Sol-Gel Routes to Supported Friedel-Crafts Alkylation Catalysts

by

Mary E. Goodchild

A Thesis

submitted to the Department of Chemistry

in partial fulfillment of the requirements

for the degree of

Master of Science

July, 1998

Brock University

St. Catharines, Ontario

ABSTRACT

Aluminosilicate catalysts containing supported $ZnCl_2$ and metal fluoride salts have been prepared using a sol-gel based route, tested and characterized. The activities of these $ZnCl_2$ + metal fluoride catalysts, while greater than "Clayzic" ($ZnCl_2$ supported on montmorillonite K10) are not as good as supported $ZnCl_2$ only supported on aluminosilicate. Alumina supports have also been prepared *via* a sol-gel route using various chemical additives to generate a mesoporous structure, loaded with $ZnCl_2$ and tested for activity. The activities for these alumina-supported catalysts are also significantly higher than that of "Clayzic", an effective Friedel-Crafts catalyst. Characterizations of these two types of catalysts were done by magic angle spinning (MAS) NMR, diffuse reflectance infrared (DRIFT) spectroscopy and additionally for the alumina nitrogen adsorption studies were done. Supported aluminum trichloride was also investigated as an alternative to the traditional use of aluminum trichloride.

ACKNOWLEDGMENTS

In a major project like this there are many people who give support and advice. First, I would like to thank my supervisor, Dr. Jack Miller for the opportunity to work on such an interesting project and for his advice, patience and support. Thanks also to the members of my committee, Dr. M.F. Richardson, Dr. A. Capretta, Dr. J.S. Hartman and to Dr. S. Rothstein for their time and suggestions. I would also like to thank Dr. C.I. Ratcliffe for serving as the external examiner on the committee

A special thank you to Dr. David Wails for his time, patience, advice and for making the lab a fun place to work. The past two years would not have been the same without him.

Thanks to my family, my parents especially for their love and support. To my friends, your support and encouragement is appreciated.

Last but by no means least, I would like to thank my husband Scott for his love, support, patience, and encouragement when I needed it most.

Table of Contents

page

page

List of Tables

List of Figures

page

1. INTRODUCTION

1.1 Supported Reagents

Supported reagents have become increasingly important in chemical synthesis due to increased environmental awareness and the need for selective catalysts with high yield. Supported reagents are environmentally friendly alternatives to conventional reagents for several reasons: smaller amounts of a supported reagent can be used for a reaction, conventional reagents are often corrosive and difficult to dispose of, and the supports themselves are environmentally benign.[1]

Environmental concerns aside, there are other advantages in using supported reagents for purely chemical reasons. Supported reagents generally have high surface areas and a layered or porous nature. These details may affect the reaction energetics, allowing reactions to be done rapidly and in high yields under mild conditions. Isomer selectivity may also be enhanced using supported reagents as their porous or layered nature only allow reagents of specific size and conformation into the reaction centre in the support. An example is the nitration of estrone using clay-supported iron(III) nitrate, "clayfen"[2,3] shown below in Scheme I:

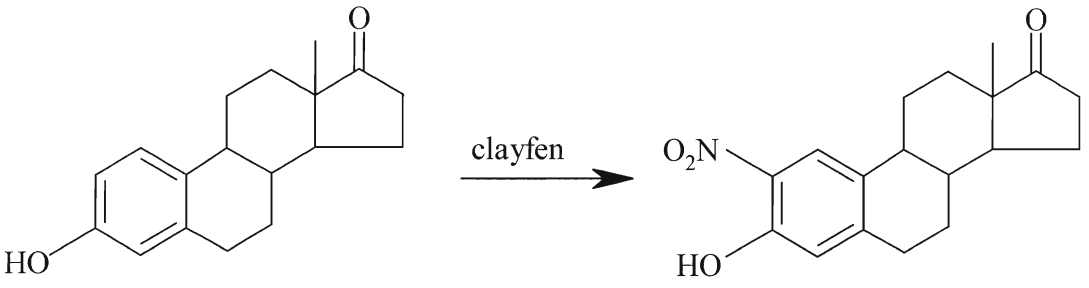

Scheme I

The traditional route of this reaction uses concentrated nitric acid in glacial acetic acid and may result in further nitration and no regioselectivity. The use of clayfen has achieved the highest yields with the best regioselectivity for this reaction.

With respect to reaction energetics, supported reagents with a high surface area having an inorganic reagent dispersed on the surface may have a great increase in the number of accessible sites for reaction. This is useful for reagents that may be insoluble in organic solvents. Supported reagents used in heterogeneous catalysis also have another advantage: reduced dimensionality. This means that the substrate and the reactant are more likely to meet in the two-dimensional space of supported reagents than with traditional reagents.

The chemical nature of the support must also be considered in combination with the surface area. The most important features are generally the Brønsted and Lewis acids sites and the degree of hydration at the surface. Clark[1] illustrates this with alumina which usually contains a large amount of physisorbed water, polarized surface =Al-O-H groups giving Brønsted acidity and Lewis acid sites of the alumina. The following section describes three of the more common supports encountered.

1.1.1 Aluminosilicates

The framework of aluminosilicates consists of SiO_2 sheets with complete sharing of oxygen atoms and some Si^{4+} replaced by Al^{3+} atoms. This results in a net anionic charge that is balanced by exchangeable cations between the sheets. Aluminosilicates have Al-O-Si and Si-O-Si tetrahedral linkages but not Al-O-Al due to Löwenstein's Rule which is derived from Pauling's third rule.[4]

Zeolites and clays are aluminosilicates and both exhibit Brønsted and Lewis acidity. The clay montmorillonite is described below. $ZnCl_2$ supported on aluminosilicate made *via* the sol-gel route is an effective Friedel-Crafts catalyst.[5]

1.1.1.1 Montmorillonite K10

Montmorillonite is a clay from the smectite family of clay minerals. Smectites are characterized by their capacity to absorb water molecules between the layers thus producing a marked expansion of the structure. Smectites are composed of *t-o-t* layers (tetrahedra-octahedra-tetrahedra) where each tetrahedron shares three of its oxygen with adjacent tetrahedra along the base of the sheet and the fourth oxygen bonds to other cations in the octahedral site formed with the addition of another plane of hydroxyls. Montmorillonites can be either di- or trioctahedral where the octahedral sites are occupied by either two or three cations (for charge balance) usually Al, Mg, or Fe. The sheets or layers are bonded together through weak electrostatic bonds or through larger interlayer cations like Na, K, and Ca.[6,7] Figure 1 shows a basic structure of montmorillonite.

When acid treated, montmorillonite shows an increase in Brønsted acidity and thus increased effectiveness as a support for a reagent.[8] This is illustrated with $ZnCl_2$ supported on montmorillonite K10 (also known as Clayzic™).[9,10] Montmorillonite K10 is acid treated montmorillonite and Clayzic is an effective Friedel-Crafts alkylation catalyst. $ZnCl_2$ on untreated montmorillonite shows little Friedel-Crafts alkylation activity.[11] Friedel-Crafts alkylation catalysts are the focus of this work and Clayzic represents some of the pioneer work into this type of catalyst.

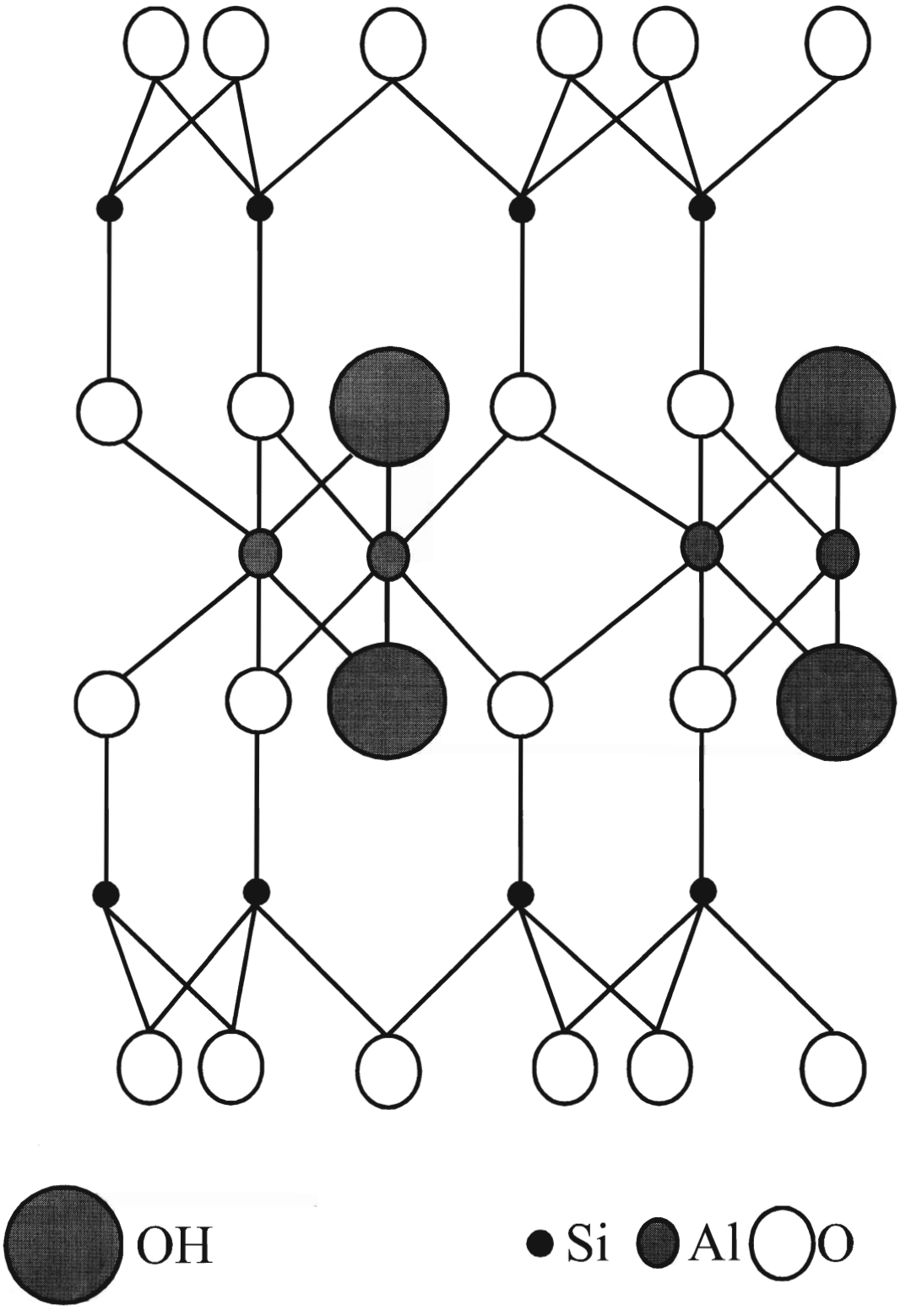

Figure 1: The layer structure of montmorillonite K10. (ref.12)

1.1.2 Alumina

Alumina is a widely used support for the catalysis of a variety of organic reactions. Alumina has a basic structure of Al_2O_3. There are two basic types of alumina: α- alumina (corundum) is arranged in a hexagonal close-packed oxygen lattice and β-alumina has an alternating close-packed lattice and contains sodium. β-alumina is of interest in supported reagent chemistry as the oxide layers are stacked in three dimensions but every fifth layer has three quarters of its oxygens missing so tunnels exist through which alkali metal ions can move.[12,13]

KF-alumina reagents are effective for Michael additions and have been studied extensively. The adsorption of inorganic salts onto the surface of alumina has also provided a way to study the nature of the reagent surface.[14-16]

1.1.3 Silica

Silica is a widely used material in supported reagents and for other applications such as chromatography column packings.[12,17-20] Silica is a common metalloid oxide and has a three dimensional polymeric structure. The coordination of silicon in silica is four and two for the oxygen.

Miller and co-workers[18] presented a sol-gel synthesis of silica with $ZnCl_2$ as an effective Friedel-Crafts catalyst that shows a considerable increase in activity over Clayzic.[9,10] Oxidation-reactions can be carried out with the use of chromium (VI) and permanganate compounds supported on silica giving good yields.[17] Silica is one of the most widely used supports.

1.2 Friedel-Crafts Reaction

The Friedel-Crafts reaction is an electrophilic substitution type reaction. It was first reported in 1877 and is used for alkylation and acylation reactions. The Friedel-Crafts reaction has conventionally been for aromatic substrates but is not necessarily confined to them. The reaction is generally an acid-catalyzed process which generates a carbocation intermediate from haloalkanes. Traditionally, metal halides (i.e. Lewis acids) have served as the catalysts for this reaction with $AlCl_3$ being the most predominant. Ferric chloride ($FeCl_3$) is also used and although it is less active than aluminum chloride it does have somewhat better selectivity. Brønsted acids such as HF and H_2SO_4 also serve as effective Friedel-Crafts catalysts.[21]

1.2.1. Alkylation Reactions

Alkylation reactions are defined as the introduction of an alkyl group to a substrate. The ease of formation of the electrophilic intermediate reflects the stability of the carbocation produced. The order of reactivity for the carbocation is usually allyl or benzyl>tertiary>secondary>primary. Because of this stability scheme the carbocation intermediate can undergo rearrangement prior to reaction with the substrate. For example, the reaction of benzene with 1-bromopropane yields a major product of isopropylbenzene with propylbenzene as the minor product (see Scheme II below)

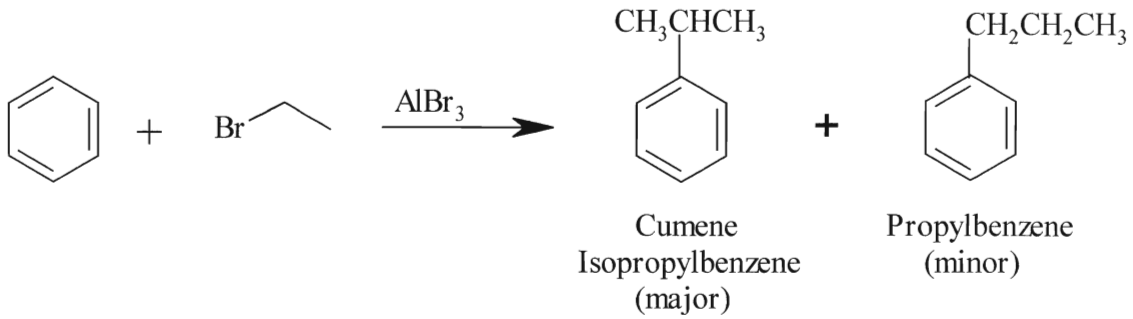

Scheme II

Another limitation of alkylation reactions is that activation of the aromatic ring occurs with one substitution and can lead to others. Hence alkylations can be unselective and are only effective if mixtures can be separated.[22]

1.2.2. Acylation Reactions

Acylation reactions are better for introducing a carbon chain to a substrate. The product is a ketone that can be utilized itself or reduced further. However, this reaction needs a 1 mole excess of catalyst because the first mole will complex to the carbonyl group. Multiple substitution does not occur here since the acyl group deactivates the aromatic ring. Rearrangement is not a problem either because para substitution predominates, presumably due to the size of the acyl-catalyst complex that forms. An example of an acylation is given below in Scheme III.[22]

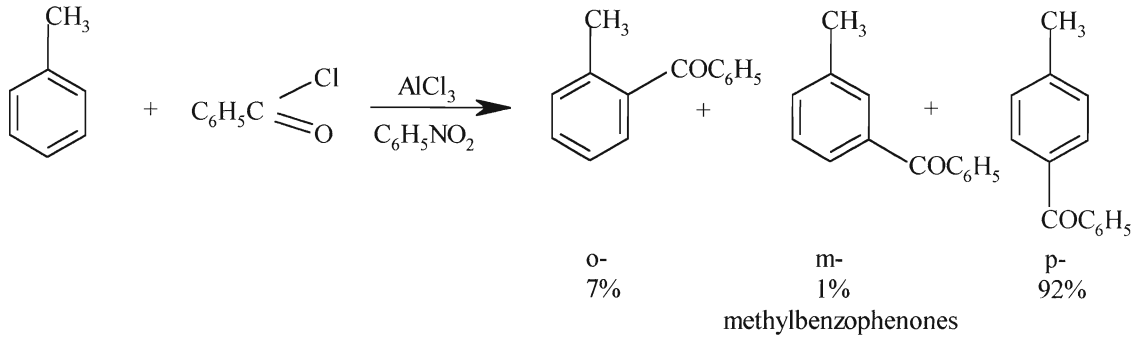

Scheme III

1.2.3 General Mechanism

A proposed general mechanism involves the formation of a complex between the catalyst and the haloalkane. A brief scheme is shown below.[23]

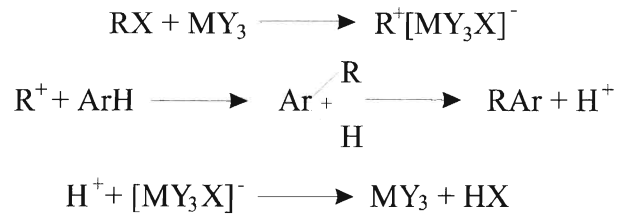

Scheme IV

1.3 Sol-Gel Chemistry

1.3.1 Basic Concepts

Sol-Gel methods are broadly defined as the preparation of ceramic materials by the preparation of a sol, gelation of the sol and removal of the solvent. The sol is produced from either inorganic or organic precursors and may consist of dense oxide particles or polymers. Sol-gel chemistry provides a very useful route to a variety of

materials including supports for catalysts (this work), thin films and ceramics. Figure 2 shows a schematic of the steps in the synthesis of these materials.

To best explain the sol-gel process a few definitions should be introduced. A colloid is a suspension where the dispersed phase is very small (≈1-1000 nm) such that the gravitational forces are negligible and interactions are dominated by short-range forces like van der Waals attraction and surface charges. The dispersed phase is so small that it exhibits Brownian diffusion, a random motion of the particles propelled by the momentum transmitted by collisions with molecules of the suspending medium. A sol is a colloidal suspension of solid particles in a liquid.

The precursors (starting materials) for the preparation of a sol are often metal or metalloid alkoxides. These alkoxides are popular precursors because they react readily with water, i.e. undergo hydrolysis, where one or more of the alkoxy groups are replaced by water. This is shown in Scheme V

$$Si(OR)_4 + H_2O \longrightarrow HO\text{-}Si(OR)_3 + ROH$$

Scheme V

The R represents any ligand that may be attached to the silicon, in this case it is an alkoxy group. Hydrolysis can proceed with the other alkoxy-silane groups present or it may stop at one, depending on the amount of water present. This reaction is important because a partially hydrolyzed molecule may link with another in a condensation reaction, shown in Schemes VI & VII.

$$(OR)_3Si\text{-}OH + OH\text{-}Si(OR)_3 \longrightarrow (OR)_3Si\text{-}O\text{-}Si(OR)_3 + H_2O$$

Scheme VI

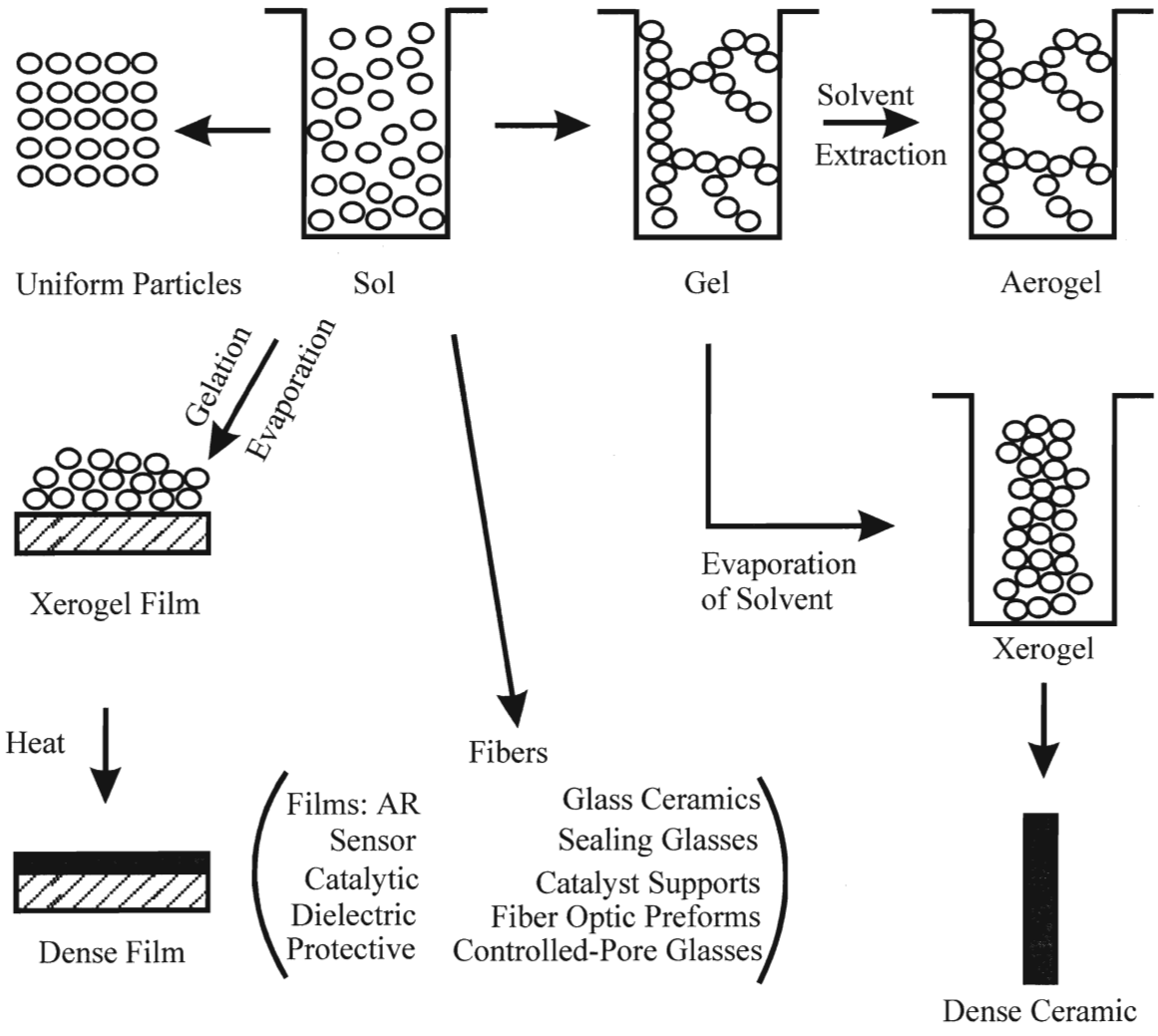

Figure 2: Overview of the sol-gel process in the synthesis of various materials. (ref. 24).

$$(OR)_3Si\text{-}OR + OH\text{-}Si(OR)_3 \longrightarrow (OR)_3Si\text{-}O\text{-}Si(OR)_3 + ROH$$

Scheme VII

Condensation can be defined as two molecules linking together with the release of a small molecule such as water or an alcohol. If this reaction were to continue a larger molecule could be formed from the alkoxy-silane species, i.e. polymerization. Polymers are, by definition macromolecules made up of hundreds or thousands of units (monomers) that are capable of forming at least two bonds. Specifically, polymerization of tetraethyl orthosilicate (TEOS) and aluminum tri-*sec*-butoxide (ATSB) leads to extensive branching as these molecules are tetra- and tri-functional, respectively.

As shown here, since a polymer can form three-dimensional structures, the definition of a polymer can be extended to include most solids. This trivializes the concept so the definition of a polymer is confined to structures with random branching. Thus, crystalline solids are excluded from being categorized as a polymer.

Another ambiguous situation encountered is: if a solution of monomers is prepared and allowed to condense into cross-linked polymers it is unclear what the result is, either a solution or a sol. The most obvious answer is a sol but if the polymer is a linear chain that has coiled into a ball this answer may not be correct. The problem arises from previous definitions of colloid and polymeric systems. Hence the definition of a polymeric sol has been refined to be one in which the solid phase contains no dense oxide particles larger than 1 nm which is the lower limit of the colloidal range. This definition is sufficient to make the distinction between sols and polymeric sols since most systems of interest contain dense particles larger than 5 nm so for these systems the term sol is used.

When condensation reactions are allowed to progress throughout a sol the molecule can reach macroscopic dimensions and the substance is then called a gel. Further, a gel is a substance that contains a continuous solid skeleton enclosing a continuous liquid phase. Gels are also formed from particulate sols when attractive dispersion forces causes the particles to stick together so that a network is formed. When the last bond to complete the macromolecule is formed it is considered to be the gel point (usually measured in hours). However, bond formation does not stop at the gel point because the network is still flexible so segments of the gel network can move close enough to allow more condensation reactions to progress. In addition, there is a sol within the gel network and the smaller polymers may continue to attach themselves to the network. This process is called aging and may involve further condensation, phase transformations within the solid or liquid phases, or dissolution and reprecipitation of oligomers and monomers. Some gels exhibit spontaneous shrinkage (syneresis) as bond formation or attraction between the particles causes contraction of the network and liquid is expelled from the pores.

Drying of the gel by evaporation under normal conditions gives rise to capillary pressure causing shrinkage of the network. The resulting dry gel is called a xerogel and the reduction in volume may be 5-10 times compared to the wet gel. If the gel is dried in an autoclave under supercritical conditions there is no capillary pressure and little shrinkage. This is called an aerogel and may be mostly air. Most gels are amorphous in nature but can crystallize on heating or with the use of templates the framework can be "grown" around a molecule (template). Xerogels and aerogels are used in the preparation

of dense ceramics but are interesting in their own right due to their high porosity and surface area.[24]

1.3.2 Chemical Additives in Substrate Synthesis

It is possible to control the surface area, pore volume and pore size distribution of a support by introducing a chemical additive in the preparation. The additive is usually organic and is referred to in the literature as a template or drying chemical control additive (DCCA). In this work they will be referred to simply as "chemical additives" for reasons discussed later in this section. The sol-gel route to the preparation of supports allows for the easy introduction of the additive. The additive is usually added before the hydrolysis of the sol. After drying the reagent is calcined at high temperatures to burn off the organic additive and leave the porous support. The goal is to choose the chemical additive so a specific surface area and pore distribution is obtained. Acetylacetonate (2,4-pentanedione, H-acac) and metal acetylacetoacetates have been used for this purpose in the synthesis of zirconia and aluminosilicate supports for catalysis.[25,26] N,N-dimethylformamide and hexylene glycol (2-methyl-2,4-pentanediol) have also been used as chemical additives for controlling pore size distributions of silica gel monoliths and alumina respectively.[27,28]

The reason the organic additions to the synthesis of these supports are not referred to as templates here is simple. The term template implies that the pore left after the organic additive is burned off should be the same approximate size as the additive. This is not necessarily the case. The organic additive often will complex with the support during

synthesis to produce a larger molecule thus leading to a larger pore size. In the case of aluminosilicates, β-diketones have proven effective as chemical additives.

1.4 Characterization Techniques

There are several techniques available for characterization of supported reagents. This section describes the theory and uses of the three techniques employed in this work. They are:

1) Nuclear Magnetic Resonance (NMR)
2) Nitrogen Adsorption-Desorption Analysis
3) Diffuse Reflectance Infrared Fourier Transform Spectroscopy (DRIFT)

1.4.1 Nuclear Magnetic Resonance (NMR)

Nuclear Magnetic Resonance (NMR) is an extraordinarily powerful technique for characterization of compounds in the liquid and solid state. The focus of this work is on solid state NMR and the theoretical aspects of NMR will be discussed in relation to solids.

1.4.1.1 Basic Concepts

1.4.1.1a Magnetic Properties

There are properties inherent to the nucleus of an atom that allows NMR to occur. These properties are angular momentum or spin (I) and the magnetic moment (μ). The spin may have integral or half-integral values (0, 1/2, 1, 3/2,...), the actual value depending on the isotope. Spin is quantized so discrete values of angular momentum may

be observed, their magnitudes given by $\hbar m$ where the quantum number m can take the values I, $I-1$, $I-2,\ldots,-I$. Therefore, there are $2I+1$ equally spaced spin states of a nucleus with angular momentum quantum number I. The components of the magnetic moment μ associated with the different spin states are defined as $m\mu/I$ so μ has $2I+1$ components as well. If an external magnetic field is applied the spin states have differing potential energies and the origin of NMR lies in these energy differences.[29]

The ratio between spin and the magnetic moment is defined as the gyromagnetic ratio, γ:

$$\gamma = \frac{\mu}{I\hbar} \qquad (1).$$

The gyromagnetic ratio has a characteristic value for each magnetically active nucleus and the size of this ratio influences spin-spin coupling (not covered here).

If a nucleus has I=0 the nucleus is magnetically inactive and is of no use in NMR. Two major examples are ^{12}C and ^{16}O. A nucleus with a spherical nuclear charge distribution possesses a spin of ½ and is known as a dipolar nucleus. Examples of nuclei with I=1/2 are ^{1}H, ^{13}C, ^{29}Si, and ^{19}F. A nucleus with an ellipsoidal charge distribution possess a spin of 1 or more in integral and half-integral units and is known as a quadrupolar nucleus. Examples of quadrupolar nuclei include ^{7}Li ^{11}B, and ^{27}Al. Quadrupolar nuclei are discussed in more detail later in this section.

The NMR experiment consists of placing a nucleus (or collection of nuclei in a sample) in a magnetic field B_o to distinguish the nuclei according to their spins by aligning them with the field in a parallel or antiparallel direction. By convention, the direction of B_o is taken to be in the z-direction of three-coordinate space. A second field,

B_1 is then applied at a frequency corresponding to the energy difference between spin states. The second field is applied to generate a population inversion of the spin states and the energy absorbed to create this population inversion can be detected electronically and is referred to as resonance. It is possible to accomplish resonance with a very short pulse of B_1 (between 2 and 200 μs). Once the second field is turned off detection of the nuclear signal can take place without interference from B_1. The signal intensity eventually returns to zero as the system comes to equilibrium. The consequences of this are discussed later. The resonance frequency ν_o is given by:

$$\nu_o = \frac{\gamma B_o}{2\pi} \qquad (2)$$

The energy difference depends on the nucleus of interest, according to the equation above.[30]

1.4.1.1b The Chemical Shift

It may seem that all examples of a given nucleus in a sample would have the same resonance frequency ν_o given by γ and B_o. This is not the case. The exact resonance frequency depends on the nature of the electron cloud surrounding the nucleus of interest. A molecule placed in a magnetic field induces motion of the electron cloud so that a secondary field is set up. The secondary field opposes the main field at the nucleus and reduces the nuclear frequency at a magnitude proportional to B_o and this is referred to as shielding or screening (σ). This is a measure of the ability of the electron cloud to alter B_o and is given by:

$$\nu_o = \frac{\gamma B_o}{2\pi}(1-\sigma) \qquad (3).$$

Equation 3 illustrates that as a nucleus is shielded more the resonance frequency decreases and if this shielding is decreased, ν_o increases. In practice the measure of this variation in ν_o is the chemical shift (δ). The chemical shift is defined in the equation below,

$$\delta = 10^6 \frac{(\nu_o - \nu_{ref})}{\nu_{ref}} \qquad (4)$$

where ν_{ref} is the resonance frequency of a reference material. Using ν_{ref} allows the chemical shift to be a molecular property, independent of the magnetic field used to measure it. The factor of 10^6 scales the numerical value of δ to a convenient number so chemical shift values are quoted in parts per million, or ppm.[51] For example, in ^{1}H NMR, if an electron-withdrawing group is introduced, the electron cloud around the proton decreases and the resonance frequency increases. The chemical shift is very useful as it gives information on the environment of a particular type of nucleus.[29]

1.4.1.1c Spin-spin Coupling

The resonance frequency of a particular nucleus is altered further when there are other magnetically active nuclei in the molecule. A nucleus can "sense" the magnetic field of another nucleus *via* the bonding electrons (s electrons have a finite density at the nucleus) and a perturbation of the magnetic field occurs for both of the nuclei and the resonances are split into multiple peaks. The influence of neighbouring spins on the multiplicity of the peaks is called spin-spin coupling. The magnitude of the coupling is

measured in Hertz (Hz) because it is the same in all magnetic fields and is called the coupling constant (J). The coupling constant can give valuable information about the bonding system. This is largely useful in liquid systems only.

1.4.1.1d Quadrupolar Nuclei

As mentioned briefly before, nuclei with spins of 1 or greater are called quadrupolar nuclei. These nuclei are polarized by the magnetic field and also by any electric field gradient present, which arises from the bonding electrons and in solids, more distant electronic contributions. The nature of the interaction depends on whether the nucleus of interest possesses an integral or half-integral spin. Since aluminum possesses a half-integral spin (5/2) and is of interest here the discussion will be limited to effects seen with half-integral spins. If the electric field gradient (EFG) is zero the energy gap between spin states ($2I+1$) is the same for any pair, i.e. the energy of the possible transitions are equal and a single resonance results. When the EFG is non-zero then the energy of each spin state is altered. The result with a $I = 5/2$ nucleus is there is five different transition frequencies possible. All of the transitions except the central +1/2, -1/2 are subject to a first order quadrupole effect. This is described by the quadrupole coupling constant ν_Q

$$\nu_Q = e^2 qQ/h \qquad (5),$$

where eq is the electric field gradient and eQ is the nuclear quadrupole moment. The energy gap between the other possible transitions will change depending on the orientation of the electric field tensor with respect to the direction of the magnetic field B_o. The central +1/2, -1/2 transition is affected by the second-order quadrupole effect which causes line broadenings and frequency shifts proportional to ν_Q^2/ν_L where ν_L is

the Larmour frequency of the quadrupolar nucleus. The second order effects may be reduced by a factor of four by Magic Angle Spinning (MAS-discussed below).[30,31]

1.4.1.1e Relaxation

The application of the second magnetic field causes the resonance effect. However, the system has to come back to the equilibrium state. This is called relaxation and takes a finite amount of time to occur. The relaxation of a particular nucleus is characterized by a time T. A pulse is applied and the subsequent measurement of the free induction decay (FID) induced by the nuclear magnetic moments present is done. A Fourier transform of the FID yields the frequency domain NMR spectrum. If the magnetization is in the *z*-direction but the spin is pointing in the opposite direction of B_o the nuclei will undergo spin-lattice or longitudinal relaxation, designated T_1, where the equilibrium distribution of the spins is determined by the Boltzmann factor. If the magnetization is moved into the *xy* plane the nucleus will undergo spin-spin or transverse relaxation, designated T_2.

There are some secondary effects that affect both T_1 and T_2. Dipole-dipole relaxation is one and the motion of other magnetic nuclei or unpaired electrons causes it. Dipole-dipole relaxation has influence on the T_2 relaxation time and also on line broadening of the NMR spectrum. Quadrupolar relaxation occurs only with quadrupolar nuclei (i.e. $I>1/2$) with an asymmetrical charge distribution. A net torque is exerted on the nucleus by the resulting electric field from the asymmetry of the charge distribution as well as by the magnetic fields present. Electric field gradients exist at atomic nuclei due to the asymmetrial arrangement of the bonding electrons. The Brownian motion of the

molecule causes the direction of the electric quadrupole torque to vary randomly around the nucleus. Therefore, electric torque components exist at the nuclear resonant frequency causing an interchange of energy between the nucleus and the rest of the system affecting both T_1 and T_2.[30]

1.4.1.2 NMR of Solids

In the early days of solid state NMR, the spectra contained broad and unresolved peaks. There are two main reasons for this. Nuclear magnets can couple directly through the interaction of nuclear dipoles and gives rise to a D coupling, which is much larger than the J coupling. This is known as dipole-dipole coupling. In liquids, the dipoles constantly reorient through tumbling but in the solid phase the nuclear dipoles are held rigid and tumbling is not the dominant interaction, D coupling is. Dipole-dipole coupling is on the order of several hundred to a few thousand Hertz thus giving broad peaks.[29]

A second factor is the chemical shift anisotropy. In solutions, the observed chemical shift is from the average of the shielding around a nucleus for all orientations in space due to tumbling. In a solid the shielding is not always the same for a given type of nucleus due to the orientation as there is no averaging of the chemical shift. There are experimental techniques that have been developed to overcome these difficulties and it is now possible to obtain high resolution NMR spectra of solid samples. These techniques are discussed below.

1.4.1.3 Experimental Techniques

The combination of the techniques described below allow for the acquisition of high resolution spectra, in some cases almost as good as the spectra for liquids.

1.4.1.3a Magic Angle Spinning

To correct for the chemical shift anisotropy and dipolar interactions there are two things that are done. The first thing that is done is to tilt the sample to a specific angle with respect to B_o (i.e. in the z direction). The magnetic field of a nucleus with magnetic moment μ at a second nucleus a distance r away will have a component in the direction of B_o. This influences the frequency of the second nucleus and couples the two spins. The B_o component is given by:

$$B_o = \left(\frac{K\mu}{r^3}\right)\left(3\cos^2\theta - 1\right) \qquad (6)$$

where K is a constant and θ is the angle between the direction of B_o and the line joining the two nuclei. The angle at which B_o is zero is the angle at which $3\cos^2\theta - 1 = 0$ or $\theta = 54°44'$ and is known as the "magic angle" because it is where most dipolar interactions disappear. This is illustrated in Figure 3.[30]

The second thing that is done is to spin the sample at high speeds to correct for the chemical shift anisotropy. Chemical shift anisotropies are a few hundred to a couple of thousand Hertz so the spinning speed must be faster than this range in order to average all orientations. In a polycrystalline solid, the internuclear vectors will take any possible θ and spinning the sample will make them behave as if they were oriented at the magic angle. Thus we have "Magic Angle Spinning" or MAS.

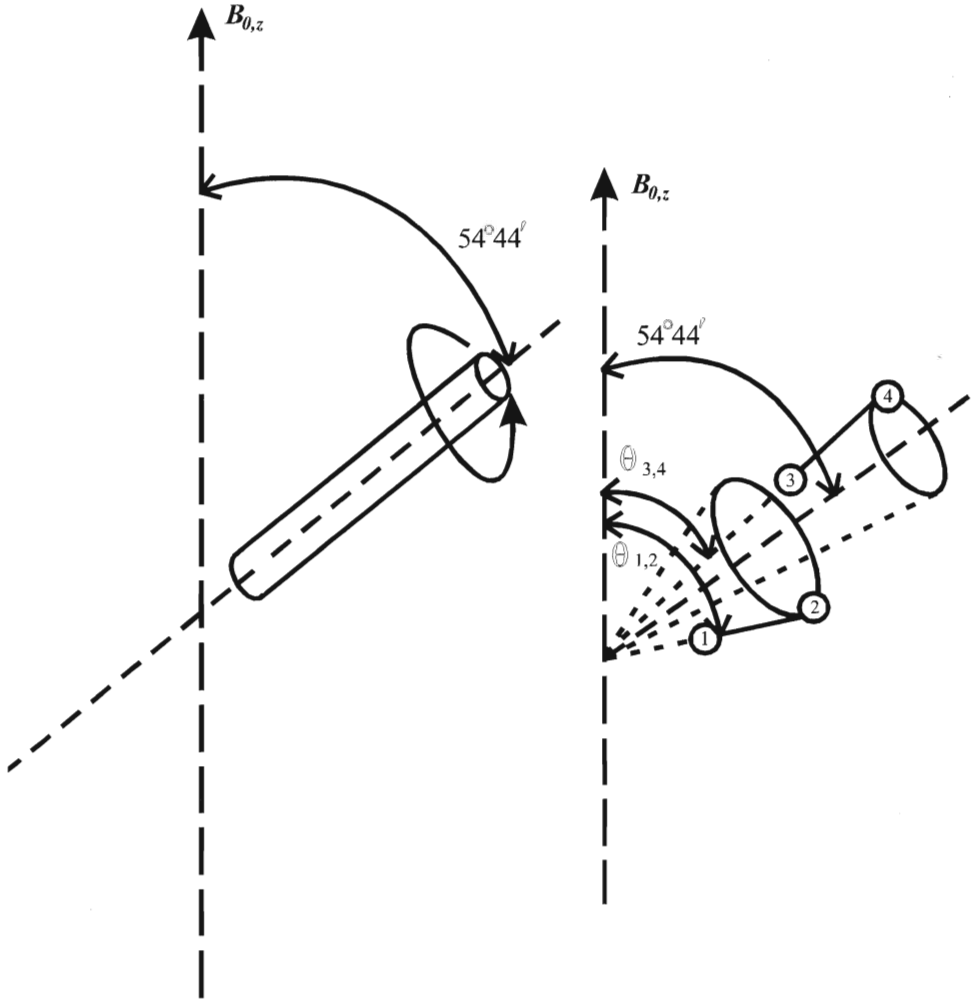

Figure 3: Illustration of Magic Angle Spinning and how MAS gives the internuclear vectors an average orientation at the magic angle. (ref. 30)

Some second order line broadening effects and frequency shifts inversely proportional to the Larmour frequency are seen with quadrupolar nuclei. The Larmour frequency is the frequency at which the magnetic moment precessess around the z axis (i.e. B_o) with a constant angular velocity. As a result, not all of the dipolar interactions are averaged out by MAS. This is significant since 74% of all nuclei with spin are quadrupolar. Two approaches are used to correct this. Double Rotation (DOR) involves simultaneous rotation about two axes, one at the magic angle the other at either 30.56° or 70.12°. This is accomplished by a stator-within-stator approach inside the probe. The second technique is Dynamic Angle Spinning (DAS) where the sample is rotated sequentially about two axes, the first at 37.38° and the second at 79.19°. In practice, switching the rotation axis cannot be performed instantaneously so an echo pulse sequence is used to preserve the magnetization during the angle switch. However, a flipping time of <9μs is possible today and could become shorter in the future. For now though, DOR is somewhat easier to accomplish than DAS as it does not involve the rapid switching of rotation axes. This will average the second order effects. Figure 4 shows schematic representations of both DOR and DAS.[33]

There is another technique that is useful for study of species adsorbed at surfaces or in the voids of molecular sieves. This is known as Multiple Quantum NMR (MQ-NMR) and it is used for characterizing homonuclear spin clusters in the solid state. The technique employs a 2D NMR pulse sequence to force nuclear spins to act collectively through their dipolar couplings. This technique has not been used very much in catalysis yet but may become more popular in the future.

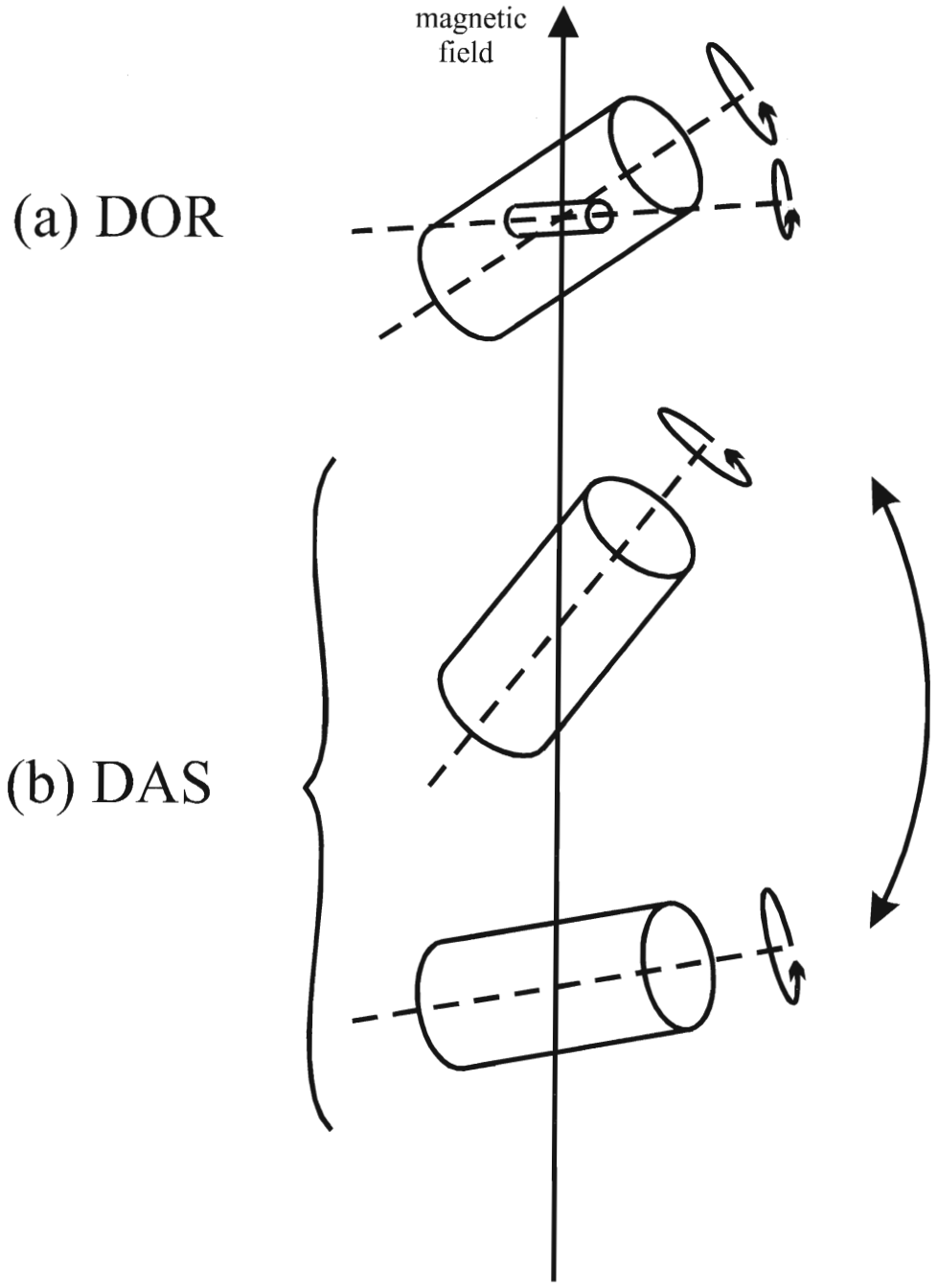

Figure 4: Schematic representation of the two approaches for averaging second-order interaction: (a) double rotation and (b) dynamic-angle spinning. (ref. 33)

1.4.1.3b High Power Decoupling/Cross-Polarization

Dipole-dipole coupling is a problem in solid-state NMR but is overcome by the use of a third magnetic field B_2 but the power levels for this field must be rather large as dipolar interactions are quite strong. A measure of the decoupling efficiency is the line width in the spectrum. Continuous high power decoupling averages the dipolar (D) coupling to zero and the spin-spin (J) coupling between the two types of nuclei involved (e.g. ^{1}H decoupling of ^{13}C-H).

Nuclei such as ^{13}C or ^{29}Si in solids have slow relaxation times and are of low natural abundance so acquisition of spectra can take a long time to accomplish. Cross Polarization (CP) makes use of the ^{1}H NMR experiment to transfer some of its high natural sensitivity to the ^{13}C or ^{29}Si experiment. In effect the magnetization of the proton (designated here as I spins) is transferred to the rare nucleus (designated as S spins). This gives a higher polarization of the rare nucleus and the long relaxation time is shortened in the magnetization build-up. This is called "cross polarization" (CP) and allows for the acquisition of spectra in a relatively short time and with a reasonable signal-to-noise ratio. In this work there is the need to wait 30 seconds-1 minute between pulses in acquiring ^{29}Si spectra due to the delay in the ^{1}H relaxation.[30]

CP is accomplished by a double resonance experiment. Magnetization of the I spins is generated by a 90° pulse at frequency ν_{oI} and after the pulse the transmitter is not turned off, the rf phase is shifted by 90°. This means B_{1I} is now applied parallel to the I magnetization. In a frame rotating with frequency ν_{oI} around the z axis, B_{1I} is the dominant magnetic field that the I spins experience. This is true only if the amplitude ν_{1I}

of the field is larger than the other interactions of the *I* spin. The *I* magnetization is then locked by the field and is known as spin locking. A similar procedure is followed for the *S* spins. Application of a second rf field B_{1S} at frequency ν_{oS}, is coincident with the lock field for the *I* spins. If the magnitudes of both rf fields are matched, known as the Hartmann-Hahn condition,

$$\gamma_S B_{1S} = \gamma_I B_{1I}, \tag{7}$$

each spin species resonates with the same frequency

$$\nu_1 = -\frac{\gamma B_1}{2\pi} \tag{8}$$

around the axis of its rf field in its own rotating frame. Since both frames share the same *z* axis, there is an oscillation of local *I* and *S* magnetization components along the *z* axis with the same frequency ν_1. Magnetization can be exchanged between both spin species by this frequency match but is only transferred from the *I* spins to the *S* spins because the *I* spin is polarized.[32]

1.4.1.4 Spectral Features

Solid state NMR is a very useful tool for elucidation of structure in supported reagents. In this work ^{29}Si (CP/MAS), ^{27}Al (MAS), and ^{19}F (MAS) NMR was used. The ^{29}Si NMR spectra of amorphous aluminosilicates generally show broad, almost unresolvable peaks in the range of approximately -70 to -120 ppm with respect to TMS. Crystalline aluminosilicates will show a lot of detail. However, the aluminosilicates in this work are amorphous so the discussion will be limited to them. The different types of Si species present are given a Q^n notation. The notations and the chemical shifts

corresponding to them are given in Figure 5.[31] The aluminosilicate spectra seen in similar work show a range of the $Q^n(Al)$ and the Q^n silanol environments.[5,34]

^{27}Al spectra of aluminosilicates basically show two or three peaks. There is the peak attributed to the non-framework octahedral species $Al[H_2O]_6^{+3}$ at about 0 ppm, the tetrahedral $[AlO_4]^-$ at about 55 ppm. The third peak is approximately 30 ppm and has been attributed to a penta-coordinate AlO_5 species.[34,35] This assignment of the "Al^V" has been disputed by MacKenzie, et.al. who claim that this peak at about 30 ppm is due to distorted tetrahedral Al species from Al triclusters sharing one oxygen.[36]

The introduction of ^{19}F into the framework allows for the acquisition of further structural information. Fluoride species also can be adsorbed to the surface of the support. There are different types of peaks that may be seen in a spectrum from aluminas (F^-, $[AlF_6]^{3-}$) or silicas; ($[SiF_6]^{2-}$, bonded $[SiF_4]^-$). The aluminum species have ^{19}F chemical shifts of about -155 ppm and the silicon species have chemical shifts of about -115 to -130 ppm.[37] A study of fluorides supported onto montmorillonite K10 shows that the fluoride species in a zeolite are all associated with aluminum and the chemical shifts of these species at approximately -155 ppm.[12]

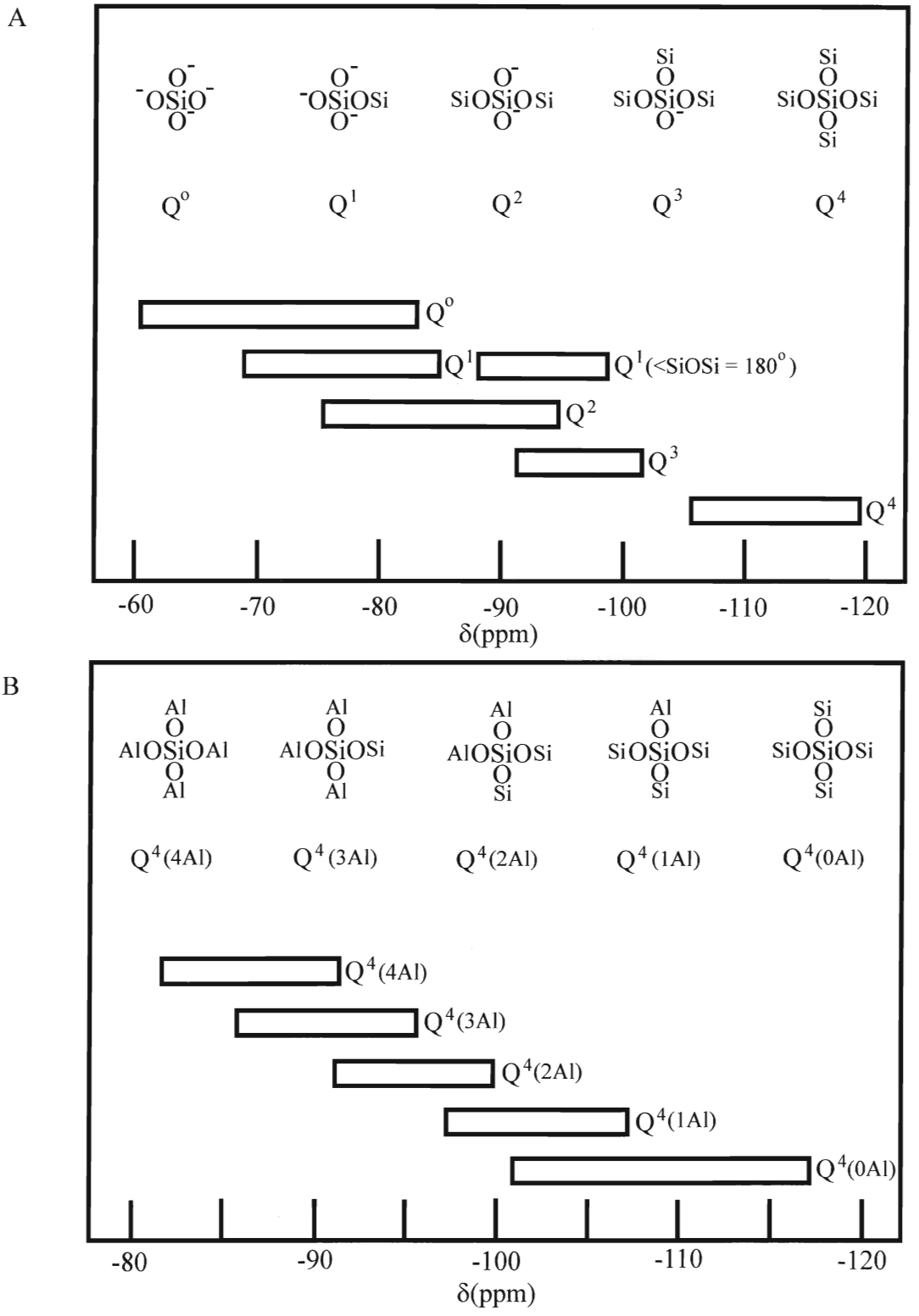

Figure 5: A-Ranges of ^{29}Si chemical shifts of Q^n units in solid silicates. B-Ranges of ^{29}Si chemical shifts of Q^4 (mAl) units in aluminosilicates. (ref. 31)

1.4.2 Nitrogen Adsorption Analysis

Gas adsorption analysis is a widely used method for determination of surface area and pore size distributions for a large variety of solid materials such as catalysts, pigments, ceramics, and industrial adsorbents.

1.4.2.1 General Considerations

1.4.2.1a Adsorption

Adsorption is defined as the enrichment of one or more components in an interfacial layer. Physisorption occurs when an adsorbable gas (the adsorptive) is brought into contact with the surface of a solid (the adsorbent). This is the phenomenon dealt with in this work. An interfacial layer has two regions; the surface layer of the adsorbent and the adsorption space in which enhancement of the adsorptive can occur. The adsorption forces involved are "dispersion" (London) forces, which are attractive, along with short-range repulsive forces. There are also electrostatic forces involved if either the solid or gas is polar in nature.[38]

1.4.2.1b Pores

The adsorption method for studying surface area and porosity is limited to bodies which are either very finely divided or possess an extensive pore system. For finely divided bodies the surface area is inversely related to the size of the constituent particles. The idealized case assumes the particles are equally sized cubes of edge length l, the specific surface area A is surface area of 1 gram of solid is given by

$$A = \frac{6}{\rho l} \tag{9}$$

where ρ is the density of the solid. However, in practice finely divided solids are made up of particles of different sizes and irregular shapes so this makes the relationship more complicated but Equation (9) serves as a rough guide.[39]

Finely divided (primary) particles will stick together due to surface forces to form secondary particles. If the connection between the particles is weak the particles can be broken down again. This is known as an aggregate. At elevated temperatures or under pressure, the primary particles will become rigidly joined and the secondary particles are known as agglomerates. The spaces between the primary particles within a secondary particle along with those between a secondary particle and its neighbours make up a pore system. The shape and size of these pores will be related to both the primary and secondary particles. In practice there are two shapes of primary particle that frequently arise: the sphere and the plate. Silica gel particles if suitably prepared are approximately spherical and of the same size. Ferric oxide and alumina gels are composed of plate-like particles. The walls of the pores in the aggregate or agglomerate will be made up of the surface of the spheres in the first case and will be planar if the primary particle is plate-like. The shapes of the pores are dependent on the size distribution of the particles and on the mode of packing. With plates, the pores tend to be wedge shaped and with spheres the closeness of the packing can be expressed by the coordination number. Figure 6 shows the different kinds of pores that can occur.[39]

There are different kinds of pore systems and the individual pores may vary in size and shape within a given solid or compared to a different solid. The width w of the

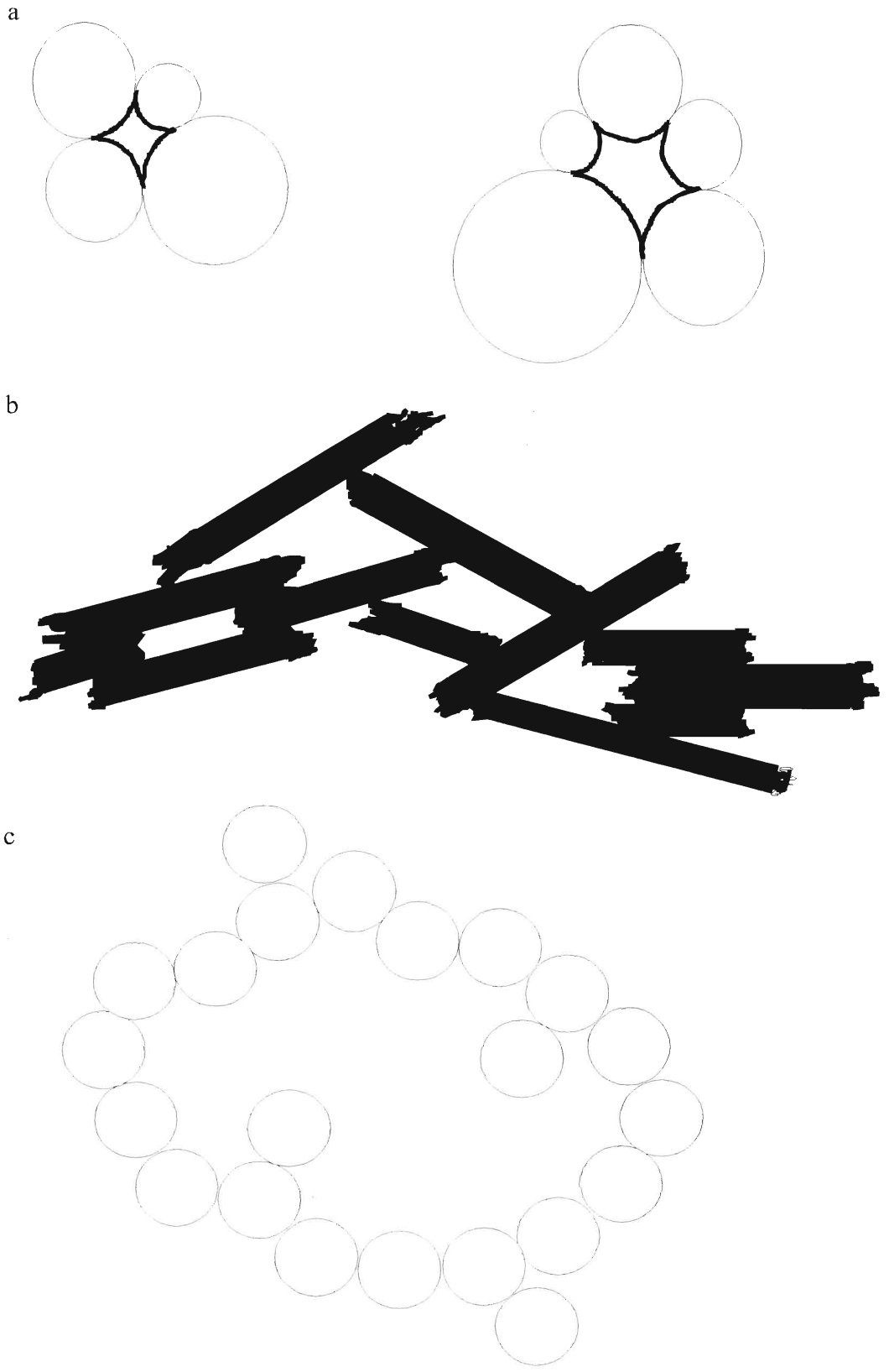

Figure 6: a) Pores in aggregates composed of spherical particles.
b) Pores in an aggregate composed of plate-like particles.
c) An aggregate of spherical particles with an open structure. (ref. 39)

pore is of interest. This refers to the diameter of a cylindrical pore or to the distance between the sides of a slit-shaped pore (formed from plate-like particles). The classification of pores is by their average width and is officially adopted by IUPAC. There are three basic classifications, given in Table 1[39]

Table 1: Classification of pores based on their width.

CLASSIFICATION	WIDTH
Micropores	Less than 2 nm
Mesopores	Between 2 and 50 nm
Macropores	More than 50 nm

The distinction between these classes are not hard and fast as they depend on the shape of the pores and on the nature of the adsorptive molecule.

The volume accessible in pores is considered to be adsorption space and the process that occurs is called filling. Micropore filling is regarded as a primary physisorption process and mesopore filling occurs in two distinct stages. The first is monolayer-multilayer adsorption and the second is capillary condensation. Monolayer adsorption is where all the adsorbed molecules are in contact with the surface layer of the adsorbent. Multilayer adsorption is where the adsorption space accommodates more than one layer of molecules so that not all adsorbed molecules are in direct contact with the adsorbent. Capillary condensation occurs when the residual pore space remaining after multilayer adsorption fills with condensate and is often accompanied by hysteresis which occurs upon desorption (discussed later).[38]

1.4.2.1c Isotherms

When a solid comes into contact with a gas in an enclosed space the solid adsorbs the gas. If the volumes of the vessel and the solid are known the amount of gas adsorbed can be calculated from the fall in pressure by application of the gas laws. The quantity of the gas taken up by a solid sample is proportional to the mass m of the sample and it also depends on the temperature T, the pressure p of the gas and the nature of the solid and the gas. If n is the quantity of gas adsorbed expressed in moles per gram of solid then,

$$n = f(p, T, \text{gas}, \text{solid}) \qquad (10).$$

For a particular gas adsorbed on a solid maintained at a fixed temperature, Equation (10) simplifies to

$$n = f(p)_{T,\text{gas},\text{solid}} \qquad (11).$$

If the temperature is below the critical temperature of the gas then the equation takes the form

$$n = f(p/p^o)_{T,\text{gas},\text{solid}} \qquad (12)$$

which is more useful with p^o being the saturation vapour pressure of the adsorptive. Equations (11) and (12) are expressions of the adsorption isotherm which is the relationship, at constant temperature, between the amount of gas adsorbed and the pressure or relative pressure.[39]

The majority of isotherms can be grouped into six classes, designated I to VI. The appearance of the different isotherms are shown in Figure 7.[39] The type I isotherm is reversible and is usually the result of adsorption of microporous solids having small

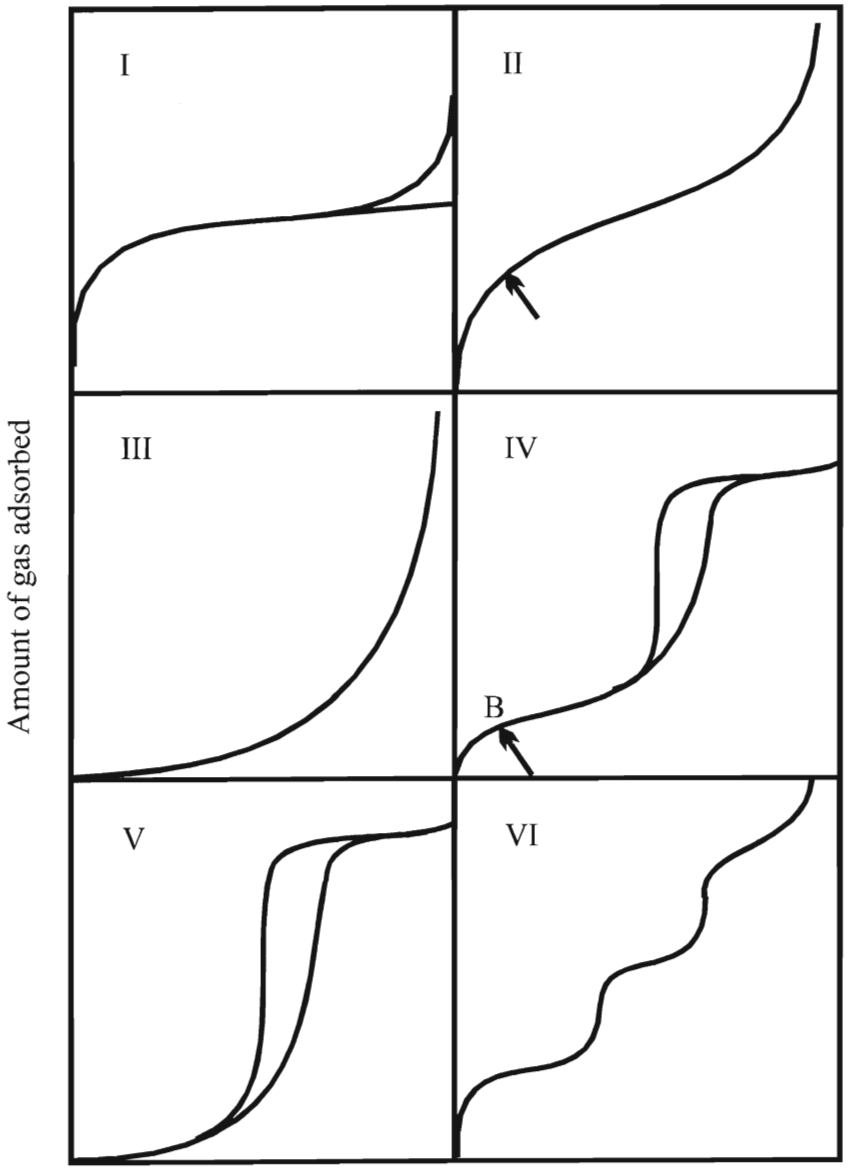

Figure 7: The six types of isotherm. (ref. 39)

external surfaces (e.g. activated carbons, molecular sieve zeolites). Type II is also reversible and is the typical form obtained with a nonporous or macroporous adsorbent This type represents unrestricted monolayer-multilayer adsorption. This is shown on Figure 7 at Point B which is taken to indicate the point at which the monolayer coverage is complete and multilayer adsorption begins. Type III is reversible and is also for non porous solids but is not very common. The type IV isotherm is attributed to mesoporous solids and has a characteristic hysteresis loop which is associated with capillary condensation occurring in the pores. Hysteresis is associated with the desorption (removal of adsorptive) branch of the isotherm. The adsorption branch is attributed to monolayer-multilayer adsorption since it follows the same path as a type II isotherm. The type V isotherm is uncommon as well but related to the type III isotherm in that they both are due to weak adsorbate-adsorbent interactions. The type VI isotherm (the stepped isotherm) represents stepwise multilayer adsorption on a uniform non-porous surface. Each step represents the monolayer capacity for each adsorbed layer. The types of solids examined in this work exhibit type IV isotherms and are thus mesoporous.[38,39]

There are also different types of hysteresis loops and these are shown in Figure 8. As mentioned before, hysteresis occurs when there is capillary condensation in the pores and pore size distributions are calculated from this branch of the isotherm. Different shapes of hysteresis loop have been recognized for specific pore structures. Type H1 is often associated with porous materials known to consist of agglomerates of compacts of approximately uniform spheres in a somewhat regular array and thus have narrow pore distributions. Type H2 loops are difficult to interpret due to network effects and in the past were associated with "ink bottle" pores. Porous glasses and oxide gels give H2 type

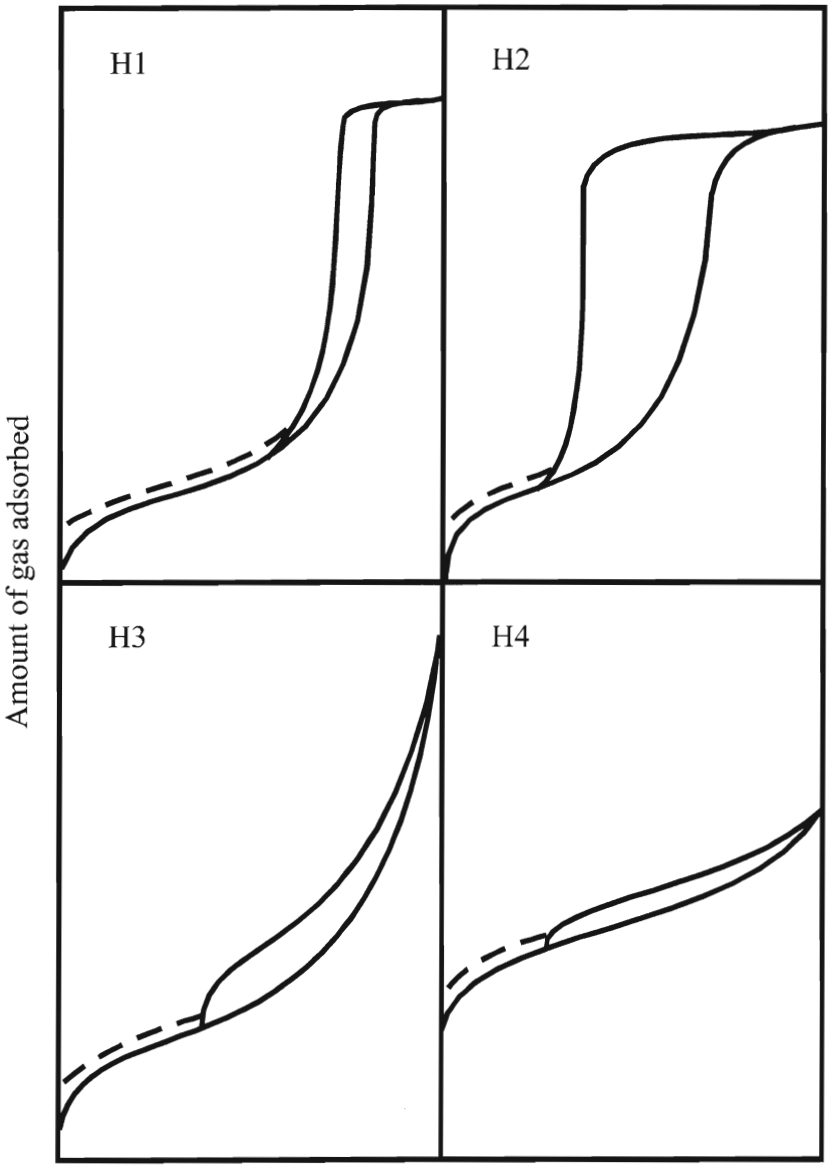

Figure 8: Types of hysteresis loops. (ref. 38)

loops. Aggregates of plate like particles giving rise to slit shaped pores exhibit type H3 loops and narrow slit-like pores give H4 type loops.[38]

1.4.2.2 Surface area by the BET method

The BET method[40] is based on a kinetic model of the adsorption process proposed by Langmuir in 1916 in which the surface of the solid was regarded as an array of adsorption sites. A state of dynamic equilibrium was assumed where the rate at which molecules arriving from the gas phase and condensing on to bare sites is equal to the rate at which molecules evaporate from occupied sites. The Langmuir model is useful for monolayer coverage but gets very complicated when applied to second and higher molecular layers. Brunauer, Emmett and Teller (BET) in 1938 introduced a model based on the Langmuir theory but with some simplifying assumptions to give an equation for multilayer adsorption. The BET equation is usually applied in the linear form

$$\frac{p}{n^a \cdot (p^o - p)} = \frac{1}{n^a \cdot C} + \frac{(C-1)}{n_m^a \cdot C}\frac{p}{p^o} \qquad (13)$$

where n^a is the amount adsorbed at the relative pressure p/p^o and n_m^a is the monolayer capacity. The variable C is related exponentially to the heat of adsorption in the first adsorbed layer. The value of C may be used to characterize the shape of the isotherm in the BET range but it does not provide a quantitative measure of the heat of adsorption, and only gives an indication of the magnitude of the adsorbate-adsorbent interaction energy. A high value of $C (\approx 100)$ is associated with a sharp knee in the isotherm which gives Point B indicating where monolayer coverage is.

The next step is to calculate the surface area (called the BET area) from the monolayer capacity. A knowledge of the molecular cross-sectional area or the average

area a_m occupied by the adsorbate molecule in the complete monolayer is needed. Therefore,

$$A_s(\text{BET}) = n_m^a \cdot L \cdot a_m \qquad (14)$$

where $A_s(\text{BET})$ is the total surface area of the adsorbent (of mass m) and L is Avogadro's constant.[38] Nitrogen is generally considered to be the most suitable adsorptive for surface area determination and full isotherms may be measured at 77 K.

1.4.2.3 Pore volume and size distribution

Porosity is related to texture (geometry of pore spaces and voids) and refers to the pore space in material. A pore is a cavity or channel in contact with the surface of a particle and a void is the space or interstice between particles. These terms are a classification of the accessibility of the pore space to the adsorptive. The total pore volume V_p is derived from the amount of vapour adsorbed at a relative pressure close to unity by assuming that the pores are then filled with condensed adsorptive in the normal liquid state. If the solid does not have any macropores the isotherm is nearly horizontal over a range of p/p^o approaching unity and the total pore volume is well-defined.

The pore distribution is derived from the Kelvin equation and there are several approaches to this. The approach taken here is the Barrett, Joyner, Halenda (BJH) method.[41] The Kelvin equation is used in the form

$$\frac{1}{r_1} + \frac{1}{r_2} = -\frac{RT}{\sigma^{lg} v^l} \ln\left(\frac{p}{p^o}\right) \qquad (15)$$

that relates the principal radii, r_1 and r_2, of curvature of the liquid meniscus in the pore to the relative pressure, p/p^o, at which condensation occurs. The other variables, σ^{lg} and v^l, are the surface tension of the liquid condensate and its molar volume respectively. To use this approach there are two assumptions that must be made: (i) a model for the pore shape and (ii) that the curvature of the meniscus is directly related to the pore width. The pore shape is usually assumed to be either cylindrical or slit-shaped: in the former the meniscus is hemispherical (thus $r_1 = r_2$) and in the latter the meniscus is hemicylindrical (thus r_1 = width of slit and $r_2 = \infty$). If a substitution is made, i.e.,

$$\left(\frac{1}{r_1}+\frac{1}{r_2}\right) \text{ by } \frac{2}{r_\kappa},$$

then with rearrangement the Kelvin equation becomes

$$r_\kappa = \frac{2\sigma^{lg}v^l}{RT\ln\left(p/p^o\right)} \tag{16}$$

where r_κ is the Kelvin radius. One must realize that this is applied for a liquid in a pore as the pore walls are already covered with multilayers of adsorptive so a correction must be made. For a multilayer thickness t and a cylindrical pore with radius r_p the relation is

$$r_p = r_\kappa + t \tag{17}$$

and for a slit-shaped pore with slit width d_p the relation is[38,39]

$$d_p = r_\kappa + 2t \tag{18}.$$

The BJH method for calculating pore distribution of mesoporous solids uses both the length and area of the pore walls. Thus only the pore radius and not the core radius (as in Kelvin equation) is used and the correction for the thickness of the adsorbed layer(s) is

made. The pore size distribution is usually expressed in a plot of $\Delta V_p/\Delta r_p$ vs. r_p . The shape of the pore distribution curve is dependent on which branch of the hysteresis loop is used. Due to complexities of capillary condensation in pore networks the pore size distribution curve can be unreliable if pore blocking effects occur (i.e. ink bottle pores) and the distribution should not be calculated from the desorption branch of the isotherm.

It should be mentioned that physisorption is one of the few non-destructive methods available for researching porous solids. Microporous and mesoporous inorganic solids have great use as catalysts because of their large surface area. It is also possible to control pore sizes and pore distribution with the use of chemical additives in the synthesis of these materials. Nitrogen adsorption is an important tool in the characterization of these supports.

1.4.3 Diffuse Reflectance Infrared Fourier Transform Spectroscopy (DRIFT)

Fourier Transform Infrared Spectroscopy (FTIR) is a very well-known technique for characterization of compounds. The incident infrared radiation sets the molecule of interest vibrating and these vibrations are what is measured. A specific bond in a moiety will vibrate with approximately the same frequency no matter which type of molecule it is in (e.g. the carbonyl will always vibrate in the 1870-1650 cm^{-1} region). This is what gives clues to the structure of a compound. Diffuse Reflectance Infrared Fourier Transform (DRIFT) spectroscopy is a method for studying surfaces and powdered materials that both scatter and absorb radiation.

1.4.3.1 Theoretical Aspects

The theory of diffuse reflectance at scattering layers within a powdered sample relates sample concentration and scattered radiation intensity. For an "infinitely thick" layer (usually on the order of <5mm), the Kubelka-Munk equation is:

$$f(R_\infty) = \frac{(1-R_\infty)^2}{2R_\infty} = \frac{k}{s} \qquad (19)$$

where R_∞ is the absolute reflectance of the layer, s is the scattering coefficient, and k is the molar absorption coefficient. Since there is no perfect standard the R_∞ is replaced by R'_∞ where

$$R'_\infty = \frac{R'_\infty(\text{sample})}{R'_\infty(\text{standard})} \qquad (20).$$

The standard is non-absorbing and exhibits high diffuse reflectance throughout the wavelength region studied. Potassium chloride or bromide with a particle size <10μm is often used. "Infinite thickness" is the point at which changing the thickness of the sample causes no change in the spectrum.

The advantages of DRIFT are short sample preparation time, strong spectra obtained from less than 100μg of sample, and it can be used for *in situ* studies of catalytic reactions. There are cells available for both high temperature and high pressure work.[42-44]

1.4.3.2 Spectral Features

In this work both aluminas and aluminosilicates were studied. Past studies show that for aluminosilicates there are various Si-O stretches in the 1040 cm^{-1} region and broad peaks corresponding to Al-O bending from 700-450 cm^{-1}. There are also Si-OH

peaks in the 3000 cm^{-1} region and Al-O coupled to Si-O at 525 cm^{-1}.[5,12,45] Studies of alumina show that there are Al-OH bands from 3600-3400 cm^{-1}, from 900-750 cm^{-1} vibrations corresponding to tetrahedral aluminum, 750-600 cm^{-1} vibrations for octahedral aluminum. At 900 cm^{-1} vibrations in the surface layer are seen and they are most likely due to deformation of surface hydroxyls. Upon dehydration a weak band at 1050 cm^{-1} develops due to a Al-O deformation in a strained group. This band will disappear upon rehydration.[46,47] DRIFT is useful for looking at adsorbed species on the surface of a support.

1.5 Aim of This Work

This work can be broken down into three components. The first takes the study of $ZnCl_2$ on aluminosilicate further and investigates the effect fluoride has on the catalyst.[5] Metal fluoride salts were incorporated into the sol-gel synthesis and characterized by MAS-NMR and DRIFT spectroscopy in addition to testing in a model reaction. The second component involves the synthesis of pure alumina *via* the sol-gel route as a support for $ZnCl_2$. The mesoporous alumina supports were synthesized using ketones and β-diketones as chemical additives in an attempt to control surface area, pore size distribution and pore volume. The third component in this work involves further investigation into supported $AlCl_3$ on various supports.[48] The precursors used for this work are tetraethyl orthosilicate (TEOS) and aluminum tri-*sec*-butoxide (ATSB).

2. EXPERIMENTAL

This section describes the work done on the project and is divided into four parts:

1) Instrumentation used to characterize catalysts
2) Preparation of supports and catalysts
3) Gas Chromatography
4) Test reactions used

2.1 Instrumental Techniques for Characterization

There are three instrumental techniques that have been employed to characterize the supports and catalysts. They are:

1) Nuclear Magnetic Resonance (NMR), ^{29}Si, ^{27}Al, ^{19}F
2) Diffuse Reflectance Infrared Fourier Transform Spectroscopy (DRIFT)
3) Nitrogen Adsorption Analysis

2.1.1 Nuclear Magnetic Resonance

The solid state samples were run on a Bruker DPX300 multinuclear Fourier transform NMR instrument using a standard bore Bruker 4 mm high speed MAS probe. The samples were packed into 4mm zirconia rotors. The ^{27}Al spectra were obtained at 78.21 MHz with a 30° pulse and 250 ms delay between the pulses and a spectral window of 50,000 Hz. The external reference was aqueous aluminum nitrate calibrated to 0 ppm. The samples were spun at 10,000 Hz and 1024 FID's were accumulated. The ^{29}Si spectra were collected at 59.62 MHz using cross-polarization with proton decoupling during acquisition. Spectra were referenced to tetramethylsilane (TMS) at 0 ppm using an

external standard (tetrakis(trimethylsilyl)silane (TTMSS), -10 ppm). Samples were spun at 4,000 Hz with a 5 ms cross-polarization contact time and a 5 s delay between pulses. The spectral window was 18,000 Hz with approximately 4,000 FID's collected. The ^{19}F spectra were collected at 282.38 MHz using the depth background suppression program.[37] Spectra were referenced to trichlorofluoromethane ($CFCl_3$) at 0 ppm using Teflon as a secondary external reference at -123.01 ppm.

2.1.2 Diffuse Reflectance Infrared Fourier Transform Spectroscopy (DRIFT)

Samples were run on a Matteson Research Series I spectrometer. The samples were ground up with potassium bromide in approximately a 1:10 ratio of sample:KBr. The sample was placed in the sample cup and pressed flat. It was heated to 200°C using a Spectra Tech variable temperature accessory under vacuum then 256 scans were collected. Transmittance spectra collected were converted to Kubelka-Munk plots to show the diffuse reflectance spectra.

2.1.3 Nitrogen Adsorption Analysis

The samples were run on a Coulter SA3100 instrument using an automated gas volumetric method. Approximately 0.08-0.12 g of sample was outgassed for approximately 1 hour at 200°C under high vacuum to remove residual water, nitrogen, oxygen and other materials physisorbed onto the surface. Surface areas were determined using the BET adsorption method and pore volumes using the BJH method on the desorption branch of the isotherm at 77K using N_2 as the adsorbate.

2.2 Preparation of supports and catalysts

This section is also divided into three sections:

1) Fluoride-based aluminosilicates
2) Alumina supports
3) Supported $AlCl_3$

2.2.1 Fluoride-based Aluminosilicates

The aluminosilicate sol was prepared by mixing Aluminum tri-sec-butoxide (20.0 g, 0.08 mol, Aldrich, 97%) with 1-butanol (200 ml, Caledon, reagent grade) while stirring. Tetraethyl orthosilicate (17.4 ml, 0.08 mol, Aldrich, 98%) was then added. The mixture was stirred with heating to 70°C for five to ten minutes until a clear solution was obtained. The solution was cooled to room temperature, divided into five equal portions so that further additions (e.g. $ZnCl_2$, MF) could be made to an identical sol. The optimum amount of zinc chloride (Aldrich, 98+%) for maximum catalytic activity for a portion has been determined (1.5 g, 0.012 mol).[5] This amounts to approximately 5 mmol zinc chloride per gram of support. Each set of five samples contained a control where 1.0 g (0.007 mol) of $ZnCl_2$ in 7.5 ml of water was made. A sample with the optimum amount of $ZnCl_2$ was also made for comparison. The fluoride samples contained various amounts of KF, NaF, or NH_4F with 1.0-1.5 g of $ZnCl_2$. The catalyst is introduced into the system by dissolution of the salt in water that is used for gelation of the sol. The optimum amount of water for gelation of each portion was 7.5 ml (0.416 mol) was determined in previous research.[5] However, mixing zinc chloride with a fluoride salt results in a precipitate of zinc fluoride which has a low solubility in water. This problem was

overcome by dissolving the salts into separate portions of water and adding the two solutions to the sol at the same time so that precipitation could occur on the support. The two portions of water added up to 7.5 ml for each portion. The gelled samples were stirred for 10 minutes and left to stand overnight. The remaining solvent was removed by heating in an oven at 120-150°C. The dry catalyst was ground into a powder and dried in air overnight at 225°C. The catalyst was then tested and characterized by methods described below.

A study of preparing the support and then loading with $ZnF_2 \cdot xH_2O$ (Aldrich, 98%), where x=3-4 was undertaken. A blank support was prepared by the procedure described above except the sol was not split into 5 portions and the solution was hydrolyzed with 37.5 ml (2.08 mol) water. The dried support (1.00 g) was added to a solution of zinc fluoride in water or methanol (100 ml). The solvent was slowly removed by rotary evaporation over the course of 1 hour. The catalysts were dried overnight at 225°C and then tested.

2.2.2 Preparation of Alumina Supports

The alumina samples were prepared in a similar manner. Aluminum tri-sec-butoxide (20.0 g, 0.08 mol) was vigorously stirred in 1-butanol (100 ml) and heated to 70°C for 5-10 minutes until the solution was clear. The solution was cooled to room temperature. If a variation in the support was to be made the solution was split into 5 equal portions. There were two variables that were altered with the alumina supports as detailed in Chapter 3, section 3.2. Aldrich supplied all chemical additives. The additive was added to the cooled sol and stirred in before the water was added. The gel was stirred for 10 minutes then left to stand overnight. The solvent was removed by

heating in an oven at 120-150°C and the dried support was ground into a powder. The support was then calcined at 500°C to burn off the organic compound to leave a mesoporous support which was characterized by nitrogen adsorption methods. Alumina supported $ZnCl_2$ catalysts were made by impregnation of the support with methanolic solution containing calculated amounts of $ZnCl_2$. The solvent was removed by rotary evaporation then dried overnight at 225°C. The catalysts were then tested by the method described below. The activity of the alumina catalysts were also compared to "clayzic", the preparation of which has been described.[9,10]

2.2.3 Supported $AlCl_3$

Aluminum trichloride (Aldrich, 99%) is very moisture sensitive so the catalyst must be prepared and tested *in situ*. Typically, the catalyst is prepared by refluxing 1 gram of an aluminosilicate support with a small amount of $AlCl_3$ in benzene (Caledon, reagent grade) for 1 hour and then adding the alkylating agent to test it.[48] There were three alkylating agents tested; 1-octene, 1-octanol and 1-chlorooctane. All of the alkylating agents were obtained from Aldrich. The mixture was allowed to cool to room temperature before addition of the 1-octene and with the other two agents the reaction was done at reflux temperatures. The amount of benzene was varied from a 2:1 molar ratio of benzene:alkylating agent to a 20:1 ratio. The amounts of $AlCl_3$ were also varied from 0.1 mmol/g support to 1.5 mmol/g. The test reaction is described below.

2.3 Gas Chromatography

A Perkin-Elmer Sigma 3B gas chromatograph interfaced to a Hewlett-Packard 3396 Series II integrator was used to analyze test reactions. Packed columns containing 3% OV-17 on Gas Chrom Q were used. Percent conversion is defined as the sum of the areas of the peaks due to products divided by the sum of the areas of the peaks due to products added to the area of the peak due to the limiting reagent, benzyl chloride. The products have been previously identified by electron impact GC-MS.[5]

2.4 Test Reactions

2.4.1 Benzene + Benzyl chloride

The typical reaction for all catalysts (except for $AlCl_3$) is between benzene and benzyl chloride. Benzene (22 ml, 0.25 mol) is stirred and 0.5 g of dried catalyst is added. Benzyl chloride (5.8 ml, 0.05 mol) is added in one aliquot and the reaction is allowed to progress for 15 minutes. A sample is taken, the solid catalyst is filtered off, and the filtrate is diluted with chloroform and analyzed by GC. The major product is diphenylmethane with small amounts of ortho, meta and para isomers of dibenzylbenzene shown in Scheme VIII.

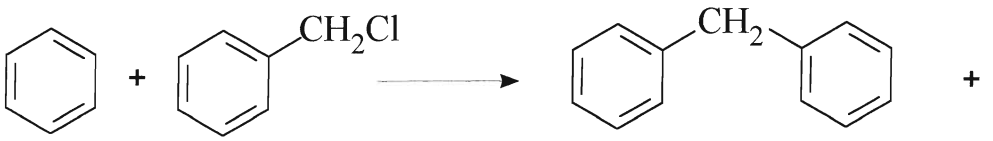

o, m, p dibenzylbenzene

Scheme VIII

2.4.2 Benzene + 1-octene in $AlCl_3$ Study

The reaction conditions are described above with the preparation of the catalyst done in benzene. The alkylating agent is added dropwise with a pressure-equalizing dropping funnel and the reaction is allowed to progress for 15 minutes and the activity is monitored by GC. The products were identified by electron impact GC-MS using a Carlo-Erba MFC 500 GC linked to a Kratos Concept 1S Mass Spectrometer. The reaction is shown in Scheme IX and the products were identified by library search. In Scheme IX the other products were disubstituted benzene products.

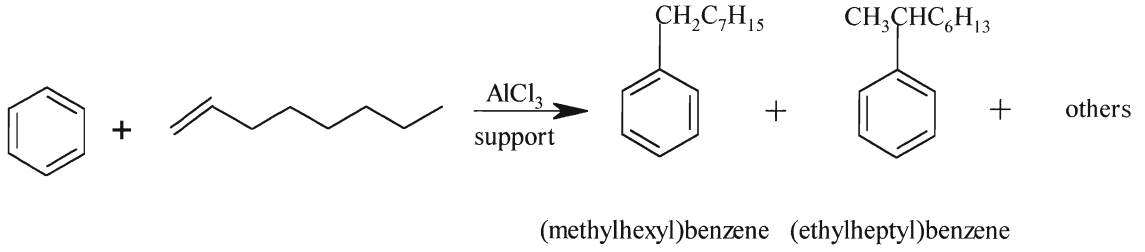

Scheme IX

The following table gives the eight most abundant peaks for the two major products formed in this reaction. The mass spectra are shown in the results and discussion.

Table 2: Mass spectral data for reaction products.

(ETHYLHEXYL)-BENZENE		(METHYLHEPTYL)-BENZENE	
m/z	intensity	m/z	intensity
91	100	105	100
119	35	91	14
161	16	106	12
190	12	115	11
92	7	190	11
105	7	41	8
104	7	77	6
41	7	39	5

3. RESULTS & DISCUSSION

3.1 Aluminosilicate Work

Clayzic has proven to be an effective Friedel-Crafts catalyst. Further work has produced a better catalyst. Acid treatment of the montmorillonite K10 destroys much of the original framework structure generating mesoporous materials where the optimum pore size for catalytic activity is 8-12 nm.[49,50] These studies were limited to commercially available materials (K10, silica). The sol-gel route for supported reagents is attractive due to the low temperature processing over the traditional high temperature melt processes for supported reagents. A synthetic aluminosilicate with controlled chemical composition, porosity and surface area with $ZnCl_2$ incorporated into the synthesis in a one- or two-step process has shown a considerable increase in activity over Clayzic.[5] As mentioned in the experimental section, the optimum amount of water needed for gelation of the sol has been determined. Theoretically, this molar ratio is 6:1 (H_2O:(Al+Si)) whereas experimentally this ratio is 13:1. The reason for this discrepancy is due to the fact that not all of the Al is incorporated into the framework. The majority of the aluminum is in the octahedral form as the charge balancing species $[Al(H_2O)_6]^{3+}$ and thus requires more water for hydrolysis than the tetrahedral species.[5] Studies on ZnF_2 supported on K10 showed an active catalyst. The surface hydroxyls are replaced by fluorine, thus introducing Lewis acid sites. The remaining surface hydroxyls have enhanced acidity due to the high electronegativity of the fluorine which contributes to the activity of the catalyst.[12] This work describes the incorporation of metal fluorides into the

aluminosilicate synthesis in an attempt to increase activity further and to provide an additional tool in the structural studies, ^{19}F MAS-NMR. Four fluoride salts were investigated, KF, NaF, NH_4F, and ZnF_2. The sections below describe them in more detail.

3.1.1 Potassium Fluoride

Incorporation of the KF into the support was attempted with dissolution of the KF into the gelation water along with the $ZnCl_2$ but it was soon discovered that dissolving both of these salts into water results in a precipitate of ZnF_2. Zinc fluoride is almost insoluble in water. To solve this problem, the gelation water for the sol was split into two portions, the salts dissolved separately, and then the solutions were added to the sol simultaneously in an attempt to precipitate the ZnF_2 onto the support. The amount of $ZnCl_2$ for optimum Friedel-Crafts activity has been determined to be 1.5 g per 1/5 portion of the sol (approximately 8 mmol/g loading). Experiments using less than this optimum amount of $ZnCl_2$ using KF to make up the molar difference were carried out. In addition, experiments using the optimum amount of $ZnCl_2$ and KF were also completed. The test reactions show that as the amount of KF is increased, the activity decreases when compared to the optimum $ZnCl_2$ and also to less than optimum amounts of $ZnCl_2$. This is shown in Table 3 below, the amounts of the salts are per 1/5 of the sol.

Table 3: Activity of catalysts with $ZnCl_2$ + KF (0.75 g used in test reaction)

AMT. $ZnCl_2$ (g)	AMT. KF (g)	% CONVERSION
1.0	0	75
1.0	0.05	65
1.0	0.10	38
1.0	0.15	31
1.0	0.21	19

The catalysts were characterized by DRIFT and MAS-NMR (^{29}Si, ^{27}Al, and ^{19}F). Figure 9 is the DRIFT spectrum for various amounts of KF compared to the catalyst with the optimum amount of $ZnCl_2$. The infrared spectra of the catalysts show vibrations corresponding to a Si-O stretch at 1050 cm^{-1}, an Al-O-Si deformation at 650 cm^{-1} and a Si-O deformation at 450 cm^{-1}. There is also a silanol peak at 3500 cm^{-1}. Any further interpretation is not possible due to the broadness of the peaks and all of the spectra look approximately the same.

Figure 10 shows the ^{29}Si NMR spectra for a series of catalysts with increasing amounts of KF. These were made with a relatively large amount of KF to exaggerate the changes in the structure that may occur upon addition of the fluoride. The silicon spectra unfortunately are broad and unresolved and show a range of Q^n silanol and $Si(OAl)_n(OSi)_{4-n}$ sites. As the amount of fluoride introduced into the system is increased the centre of the band shifts from -100 ppm to -95 ppm. The ^{27}Al NMR in Figure 11 show the 3 different aluminum species present in all of the catalysts. The octahedral $[Al(H_2O)_6]^{+3}$ species at approximately 0 ppm, the tetrahedral AlO_4^- species at approximately 55 ppm and the $Al^{"V"}$ peak at 30 ppm. As the amount of fluoride in the catalysts is increased the $Al^{"V"}$ peak decreases (and almost disappears), the tetrahedral aluminum peak increases. This supports the claim that the $Al^{"V"}$ is important to enhanced activity in the aluminosilicate system since as the amount of fluoride is increased the catalytic activity decreases. The shift to lower field observed in the ^{29}Si spectra is consistent with an increase in the amount of framework Al species. ^{19}F NMR were obtained only for the higher loadings of KF as there was no fluorine detected in the samples with smaller amounts of KF. This may be due to the sensitivity of the instrument

or perhaps some of the fluorine species are burned off as HF in the drying stages. Figure 12 gives the fluorine spectra obtained. There is one discernible peak at approximately -140 ppm due to the AlF_4^- species which is tetrahedral and could account for the decrease in $Al^{"V"}$ observed in the ^{27}Al spectra.[37] With the addition of the fluoride there is a decrease in non-framework species, an increase in tetrahedral aluminum from incorporation of the aluminum into the support and also from the formation of AlF_4^-.

3.1.2 Sodium Fluoride

The synthesis procedure is the same as with KF because NaF makes the precipitate ZnF_2 with $ZnCl_2$ when solutions of them are mixed together. The activity of this catalyst is fairly good compared to a non-optimum amount of $ZnCl_2$ but not as good as with the optimum $ZnCl_2$. Table 4 shows the results for reactions with both 0.75 g and 0.50 g of catalyst used in the test reaction.

Table 4: Activity of catalysts with $ZnCl_2$ + NaF.

AMT. $ZnCl_2$ (g)	AMT. NaF (g)	% CONVERSION (0.75 g)	% CONVERSION (0.50 g)
1.0	0	70	63
1.0	0.04	89	54
1.0	0.08	85	51
1.0	0.12	43	41
1.0	0.15	61	27

From the table it seems like this catalyst is better but as I will show later this is not the case. If more catalyst is used here the activity increases but this is somewhat counterproductive as one of the goals is to obtain an active catalyst with as little reagent as possible. Unfortunately, it is not a trivial thing to compare results from two different

days for the same catalyst, that is, comparison of these results with a result from the optimum $ZnCl_2$ catalyst made with a different batch is not possible. Variations in humidity, temperature and reagents make direct comparisons impossible. For example, if the same catalysts were made on two different days under seemingly identical conditions, the activities would not be the same. However, the activity trends were the same from day to day. That is, the trend shows an increase in activity to a maximum and then as the amount of fluoride is increased the activity falls off. This is similar to the trend observed with the original $ZnCl_2$ study.[5]

DRIFT and MAS-NMR spectra were obtained for characterization. The DRIFT spectra in Figure 13 shows two different loadings of NaF compared to the optimum $ZnCl_2$ spectrum. There is the silanol stretch at 3500 cm^{-1}, the Si-O stretch at 1050 cm^{-1}, and the Si-O deformation at 450 cm^{-1}. The Al-O-Si deformation is not very strong here. Any other interpretation is difficult due to the broadness of the peaks. The ^{29}Si MAS-NMR spectra (Figure 14) shows only a range Q^n silanol and $Si(OAl)_n(OSi)_{4-n}$ sites as the spectra are broad and unresolved. The ^{27}Al MAS-NMR spectra (Figure 15) show the three different aluminum species; octahedral $[Al(H_2O)_6]^{+3}$ at 0 ppm, $Al^{"V"}$ at 30 ppm and tetrahedral AlO_4^- at 55 ppm. As the fluoride increases the $Al^{"V"}$ intensity decreases and the tetrahedral aluminum species increases. The maxima for the ^{29}Si spectra decrease as the NaF is introduced. The fluorination process causes replacement of Si by Al in the SiO_2 framework. The F^- may attack the silica layer and forms SiF_6^{2-} which decomposes to SiF_4 and F^- at elevated temperatures. As the Si atoms are removed Al atoms replace them in the tetrahedral layer.[5] The maximum number of Si atoms that may be replaced is 50% due to Löwenstein's Rule.[4] Also, there is a small shift to lower field in the ^{29}Si

spectra from -98 ppm to -96 ppm as the amount of fluoride is increased. Evidence for this is also seen the ^{27}Al spectra with the increased intensity of the tetrahedral species in the aluminum spectrum. As with potassium fluoride, the activity of the catalyst decreases as the amount of fluoride introduced is increased showing that the presence of the $Al^{"V"}$ is important for enhanced Friedel-Crafts activity. This phenomenon is observed with the other two metal fluorides (KF, NH_4F) studied. There was no detected signal in the ^{19}F NMR experiment, presumably due to the small amounts of fluoride used.

3.1.3 Ammonium Fluoride

The synthesis procedure is the same as with KF and NaF. The activity of this catalyst was the best but still did not exceed the optimum loading of $ZnCl_2$ on synthetic aluminosilicate.[5] Table 5 shows the activities for this system.

Table 5: Activity of catalysts with $ZnCl_2$ + NH_4F (0.75 g used in test reaction)

AMT. $ZnCl_2$ (g)	AMT. NH_4F (g)	% CONVERSION
1.0	0	98
1.0	0.03	95
1.0	0.06	93
1.0	0.09	87
1.0	0.12	90

Characterization by DRIFT and MAS-NMR was also done for this system. DRIFT spectra (Figure 16) shows a high and low loading of the fluoride compared to the optimum $ZnCl_2$. The peaks that are present are the silanol at 3500 cm^{-1}, Si-O stretch at 1050 cm^{-1}, Al-O-Si deformation at 600 cm^{-1}, and the Si-O deformation at 455 cm^{-1}. There is also a sharp peak at 1400 cm^{-1} that is only in the fluoride samples. This peak increases

in intensity from the low to high loading due to either an Al-F stretch or due to the diffusion of the NH_4^+ cation into the aluminosilicate lattice.[15,45] It seems most likely that this band is from the exchangeable ammonium cation as this band is not observed in the other metal fluoride DRIFT spectra. Other metal cations can be incorporated into the aluminosilicate lattice but this occurs at higher temperatures than was used here.[12] The maximum temperature that these catalysts were subjected to was 225°C. The Si-O stretch broadens with increasing fluoride concentration but does not shift to a higher field. As with the other catalysts, the ^{29}Si MAS-NMR spectra (Figure 17) show only the broad range of Q^n silanol and $Si(OAl)_n(OSi)_{4-n}$ peaks at about -95 ppm. The ^{27}Al spectra (Figure 18) show the three different Al environments with the octahedral chemical shift of 0 ppm, the $Al^{"V"}$ shift at 30 ppm and the tetrahedral shift at 55 ppm. Again, there is a reduction in the intensity of the $Al^{"V"}$ signal as the amount of fluoride present increases but it is not as pronounced as the others and only a slight increase in the tetrahedral intensity as the fluoride increases. This supported catalyst gave the best activity of the three and may be attributed to the relatively high intensity of the $Al^{"V"}$ peak.

In summary, it is evident from the NMR spectra that as the fluoride is introduced to the system the so-called penta-coordinate aluminum decreases with a corresponding increase in the tetrahedral aluminum species. This may account for the reduction in activity that accompanies the increase in fluoride. The presence of the distorted tetrahedral aluminum or $Al^{"V"}$ has been linked to enhanced activity.[35] The ^{29}Si spectra show broad and unresolved peaks but in the case with NaF and KF modified supported catalysts there is a shift of the centre of the band to a higher field which can be attributed to the increase in the tetrahedral aluminum present in the framework. The ammonium

fluoride modified catalysts do not show this shift and showed the highest activity of the modified catalysts, as shown below. The diffusion of the ammonium cation into the aluminosilicate lattice may play a role in these observed differences between the catalysts described above.

An experiment was carried out where the best combination of the three different salts was made along with the optimum catalyst for $ZnCl_2$ alone and tested. These results are given in Table 6.

Table 6: Activity of catalysts with $ZnCl_2$ + MF (0.50 g used in test reaction)

AMT. $ZnCl_2$ (g)	AMT. MF (g)	% CONVERSION
1.0	0	85
1.0	0.05 KF	64
1.0	0.10 NaF	74
1.0	0.02 NH_4F	83
1.5	0	86

The catalyst made with the NH_4F and $ZnCl_2$ resulted in activity comparable to that of $ZnCl_2$ alone. On the whole, the activity of the $ZnCl_2$ catalyst was greater than the fluorides so in that sense this investigation was not successful but with the spectra a better idea of what is happening in these systems was ascertained. From these results it would seem that the presence of the $Al^{"V"}$ in these aluminosilicates does possibly work to enhance the activity.

3.1.4 Zinc Fluoride

A study to determine if ZnF_2 loaded on an aluminosilicate framework resulted in an active Friedel-Crafts catalyst was done. Zinc fluoride is almost insoluble in almost any solvent and thus a difficult salt to work with. It is slightly soluble in water so that was the

solvent used. The ZnF_2 was impregnated into the support in an aqueous solution containing calculated amounts of ZnF_2. The solvent was removed by rotary evaporation. There were two different types of supports used; one aluminosilicate (designated blank) with no additive and the other with 2,4-pentanedione (designated H-acac) as the additive on the aluminosilicate. The table below shows the results of the ^{19}F MAS-NMR experiments as well as the activity of the supports.

Table 7: ZnF_2 catalysts NMR shifts and % conversion (0.5 g catalyst)

LOADING/TYPE OF SUPPORT	^{19}F CHEMICAL SHIFTS (ppm)	% CONVERSION
1 mmol/g - blank	-155, -125	0
1 mmol/g - H-acac	-155, -120	3
3 mmol/g - blank	-155, -120	19
3 mmol/g - H-acac	-155, -125	52
4 mmol/g - blank	-155, -120	36
4 mmol/g - H-acac	N/A - not enough sample	60
5 mmol/g - blank	-155, -120	9
5 mmol/g - H-acac	-155, -115	2

The supports made with the additive gave better conversions, probably due to better coverage and the porosity of the support. However, the overall activity was not very good so the study was discontinued. The ^{19}F MAS-NMR (Figure 19a and Figure 19b) shows the presence of AlF_6^{3-} at -155 ppm and possibly the presence of SiF_6^{2-} at -120 ppm. The -120 ppm peak may simply be a spinning side band of the -155 ppm peak. Spectra obtained at different spin rates of 10,000 and 15,000 Hz were acquired to determine isotropic chemical shifts are shown in Figure 20. The peak at -120 ppm was partly a spinning side band but the spectrum on the sample spun at 15 kHz shows a small peak remaining. In both spectra there is a shoulder on the -155 ppm peak at approximately -

175 ppm due to the presence of F^- as the intensity of this peak increases with increasing loadings.[37]

TEXT CONTINUES ON PAGE 73

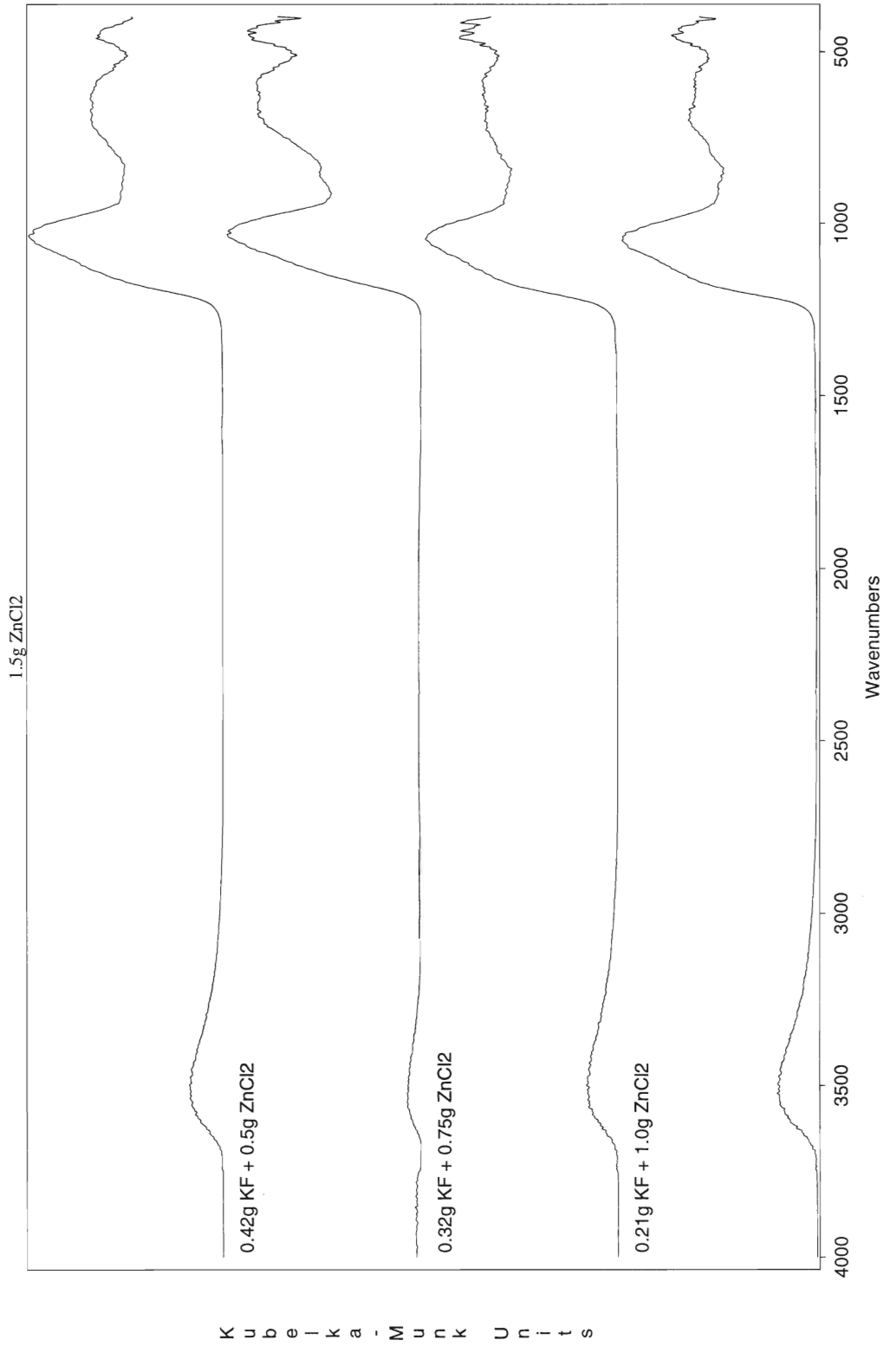

Figure 9: DRIFT spectra of aluminosilicate supports with $ZnCl_2$ and KF.

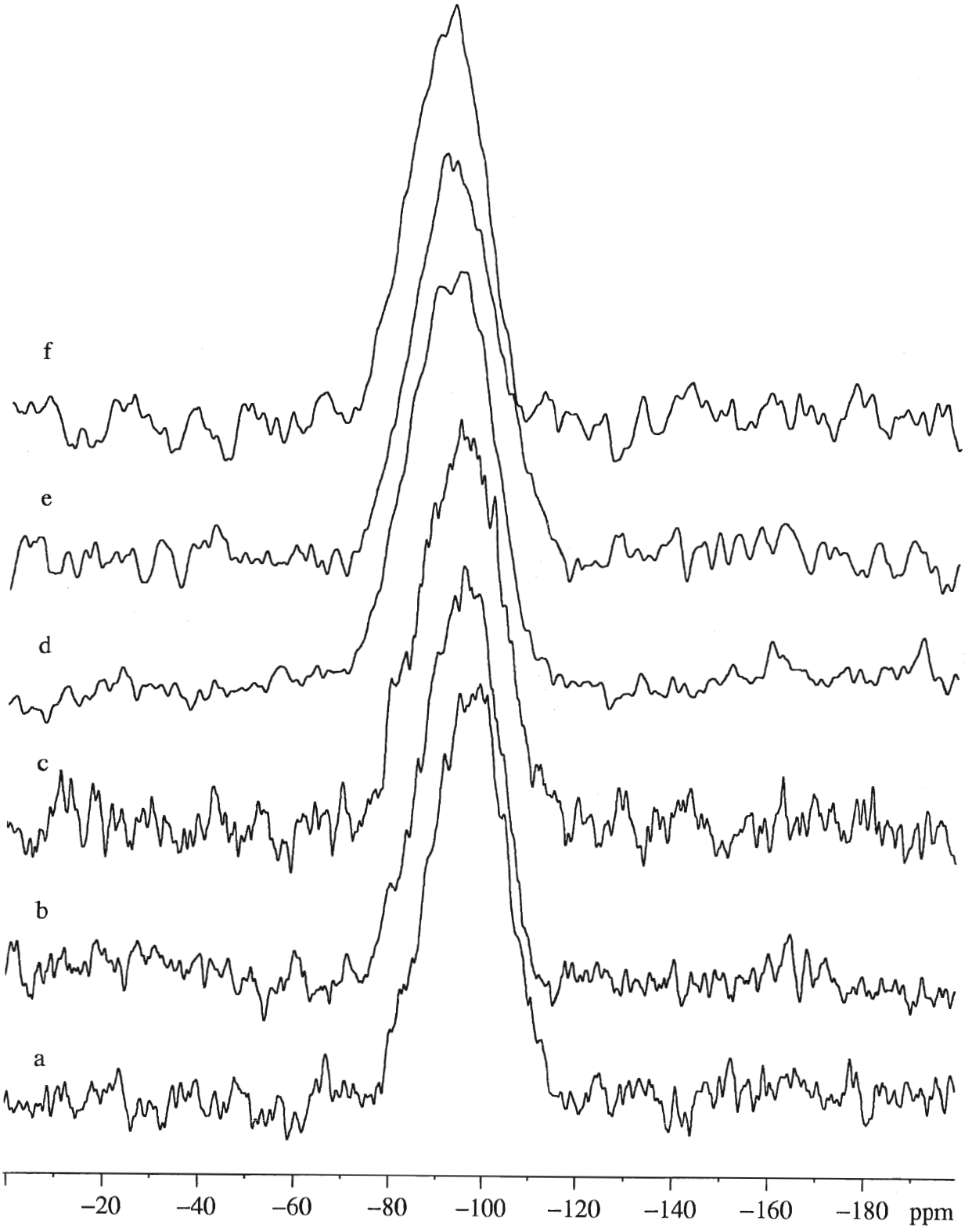

Figure 10: ^{29}Si MAS-NMR spectra for aluminosilicate catalysts with KF.

a: 1.5g $ZnCl_2$, b: 0.04g KF + 1.5g $ZnCl_2$, c: 0.15g KF + 1.5g $ZnCl_2$,
d: 0.21g KF + 1.0g $ZnCl_2$, e:0.32g KF + 0.75g $ZnCl_2$,
f: 0.42g KF + 0.5g $ZnCl_2$.

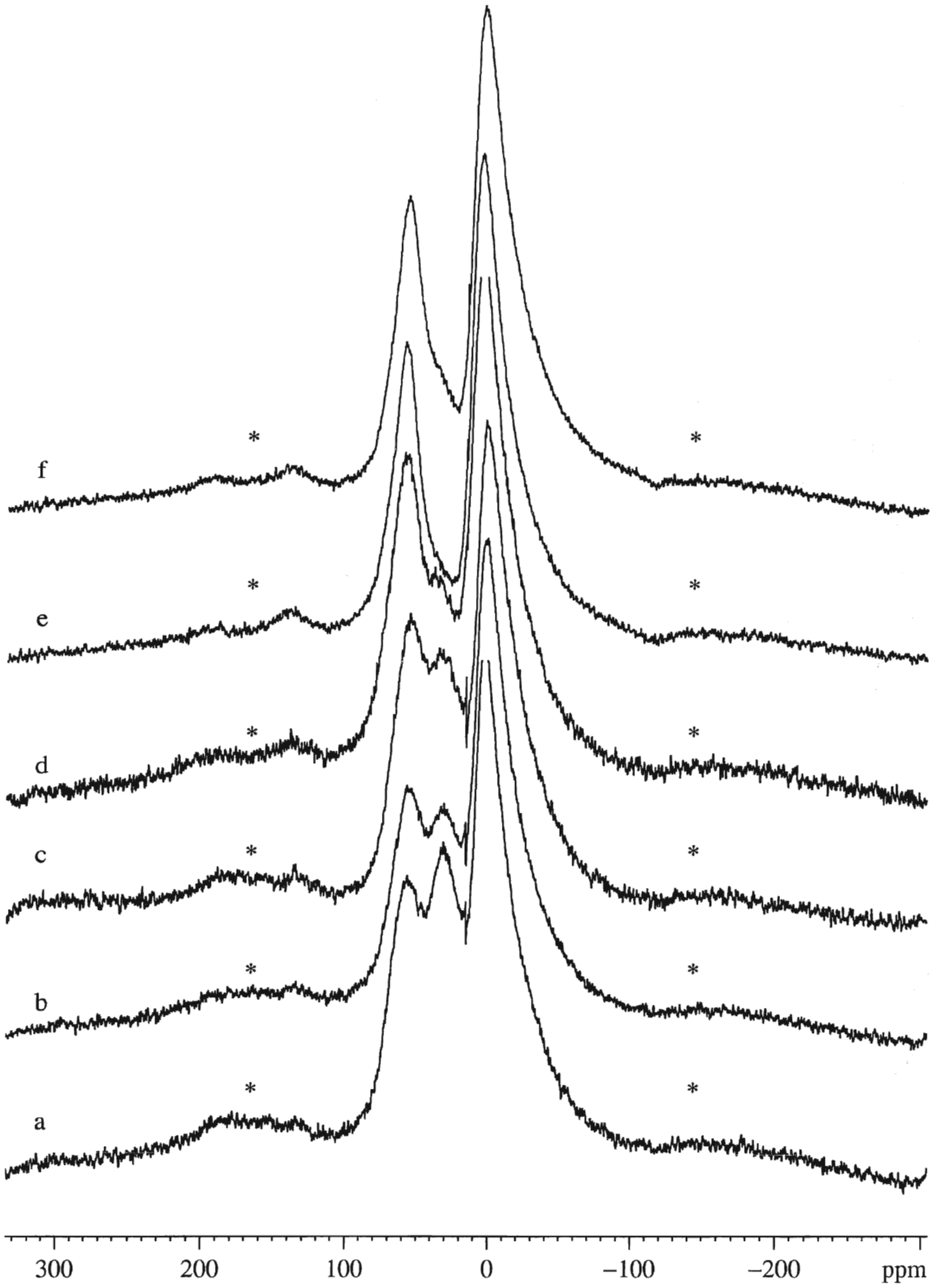

Figure 11: ^{27}Al MAS-NMR spectra for aluminosilicate catalysts with KF.

a: 1.5g $ZnCl_2$, b: 0.04g KF + 1.5g $ZnCl_2$, c: 0.15g KF + 1.5g $ZnCl_2$,
d: 0.21g KF + 1.0g $ZnCl_2$, e:0.32g KF + 0.75g $ZnCl_2$,
f: 0.42g KF + 0.5g $ZnCl_2$.

*-Spinning Side Bands

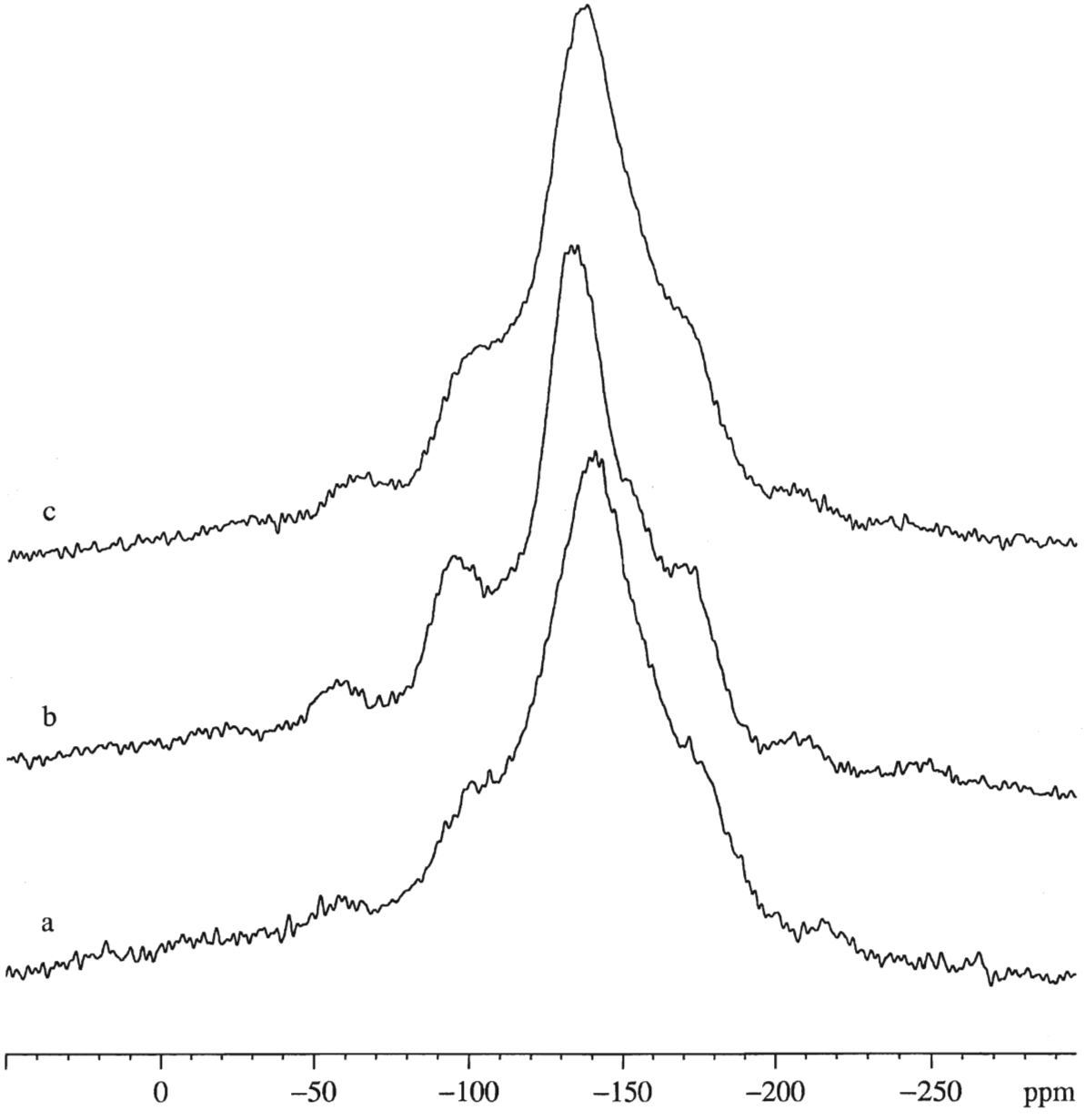

Figure 12: ^{19}F MAS-NMR spectra for aluminosilicate catalysts with KF.
a: 0.21g KF + 1.0g $ZnCl_2$, b:0.32g KF + 0.75g $ZnCl_2$,
c: 0.42g KF + 0.5g $ZnCl_2$.

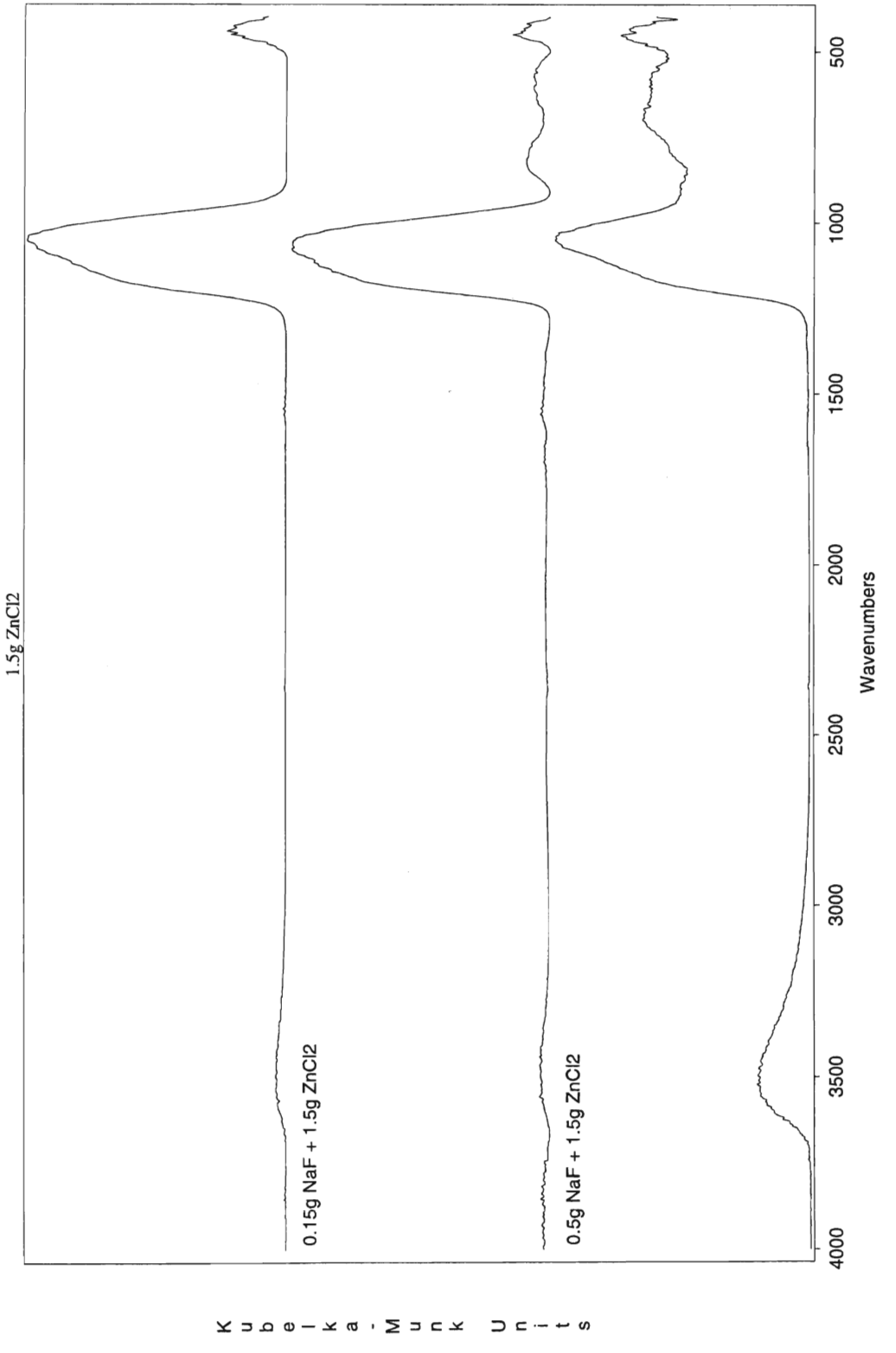

Figure 13: DRIFT spectra for aluminosilicate supports with $ZnCl_2$ and NaF.

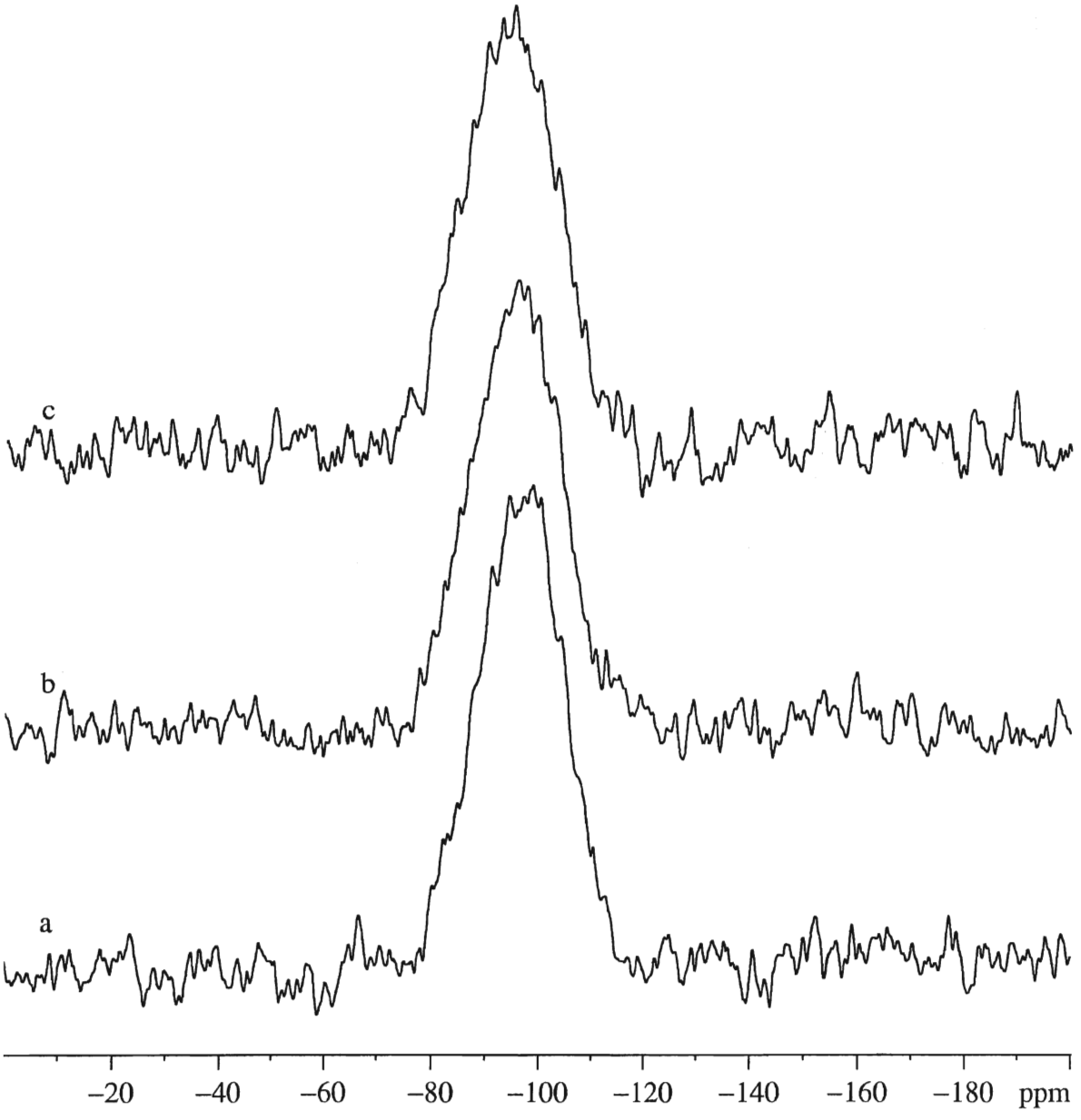

Figure 14:[29]Si MAS-NMR spectra for aluminosilicate catalysts with NaF.
a: 1.5g $ZnCl_2$, b:0.04g NaF + 1.5g $ZnCl_2$,
c: 0.15g NaF + 1.5g $ZnCl_2$.

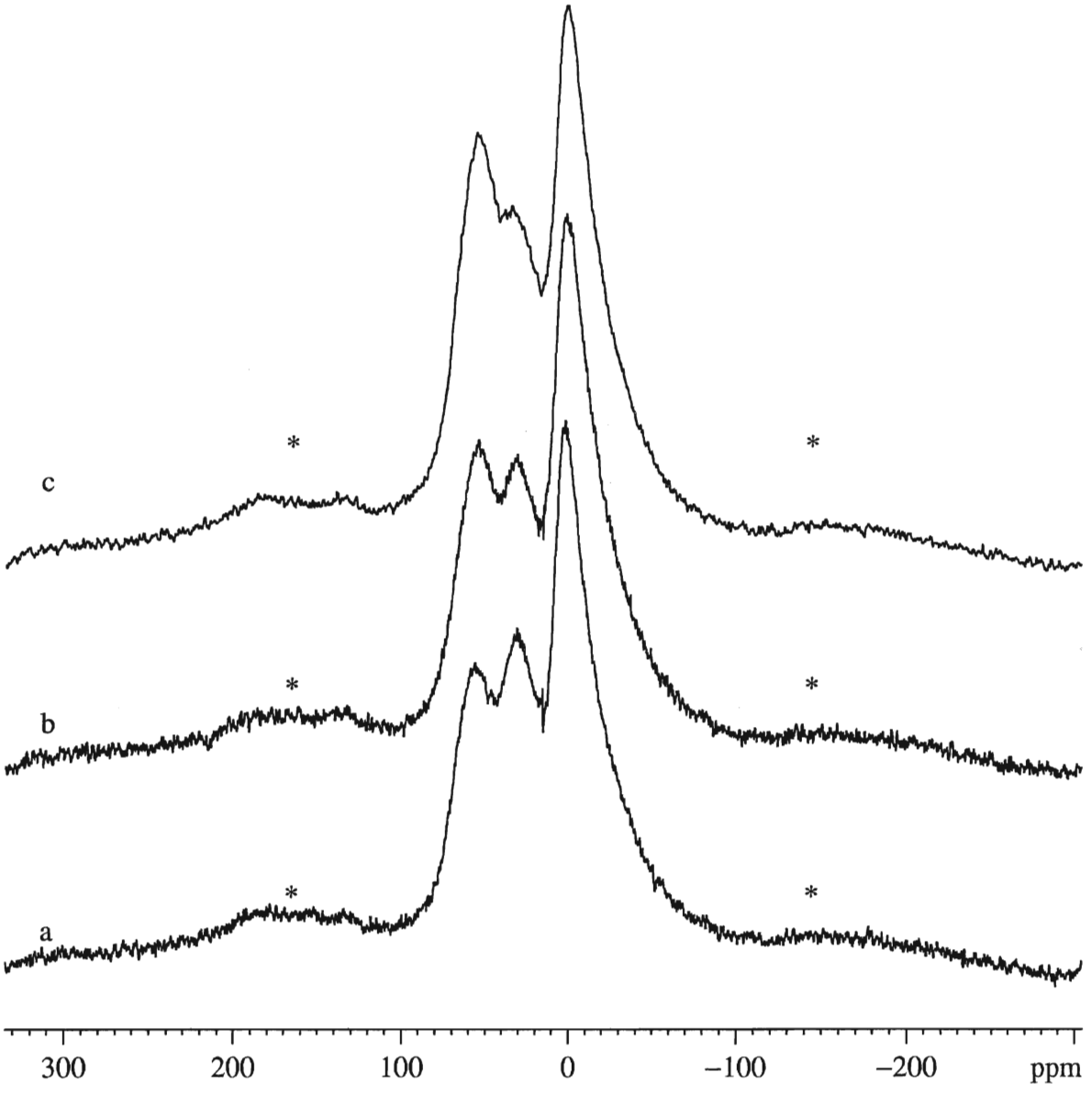

Figure 15:^{27}Al MAS-NMR spectra for aluminosilicate catalysts with NaF.
a: 1.5g $ZnCl_2$, b:0.04g NaF + 1.5g $ZnCl_2$,
c: 0.15g NaF + 1.5g $ZnCl_2$.
*-Spinning Side Bands

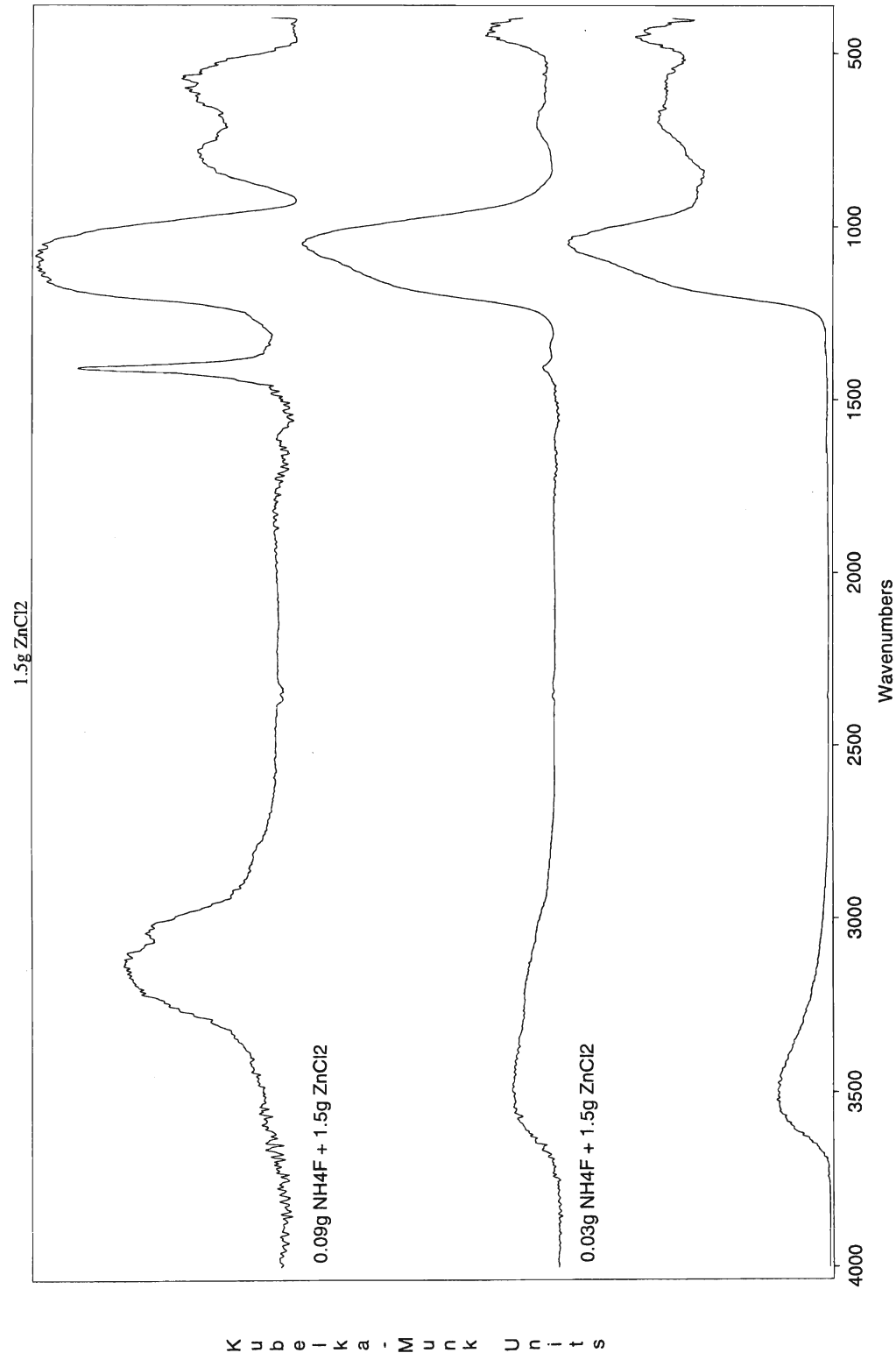

Figure 16: DRIFT spectra for aluminosilicate supports made with $ZnCl_2$ and NH_4F.

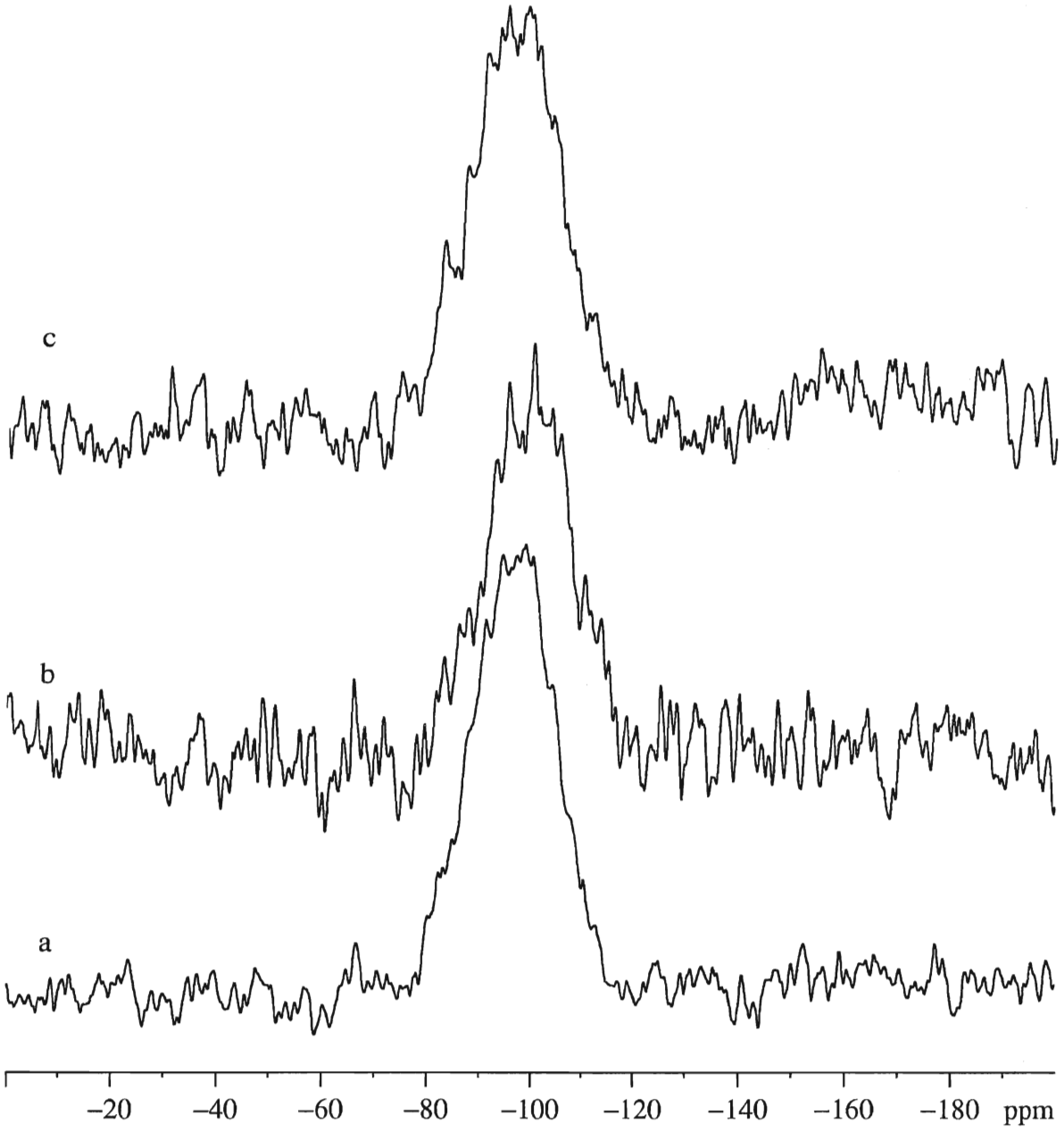

Figure 17:^{29}Si MAS-NMR spectra for aluminosilicate catalysts with NH_4F.
a: 1.5g $ZnCl_2$, b:0.03g NH_4F + 1.5g $ZnCl_2$,
c: 0.09g NH_4F + 1.5g $ZnCl_2$.

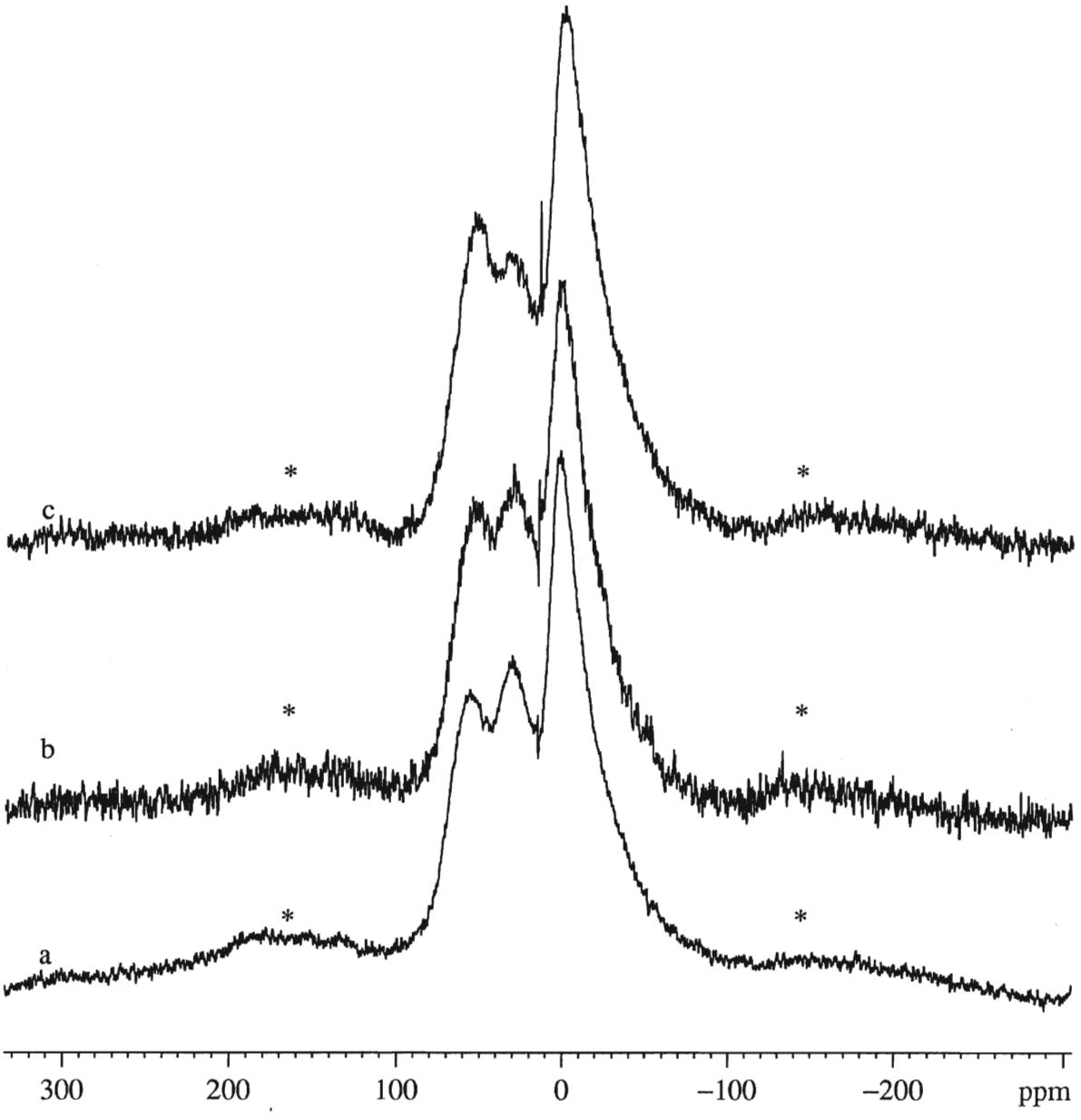

Figure 18:^{27}Al MAS-NMR spectra for aluminosilicate catalysts with NH_4F.
a: 1.5g $ZnCl_2$, b:0.04g NH_4F + 1.5g $ZnCl_2$,
c: 0.09g NH_4F + 1.5g $ZnCl_2$.
*-Spinning Side Bands

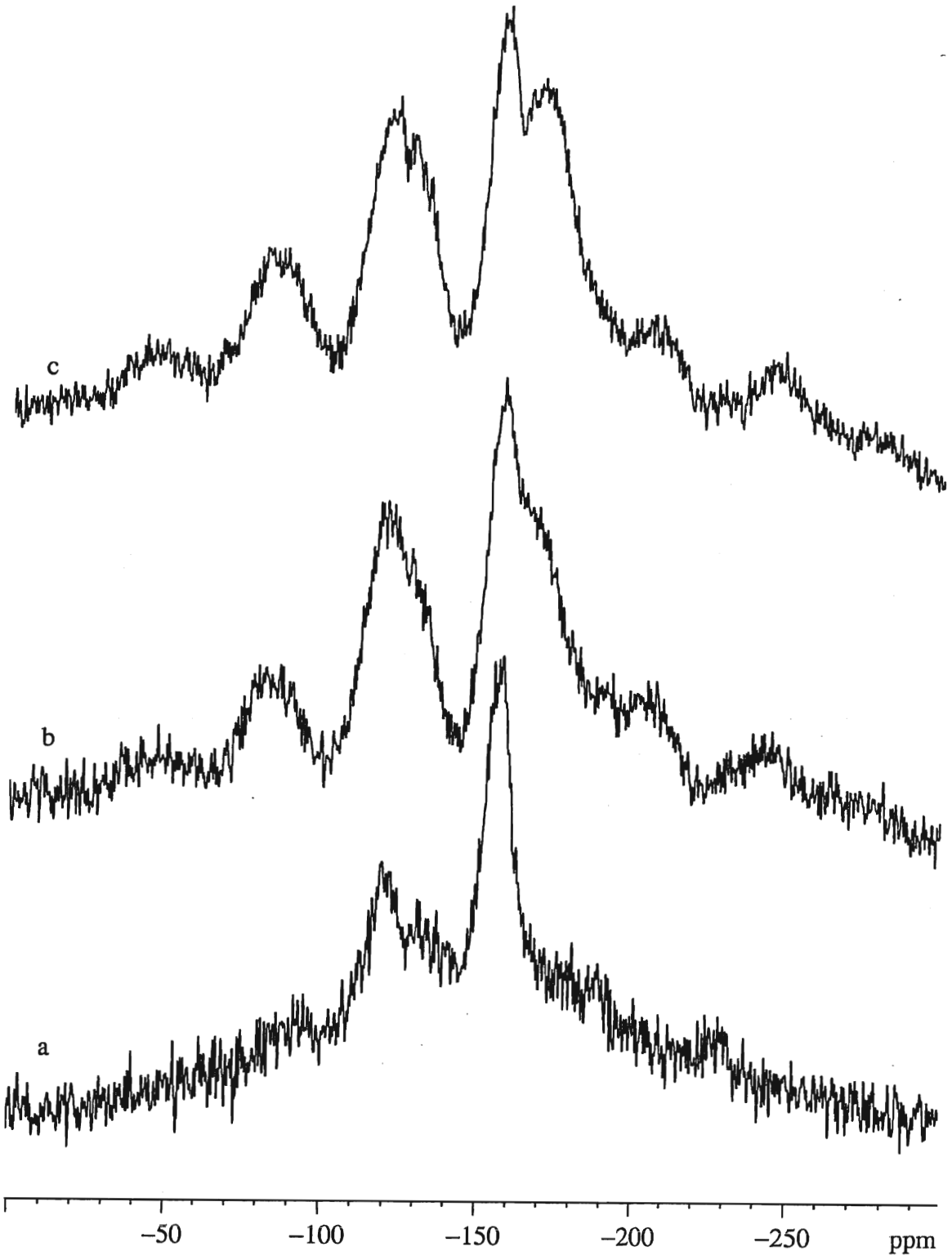

Figure 19a: ^{19}F MAS-NMR spectra for aluminosilicate with ZnF_2 loaded.
a - 1 mmol/g, b - 3 mmol/g, c - 5 mmol/g.

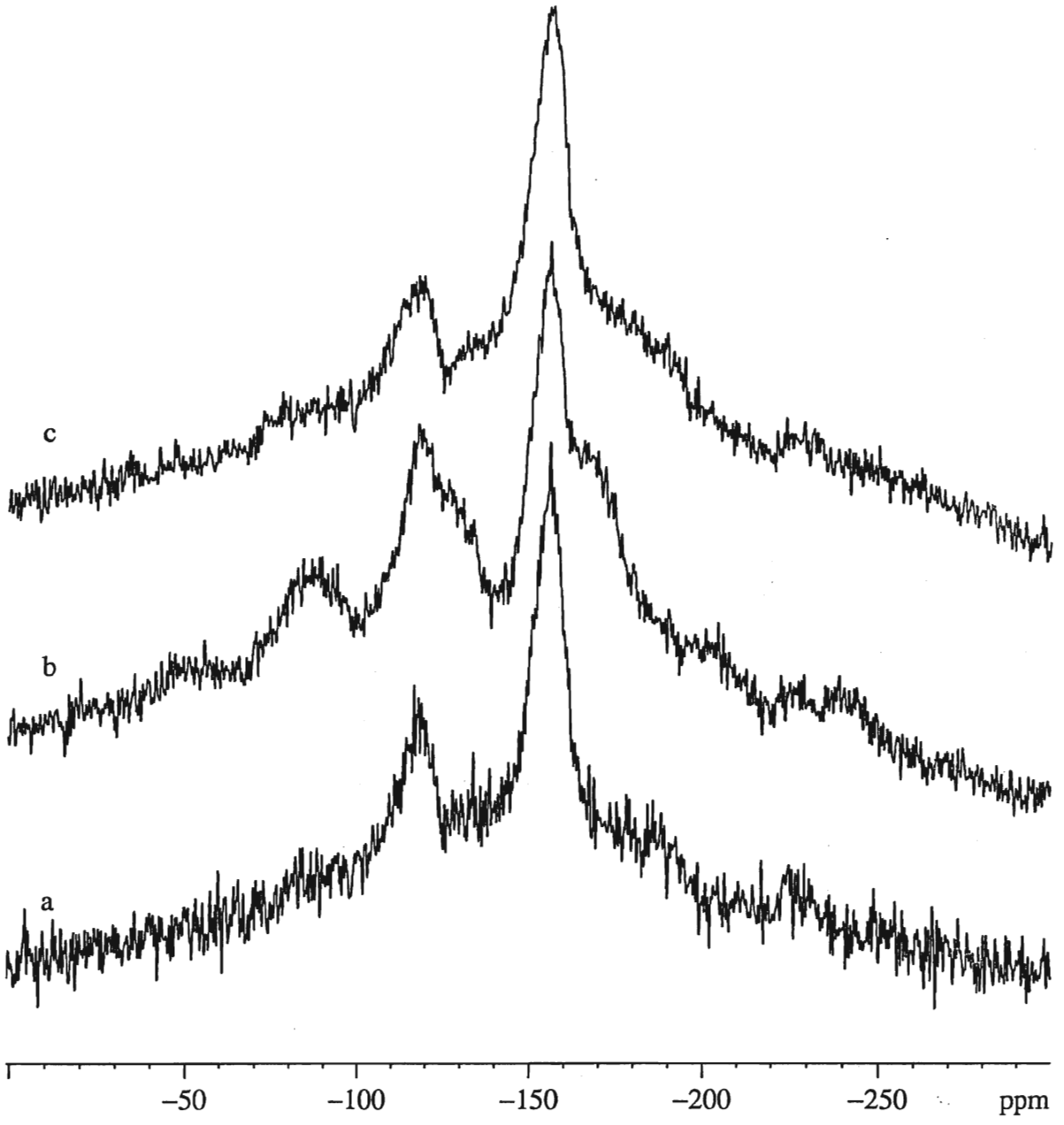

Figure 19b: ^{19}F MAS-NMR spectra for H-acac modified aluminosilicate support loaded with ZnF_2.
a - 1 mmol/g, b - 3 mmol/g, c - 5 mmol/g.

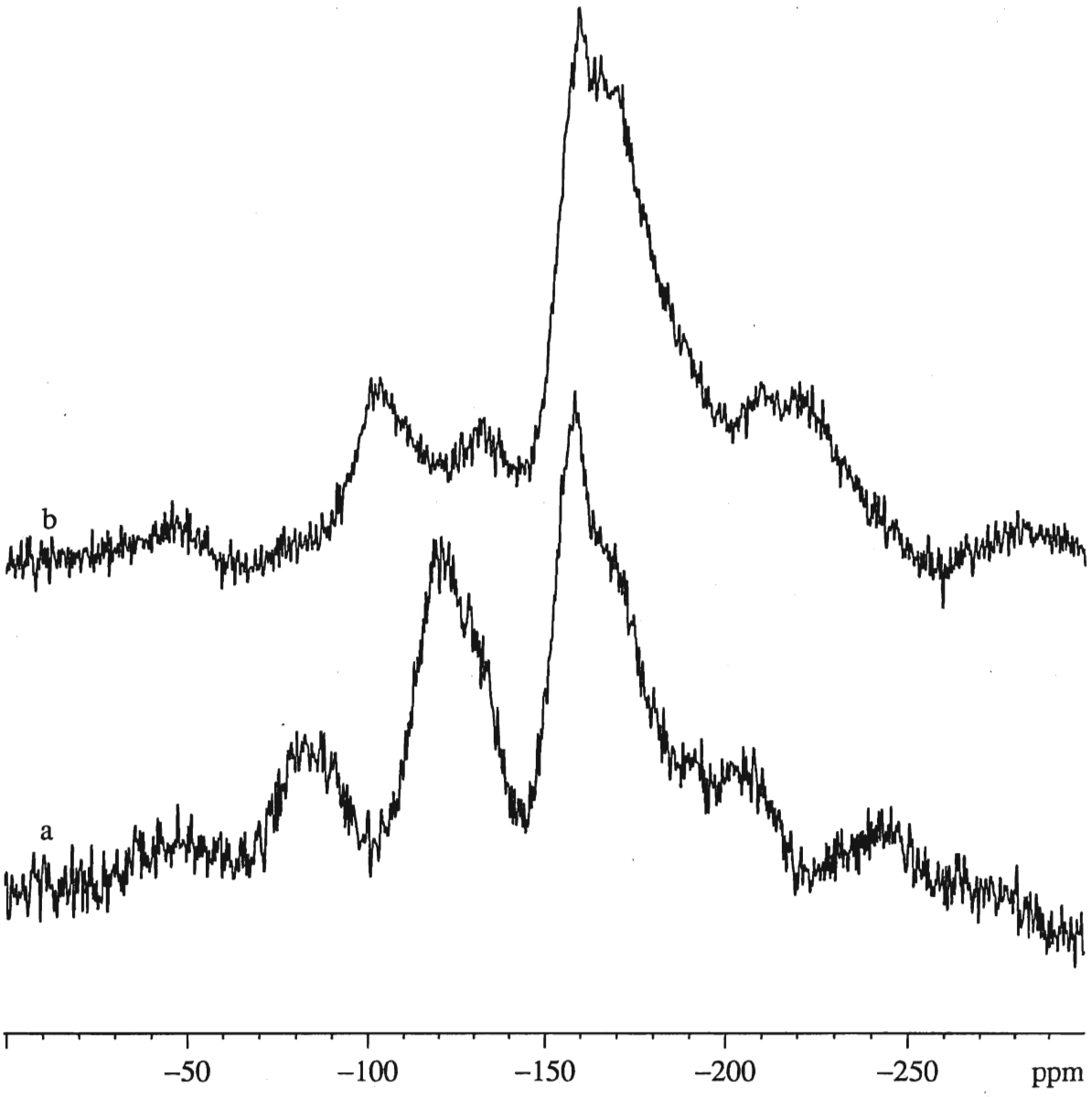

Figure 20: ^{19}F MAS-NMR for 3 mmol/g ZnF_2 on unmodified aluminosilicate support at various spinning speeds.
a - 10,000 Hz, b - 15,000 Hz.

3.2 Alumina Work

As discussed in Chapter 1, it is possible to control the pore size distribution of a support with the use of a chemical additive in the synthesis. In this work alumina was the support investigated and there were four different additives used. They were 2,4-pentanedione (H-acac), acetophenone, dibenzoylmethane, and benzophenone. This section describes the results of the synthesis of alumina using these additives, the nitrogen adsorption data, DRIFT, ^{27}Al MAS-NMR, and activity studies.

3.2.1 Synthesis Strategy

To synthesize the support the basic procedure is described in Chapter 2. This procedure was a modification of the one used for the aluminosilicates. The TEOS was eliminated from the procedure and the amount of solvent reduced to half. This seemed to be the best place to start. The variables chosen to alter were the amount of water for gelation and the amount of additive used. The first additive used was the 2,4-pentanedione as this had been a good additive for the aluminosilicate system giving large pores and high surface area. The β-diketones had proven to be effective in the aluminosilicate system so I decided to try them for the alumina system in addition to the other additives used.[26] The actual amounts tried are given in tables later in the section on nitrogen adsorption data.

3.2.2 ^{27}Al MAS-NMR & DRIFT Spectra

3.2.2.1 ^{27}Al MAS-NMR Spectra

3.2.2.1a Supports made with 2,4-pentanedione

Figure 21 shows the ^{27}Al MAS-NMR spectra with a constant amount of additive (0.25 ml - 2.4 mmol) and the amounts of water varied from 2-10 ml. The peak at 5 ppm is due to the non-framework octahedral species $Al[H_2O]_6^{+3}$ and the peak at 65 ppm is due to the tetrahedral aluminum species. This peak is situated 10 ppm more than the $Al^{"IV"}$ in the aluminosilicate system, most likely due to the absence of silicon in this system. In the alumina supports here there is very little of the $Al^{"V"}$ species, the peak seen at 30 ppm in the aluminosilicates. This only appears in the supports with small amounts of water used in the gelation. The octahedral and tetrahedral peaks in the spectra are as broad as the spectra with the $Al^{"V"}$ species present. The amount of additive used in the synthesis appears to have no effect on the so-called penta-coordinate species. Although it is not known for sure that this is actually Al^{V} or distorted tetrahedra it is a framework species.[36] Figure 22 shows spectra with a constant amount of water for gelation (10 ml) and variations in the amount of additive used (2.4, 4.8, 7.2, 9.6 mmol). The positions and intensities of the four and six coordinate aluminum species are the same as in Figure 21. There is so little of the $Al^{"V"}$ present and as it disappears with increasing amounts of gelation water it is difficult to see any change in the four or six coordinate peaks.

3.2.2.1b Supports made with acetophenone

Figures 23 and 24 show the spectra for a varied amount of water (2-10 ml in 2 ml increments) with the additive constant. Figure 23 shows the spectra for a constant amount

of acetophenone (2.1 mmol) and varied amounts of water. Figure 24 shows the spectra for a constant amount of acetophenone (4.2 mmol) and varied amounts of water. Both sets of spectra show the disappearance of the small penta-coordinate (30 ppm) as the amount of water used in gelation is increased. The six-coordinate aluminum species in this case is at 0 ppm and the tetrahedral species is at 69 ppm. The intensity of the four- and six-coordinate peaks are all the same for all spectra given here. Figures 25-26 show two sets of spectra with the amount of water used in gelation held constant (25-2 ml and 26-4 ml) respectively while the amount of additive is varied. As with the 2,4-pentanedione the amount of additive has no effect on the formation of the $Al^{"V"}$ species.

3.2.2.1c Supports made with dibenzoylmethane

Figures 27 and 28 show the spectra for the supports made with varying amounts of water (2-10 ml in 2 ml increments) with the amount of dibenzoylmethane held constant. Figure 27 is for the supports with 1.1 mmol of dibenzoylmethane and Figure 28 is for supports made with 2.2 mmol of the additive. As the amount of water is increased the "Al^{V}" peak at 30 ppm disappears. The six coordinate $[Al(H_2O)_6]^{+3}$ species is centered at 0 ppm and the tetrahedral aluminum species is at 67 ppm. Figures 29 and 30 show the spectra for a varied amount of additive with the amount of water used in gelation held constant. Figure 29 shows the spectra for 2 ml of water and 1.1, 2.2, 3.3, and 4.4 mmol of additive and Figure 30 shows the same variation in additive for 4 ml of water. As the amount of additive in Figure 29 is increased, the presence of the $Al^{"V"}$ species is decreased. In Figure 30 there is no $Al^{"V"}$ present. The intensities of the four- and six-coordinate species are all the same in all spectra.

3.2.2.1d Supports made with benzophenone

Figures 31 and 32 show the spectra for supports made with the amount of additive held constant and variation in the amount of water used in gelation. Figure 31 is for supports made with 1.4 mmol additive and Figure 32 is for supports made with 2.8 mmol additive, in this case benzophenone. Figures 33-34 show spectra for supports made with varying amounts of benzophenone (1.4, 2.8, 4.2, and 5.6 mmol) with a constant amount of water (33-2 ml and 34-4 ml). The peaks in both sets of spectra are the same. There is the six-coordinate $[Al(H_2O)_6]^{+3}$ species at 0 ppm and the four-coordinate aluminum at 62 ppm. There is a very small $Al^{"V"}$ peak for the spectra with the small amounts of water used for gelation at 30 ppm. As with all of the different additives used the intensities of the four- and six-coordinate peaks are the same in all spectra.

For all of the different additives, the reason the $Al^{"V"}$ disappears when larger amounts of water are used for gelation has to do with the amount of aluminum that gets hydrolyzed to $[Al(H_2O)_6]^{+3}$. A larger amount of water is required to hydrolyze aluminum to the octahedral form so when a smaller amount of water is used, more of the aluminum may become framework species. That is, less of the aluminum in the sol gets hydrolyzed by the water to $[Al(H_2O)_6]^{+3}$ so during aging there is the formation of a small amount of the $Al^{"V"}$.

3.2.2.2 DRIFT Spectra

3.2.2.2a Supports made with 2,4-pentanedione

Figure 35 is for the supports made with the amount of additive held constant and the water for gelation varied. In all of the spectra there is a broad band at 650 cm^{-1}

corresponding to the stretching vibration of the octahedral aluminum species At 840 cm^{-1} there is a sharper peak for the stretching vibrations of the framework tetrahedral aluminum species. As the amount of water is increased there is an increase in a broad band centered about 1100 cm^{-1} corresponding to the Al^{VI}-O surface stretching modes. Figure 36 shows the spectra when the amount of water is held constant. There is the broad band at 650 cm^{-1} for the octahedral aluminum stretches and a band at 840 cm^{-1} for the tetrahedral aluminum stretches. There is also a broad band at 3500 cm^{-1} which is the AlO-H stretch. The appearance of the band at 1100 cm^{-1} as the amount of water is increased may be related to the decrease in the "penta-coordinate" species in the NMR spectra. As more water is used for gelation, more of the aluminum in the sol is hydrolyzed to octahedral species.

A spectrum was obtained for the support dried at room temperature, i.e. before calcining, to see if the nature of the complex between the additive and the aluminum could be discerned. This spectrum was compared to that of 2,4-pentanedione, both spectra are given in Figure 37. The spectrum shows a broad peak centered at 1630 cm^{-1} corresponding to the carbonyl stretch. This peak is split into two when added to the alumina which shows that the additive does not act strictly as a template. It seems that complexation of only one of the carbonyls in 2,4-pentanedione to the alumina occurs. In the aluminosilicate system, thermal desorption-mass spectrometry studies confirmed that the complex formed with aluminum and 2,4-pentanedione is $Al(acac)_3$, however, it is uncertain as to the nature of the complex formed here. The structure on the next page shows how the complex between H-acac and the aluminum in aluminosilicate may form and that it would be octahedral in shape.

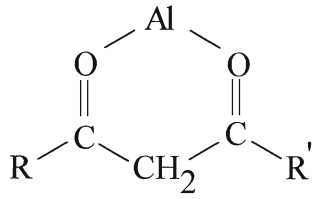

The structure involves a very stable six-membered ring.

3.2.2.2b Supports made with acetophenone

Figures 38 and 39 show the spectra for the supports made with the additive held constant and the water held constant, respectively. In Figure 38 there is the broad band at 590 cm^{-1} due to the octahedral stretch, although this band is not as broad as the one for the support made with 2,4-pentanedione. There is also the tetrahedral stretch at 800 cm^{-1} shifted slightly as compared to supports made with H-acac. The octahedral surface stretching is present at 1100 cm^{-1} along with some other peaks, presumably due to some residual organic left after calcination at 500°C. The band at 1100 cm^{-1} is present in the supports that give the best activity when loaded with $ZnCl_2$. This indicates the possibility of a strong interaction between the additive and the support. It should be noted that these spectra are from supports with very little acetophenone (2.1 mmol). The spectra with the amount of water held constant (Figure 39) show the same octahedral stretch at 600 cm^{-1} and tetrahedral stretches at 800 cm^{-1} although with higher amounts of additive this peak is broadened. The surface stretch at 1100 cm^{-1} disappears with higher amounts of additive and the residual organic peaks are gone as well.

Figure 40 is the spectrum of acetophenone compared to the support made and dried at room temperature. The carbonyl stretch for the acetophenone is at 1688 cm^{-1} while the carbonyl for the support is at 1642 cm^{-1}. There are two peaks on the spectrum of

acetophenone that are approximately 100 cm^{-1} (1600 and 1450 cm^{-1}) apart corresponding to the skeletal stretch of the aromatic ring. On the spectrum for the support these peaks are present but shifted to 1500 and 1410 cm^{-1}. This shows that in this case there is a complex formed and the carbonyl and the aromatic ring are involved. The structure shown in the previous section is most likely how the complex is formed. In this case it seems that the aromatic ring takes the place of one of the carbonyl groups. It is possible that the complex formed here is between the carbonyl and the plane of the aromatic ring where the delocalized electron cloud is although more work is needed to determine this for sure.

3.2.2.2c Supports made from dibenzoylmethane

Figures 41 and 42 show the spectra for the supports with the amount of additive held constant and the amount of water held constant, respectively. Figure 41 shows only the broad bands at 575 and 750 cm^{-1} corresponding to the octahedral and tetrahedral stretches respectively. The same peaks are in the spectra in Figure 42 as well. In both sets there is also the presence of the Al-OH stretch at 3500 cm^{-1}. This support shows the most hydroxyl stretch intensity in any of the spectra and may be related to the reason this additive did not make very good supports for the test reaction.

Figure 43 is the comparison between dibenzoylmethane and the support dried at room temperature with the additive still present. Unfortunately, the spectrum is not very good for the pure dibenzoylmethane and is difficult to interpret. There is a carbonyl peak at 1580 cm^{-1} and does not appear to be shifted in the support spectrum. The aromatic skeletal stretches are indistinguishable.

3.2.2.2d Supports made with benzophenone

Figure 44 shows the spectra for supports made with a constant amount of benzophenone, with water being varied. There are the two peaks that appear in all of the spectra, tetrahedral aluminum stretch (850 cm^{-1}) and the octahedral aluminum stretch (545 cm^{-1}). There is also a third band at 800 cm^{-1} possibly due to the deformation of the surface hydroxyls.[46] Figure 45 shows the spectra for the supports made with constant amount of water and the additive as the variable. There are the two basic tetrahedral and octahedral peaks at 825 cm^{-1} and 550 cm^{-1} respectively. There is the third peak at 800 cm^{-1} but only for the smaller amounts of the additive. There is the octahedral surface stretch at 1100 cm^{-1} but only for an intermediate amount of benzophenone (2.8 mmol) in the synthesis of the support. The presence of this peak may be related to the effectiveness of the support as this particular support gave very good activity when loaded with $ZnCl_2$. The supports made with acetophenone that were also effective had this surface stretch at 1100 cm^{-1}. There was also a small amount of Al-OH stretches present but on the supports that were not particularly effective.

Figure 46 is the comparison between benzophenone and the support dried at room temperature with the additive present (i.e. had not been burned off yet). The carbonyl peaks for both spectra are at the same frequency (1659 cm^{-1}) but the aromatic skeletal stretches are not. For the benzophenone spectrum the two peaks are at 1450 and 1325 cm^{-1}. For the alumina support spectrum these peaks are at 1435 and 1300 cm^{-1}. In this case it seems that the complex formed involves both the aromatic rings and not the carbonyl group. As with the acetophenone supports this was an effective support when loaded with $ZnCl_2$ and tested but the supports modified with acetophenone did exhibit greater activity.

The interaction between aluminum and the aromatic rings may not be as strong as the interaction between aluminum and the oxygen of the carbonyl group.

3.2.3 Nitrogen Adsorption Data

The surface area, pore distribution and pore volume analysis proved to be the most useful in determining a possible effective Friedel-Crafts support. Many supports were synthesized and tested and of these the ones with specific results (discussed later) were scaled up, loaded with $ZnCl_2$ and tested. The following sections present the data for the four different types of additives used.

3.2.3.1 Supports made with 2,4-pentanedione

Table 8 below gives the BET surface area, total pore volume and where the approximate maximum is for the supports made with 2,4-pentanedione.

Table 8: Nitrogen adsorption data for supports made with 2,4-pentanedione

AMT. $H_2O\downarrow$ / AMT. ACAC$\rightarrow$	0.25 ml (2.4 mmol)	0.50 ml (4.8 mmol)	0.75 ml (7.2 mmol)	1.0 ml (9.6 mmol)
2.0 ml	353.82 $m^2/g^{\{}$ 0.84349 cc/g^{Π} ~5-6 nm^{O}	344.25 0.58411 ~5 nm	315.37 0.37197 ~4 nm	N/A
4.0 ml	344.71 0.94509 ~6 nm	318.91 0.66754 ~5-6 nm	356.41 0.52703 ~5 nm	N/A
6.0 ml	328.91 0.94121 ~6 nm	316.95 0.64810 ~5-6 nm	298.66 0.46315 ~5 nm	N/A
8.0 ml	320.93 0.84117 ~6-8 nm	305.94 0.66425 ~6 nm	346.94 0.33992 ~4 nm	N/A
10.0 ml	325.56 0.59122 ~6 nm	310.80 0.64175 ~6 nm	345.45 0.31838 ~4 nm	348.90 0.47985 ~5 nm

$^{\{}$-BET Surface Area (m^2/g), $^{\Pi}$-Total pore volume (cc/g), ^{O}-Average pore size (nm)

All of these supports give relatively high surface areas but there is a trend where the surface area decreases with increasing amounts of water and additive. There are a couple of anomalous entries but the trend is there. The average pore sizes for all the supports are roughly the same at 4-6 nm. The pore distribution is very narrow with small pores. Figure 47 shows the pore size distribution for all four of the additives studied. The total pore volume is the one variable that shows the most fluctuation. Figure 48 shows the isotherm for the support made with 2,4-pentanedione the shape of which give clues to supports that may exhibit high catalytic activity when loaded with $ZnCl_2$. This isotherm exhibits a type H4 hysteresis loop indicating mesoporous pores and that they are most likely cylindrical in shape. The pore volume is the factor that will indicate the most promising support for the test reaction used. This will become evident as the rest of the data is presented. For the supports made with 2,4-pentanedione the pore volume is relatively small as is the pore size. The supports loaded with $ZnCl_2$ exhibited little or no activity in the benzylation of benzene.

3.2.3.2 Supports made with acetophenone

Table 9 below gives all of the surface areas, total pore volumes and approximate maxima from the pore size distribution.

Table 9: Nitrogen adsorption data for supports made with acetophenone

AMT. $H_2O\downarrow$ / AMT. ACET.$\rightarrow$	0.25 ml (2.1 mmol)	0.50 ml (4.2 mmol)	0.75 ml (6.4 mmol)	1.0 ml (8.6 mmol)
2.0 ml	338.94 2.56727 ~22-23 nm	349.78 1.84594 ~15 nm	335.05 1.85631 ~15 nm	328.31 2.02384 ~25 nm
4.0 ml	303.83 2.26009 ~21 nm	343.63 2.29356 ~20-23 nm	354.14 2.71066 ~25-30 nm	351.08 5.59633 ~25 nm
6.0 ml	276.55 1.72081 ~20 nm	300.45 1.38123 ~15 nm	341.71 2.23779 ~ 20 nm	327.01 2.60698 ~23-26 nm
8.0 ml	261.54 1.12756 ~ 19 nm	340.81 1.90746 ~15 nm	338.13 1.79296 ~25 nm	327.01 2.31937 ~20 nm
10.0 ml	255.66 1.07285 ~17 nm	338.45 1.99895 ~15, 20 nm	317.73 1.27141 ~15 nm	272.14 0.73772 ~7 nm

The units for these entries are the same as for Table 8.

The supports made with acetophenone show the same trend in the surface areas as seen with the supports made with the 2,4-pentanedione. The surface areas decrease as the amount of water used for gelation increases but this is not the case with the series of increasing amount of additive. Again, the hysteresis loop is of the H4 type. The total pore volumes are much larger for these supports and as the data will show later these supports exhibit high catalytic activity when loaded with $ZnCl_2$. The pore size distributions have larger maxima but are broad (see Figure 47) and the isotherm has a much higher volume of gas adsorbed (Figure 49). As the data is presented a trend of high pore volume corresponds to high catalytic activity emerges.

3.2.3.3 Supports made with dibenzoylmethane

Table 10 gives the nitrogen adsorption data for the supports made with dibenzoylmethane. All of the units are the same as in Table 8.

Table 10: Nitrogen adsorption data for supports made with dibenzoylmethane

AMT. $H_2O\downarrow$ / AMT. DIBE$\rightarrow$	0.25 g (1.1 mmol)	0.50 g (2.2 mmol)	0.75 g (3.3 mmol)	1.0 g (4.4 mmol)
2.0 ml	391.93 0.49867 ~5 nm	341.80 0.43354 ~5 nm	326.96 0.42813 ~5 nm	280.50 0.54103 ~6 nm
4.0 ml	342.42 0.77564 ~10 nm	321.51 0.76129 ~10 nm	294.82 0.63795 ~11 nm	308.37 0.79413 ~10-12 nm
6.0 ml	329.05 1.19554 ~15 nm	301.42 1.12364 ~15 nm	306.60 1.07662 ~15 nm	300.25 1.00464 ~15 nm
8.0 ml	326.77 1.10426 ~15 nm	294.86 1.06613 ~15 nm	278.52 0.86093 ~15 nm	298.31 0.90514 ~15 nm
10.0 ml	302.42 0.83805 ~15 nm	262.39 0.70575 ~15 nm	267.90 0.80084 ~15 nm	271.67 0.73978 ~15 nm

The surface areas for the supports made with dibenzoylmethane decrease as the amount of water for gelation is increased and as the amount of additive is increased as well. Again, there are some anomalous values but the basic trend is there. The pore size distribution (Figure 47) give relatively large pores but the activity of the support when loaded with $ZnCl_2$ is not very good. The total pore volumes are small although they are larger than those for the supports made with 2,4-pentanedione. The isotherm (Figure 50) shows an H2 type hysteresis loop indicating the possibility of ink-bottle shaped pores. This means that the pore would become easily blocked by reagents and would contribute

to the low activity exhibited. These values indicate further that the pore volume is the critical factor in determining a promising support for Friedel-Crafts alkylation.

3.2.3.4 Supports made with benzophenone

Table 11 below shows the surface areas, total pore volumes and average maximum for the pore size distributions of the supports made with benzophenone. The units are the same as in Table 8 (H-acac data).

Table 11: Nitrogen adsorption data for supports made with benzophenone

AMT. $H_2O\downarrow$ / AMT. BENZ$\rightarrow$	0.25 g (1.4 mmol)	0.50 g (2.8 mmol)	0.75 g (4.2 mmol)	1.0 g (5.6 mmol)
2.0 ml	348.37 2.09283 ~20 nm	367.59 2.36151 ~20-25 nm	344.13 2.27369 ~20 nm	318.77 1.68921 ~20 nm
4.0 ml	338.16 2.08162 ~20 nm	309.29 1.88442 ~20 nm	320.77 1.81381 ~20 nm	290.32 1.36457 ~15 nm
6.0 ml	282.66 1.13908 ~15 nm	277.91 1.35874 ~15-20 nm	343.20 1.40967 ~15-20 nm	287.04 1.06177 ~15 nm
8.0 ml	303.26 0.92048 ~15 nm	303.26 0.92048 ~15 nm	261.70 1.00049 ~15 nm	303.12 1.21878 ~15 nm
10.0 ml	278.90 0.66269 ~13 nm	243.77 0.69361 ~15 nm	264.08 0.87150 ~15 nm	249.53 0.98007 ~15 nm

The surface area data indicate the trend that as the amount of water used in gelation is increased the surface area decreases but not as the amount of additive is increased. As before the surface area does not seem to be a crucial factor in determining a suitable support. The pore size distribution indicates maxima from about 15-20 nm but the distribution is broad (Figure 47). The total pore volumes are larger here and the

isotherm shows this (Figure 51) by the shape (H4 hysteresis) and amount of gas adsorbed. These supports show data similar to that of the supports made with acetophenone and exhibit similar activity when loaded with $ZnCl_2$.

3.2.4 Activity Study

After nitrogen adsorption data was collected the supports with the highest pore volumes were scaled up and loaded with various amounts of $ZnCl_2$ to assess the activity of the catalyst. The test reaction is the benzylation of benzene. The catalyst Clayzic was also made as a control sample for all of the reactions and also to compare the activity of the alumina supports to it. Clayzic is 1 mmol/g $ZnCl_2$ on K10 montmorillonite clay, where the $ZnCl_2$ is dissolved in methanol and the clay added. The methanol is removed by rotary evaporation and the catalyst dried at 280°C overnight. Table 12 below gives all of the supports that were scaled up and tested.

Table 12: Activity of alumina supports when loaded with $ZnCl_2$ as %conversion.

LOADING→ ADDITIVE/H_2O↓	1 mmol/g	3 mmol/g	5 mmol/g	7 mmol/g	CLAYZIC
2,4-pentanedione					
2.4 mmol/4 ml	19	24	15	7	16
2.4 mmol/6 ml	22	15	12	7	7
2.4 mmol/8 ml	20	11	10	5	4
4.8 mmol/10 ml	11	19	14	6	14
acetophenone					
2.1 mmol/2 ml	38	84	95	86	15
4.2 mmol/4 ml	26	95	91	87	20
6.3 mmol/4 ml	71	88	81	71	13
6.3 mmol/6 ml	37	47	41	33	13
8.4 mmol/4 ml	2	42	45	35	8
8.4 mmol/6 ml	11	20	29	21	8
8.4 mmol/8 ml	15	76	76	57	9
dibenzoylmethane					
1.1 mmol/6 ml	5	24	17	19	4
2.2 mmol/6 ml	7	24	17	18	4
benzophenone					
1.4 mmol/2 ml	21	82	93	98	8
2.8 mmol/2 ml	14	74	89	80	8
4.2 mmol/2 ml	29	83	86	79	28

From these results it is evident that the supports made from acetophenone and benzophenone give catalysts with the best activity. The activity is considerably better than that of Clayzic. The optimum loadings are between 3 and 5 mmol/g ($ZnCl_2$/support). The monolayer coverage of the $ZnCl_2$ is presumably where the maximum activity occurs. The activity decreases when the support is overloaded or underloaded.

3.2.5 Further General Discussion

The optimum amount of water for gelation of the sol seems to vary with the additive. Theoretically the optimum molar ratio of water to aluminum tri-*sec*-butoxide is 2:1.[5] Experimentally, it was found that the optimum ratios for activity for the two

additives that did not yield good supports was 5.5:1 for 2,4-pentanedione and 4:1 for dibenzoylmethane. The supports made with additives that yielded high activity had a ratio of water to aluminum closer to the theoretical value. The ratios for acetophenone and benzophenone were 3:1 and 1.5:1 respectively. With the aluminosilicate system the discrepancy in water:(Al+Si) was due to not all of the aluminum being incorporated into the framework, i.e. some aluminum is present as octahedral species since it takes more water to hydrolyze the octahedral aluminum. The FTIR spectra of the supports before calcination showed in three out of the four cases that the aluminum complexed to the additive *via* the aromatic ring and/or the carbonyl group. This means that the amount of aluminum available for hydrolysis would be reduced, thus accounting for the smaller ratios of water required for the supports with this complex present. In the case of the H-acac, it seems that only a weak complex was formed whereas with the dibenzoylmethane there was no complex formed at all so these two systems would require more water for optimum gelation.

The MAS-NMR and DRIFT spectra gave some structural information but the nitrogen adsorption data gives the most information when determining a support that may show high catalytic activity. The NMR spectra show the different aluminum species present but do not give much else. The supports made with acetophenone show the $Al^{"V"}$ species but the supports made with benzophenone do not although both types of support exhibit high catalytic activity when loaded with $ZnCl_2$. That is, the presence or absence of the $Al^{"V"}$ species does not necessarily correlate to catalytic activity. The DRIFT spectra do show a little more than that. The supports that gave the best activities possess the surface octahedral stretch at 1100 cm^{-1} so this may be used as an indicator.

All the supports give relatively high surface areas (250-350 m^2/g) but as mentioned before there is a trend where as the amount of water and/or additive is increased the surface area does decrease. The supports made with acetophenone do not really show this trend, as all the surface areas stay approximately the same. This is true for the supports made with benzophenone as well but not to the same degree. Since these two types of supports gave the best results from the activity study the trend could be used as another indicator for a good support. The supports made from 2,4-pentanedione and dibenzoylmethane still have high surface areas but do show the decreasing trend. The shape of the hysteresis loop is also an indicator for the effectiveness of a support. The supports made with dibenzoylmethane showed "ink bottle" type pores indicating that they would be easily blocked by both catalyst and reagents making it an ineffective catalyst. The supports made with the other three additives exhibited H4 type hysteresis loops that indicate a mesoporous structure with wider pore openings.

The pore size distribution data can be revealing for determining suitable supports. The 2,4-pentanedione supports exhibit small pores with a sharp pore size distribution and the supports made from dibenzoylmethane are larger but the pore size distribution is still relatively sharp. These two supports gave poor results in the activity study although they were an improvement over Clayzic. The acetophenone and benzophenone supports had large pores but with broad pore size distributions and gave very good results in the activity study. This may allow for better monolayer coverage of the catalyst.

The most useful data in judging a support is the total pore volume calculated from the adsorption data. Those supports with a pore volume ≥ 2 cc/g give the best activity when loaded with catalyst. The pore volume indicates how much space there is for the

reaction as it is a measure of the liquid condensate in the pore. The isotherms may give some indication of how high this pore volume is by the maximum amount of nitrogen adsorbed. From the data tables above it is clear that the supports made from acetophenone and benzophenone have the highest pore volumes (and activity) while the other two supports gave low pore volumes and activity.

In the aluminosilicate system, β-diketones proved to be the most effective additives for obtaining catalysts with high activity. A relatively sharp pore distribution with pores 8-12 nm in size give the best results.[26,49,50] At the start of this work it was thought that this may be true for alumina as well and the results show that this is not the case. The aromatic ketones give the best results possibly because the complex formed with the aromatic ring as shown by the FTIR data may be more effective at producing a useful support than complexes with the carbonyl. Perhaps a complex between both a carbonyl and an aromatic ring is the most effective of all. The complex formed may be octahedral in nature with the additive acting as a bidentate ligand as shown by the shift in the vibrational modes of the carbonyl and aromatic ring in the FTIR spectra.

Much more work needs to be done on this system. There are many ketones that can be utilized in synthesis of these supports. Chapter 5 gives a more thorough discussion on the future possibilities for this work.

TEXT CONTINUED ON PAGE 122

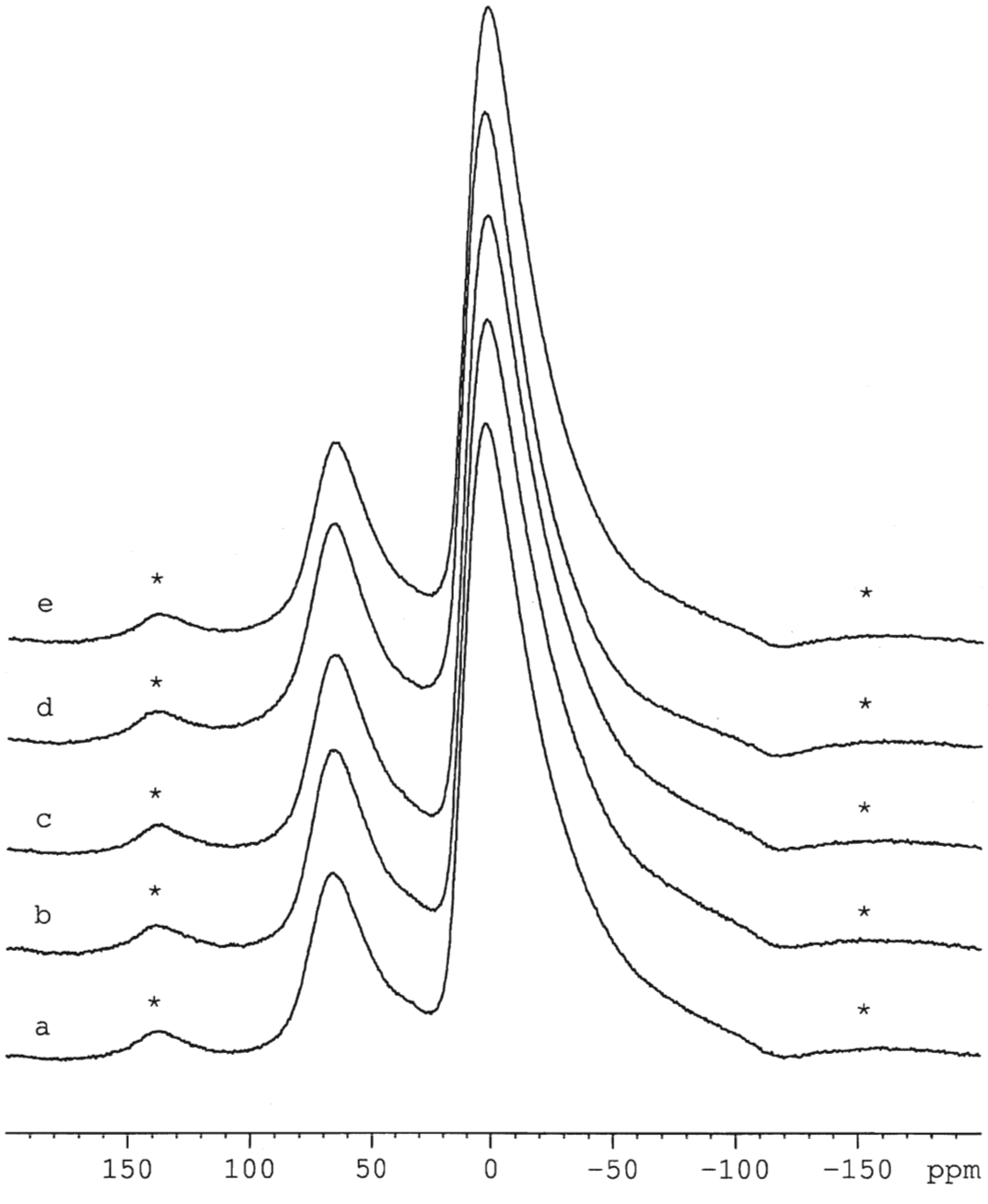

Figure 21: ^{27}Al MAS-NMR spectra for supports made with 2.4 mmol of 2,4-pentanedione. a: 2ml H2O, b: 4 ml H2O, c: 6 ml H2O, d: 8 ml H2O, e: 10ml H2O.

* Spinning Side Bands

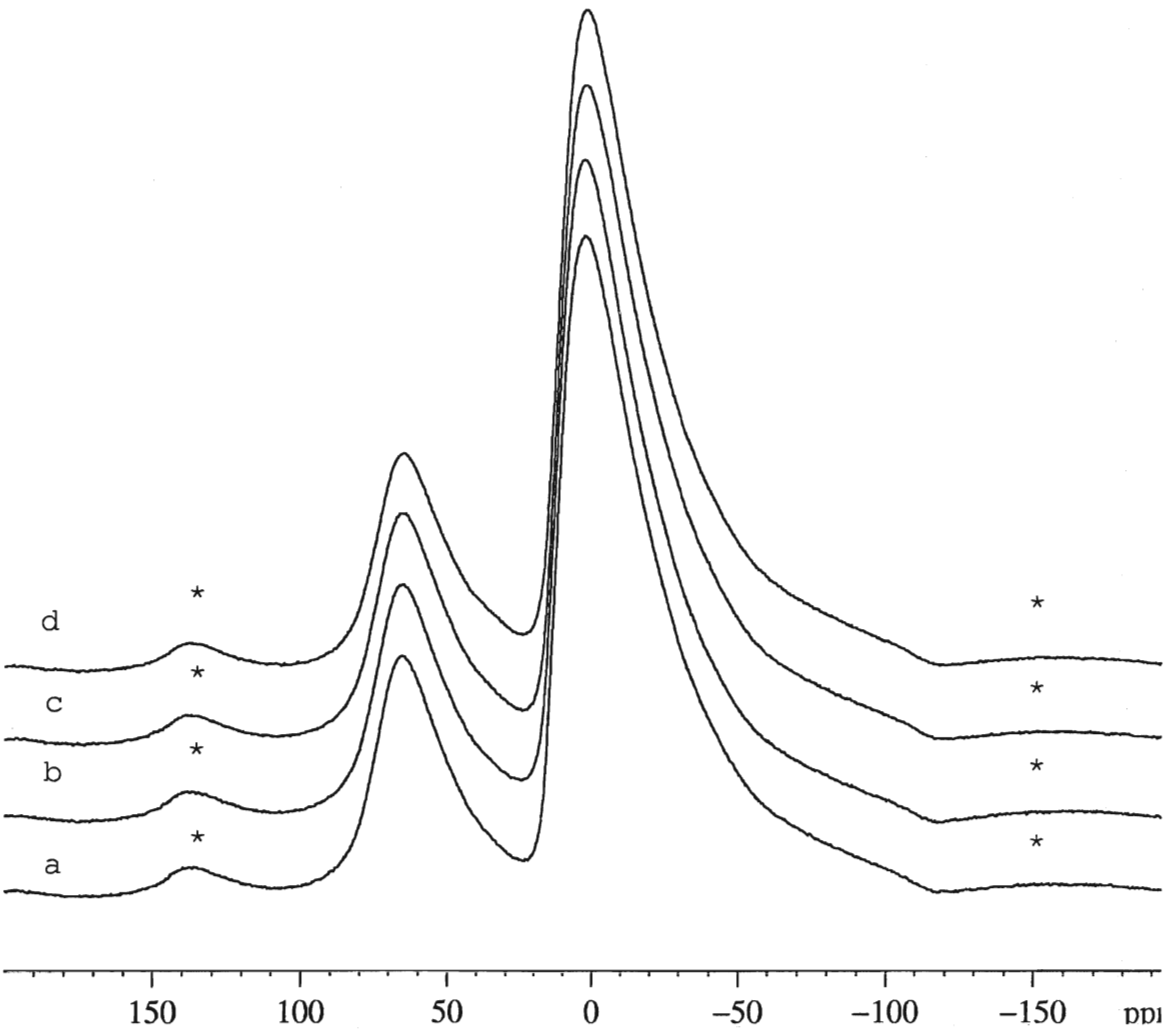

Figure 22:[27]AL MAS-NMR spectra for supports made with 2,4-pentanedione.
(10ml water for gelation)
a: 2.4 mmol H–acac, b: 4.8 mmol H–acac, c: 7.2 mmol H–acac,
d: 9.6 mmol H–acac.

* Spinning Side Bands

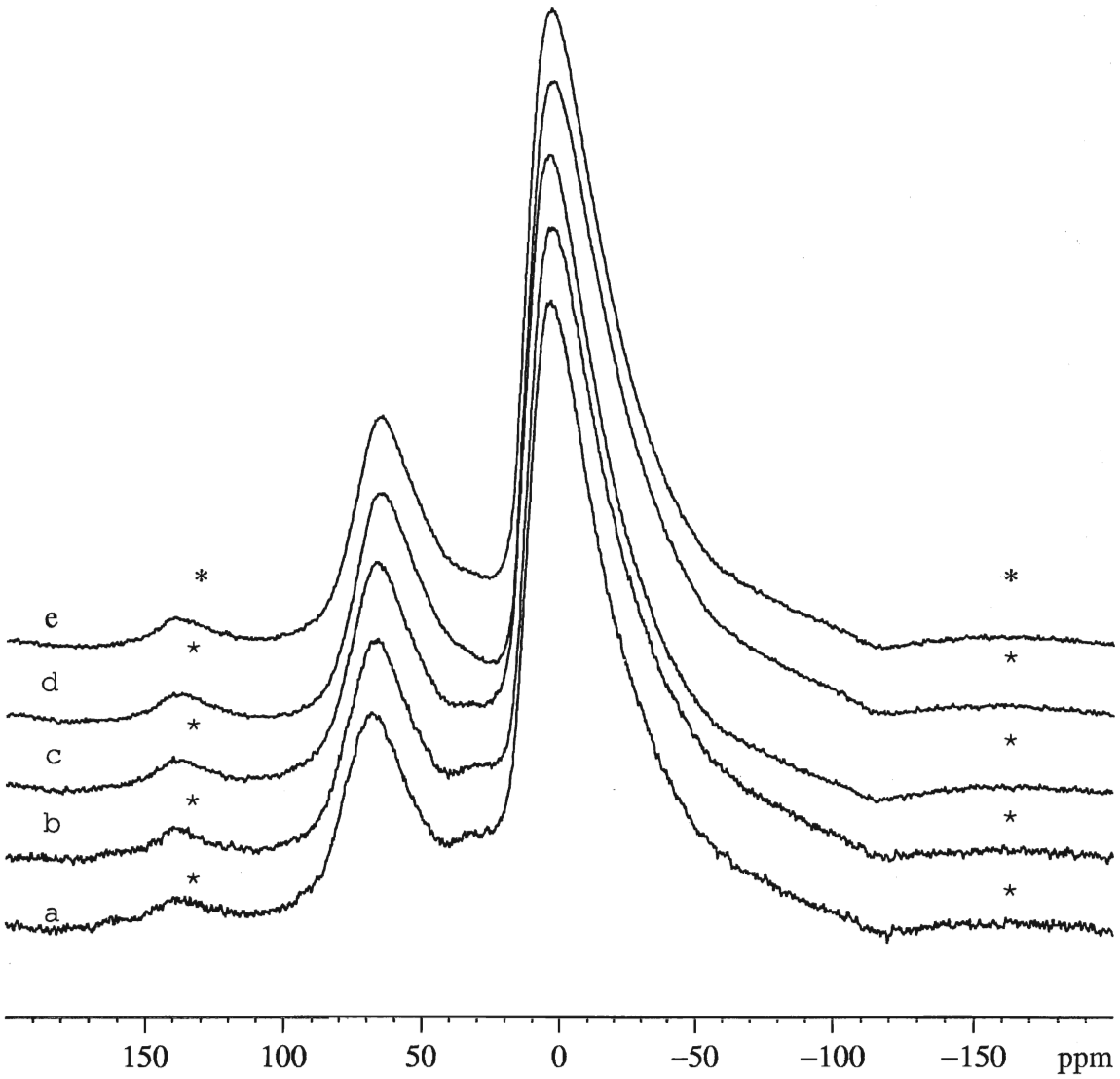

Figure 23:[27]Al MAS-NMR spectra for supports made with 2.1 mmol of acetophenone. a: 2ml H2O, b: 4 ml H2O, c: 6 ml H2O, d: 8 ml H2O, e: 10ml H2O.

* Spinning Side Bands

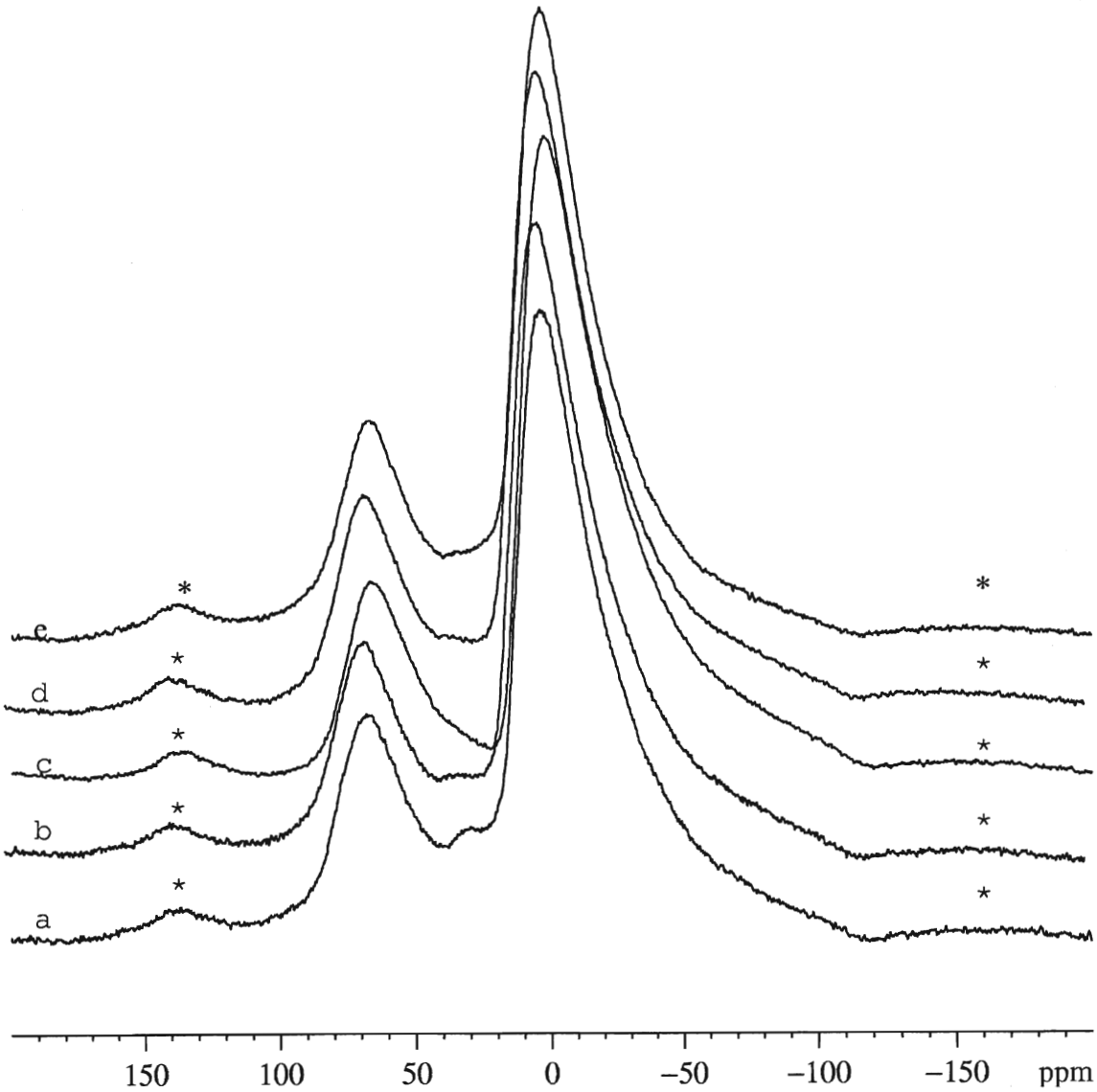

Figure 24:[27]Al MAS-NMR spectra for supports made with 4.2 mmol of acetophenone. a: 2ml H2O, b: 4 ml H2O, c: 6 ml H2O, d: 8 ml H2O, e: 10ml H2O.

* Spinning Side Bands

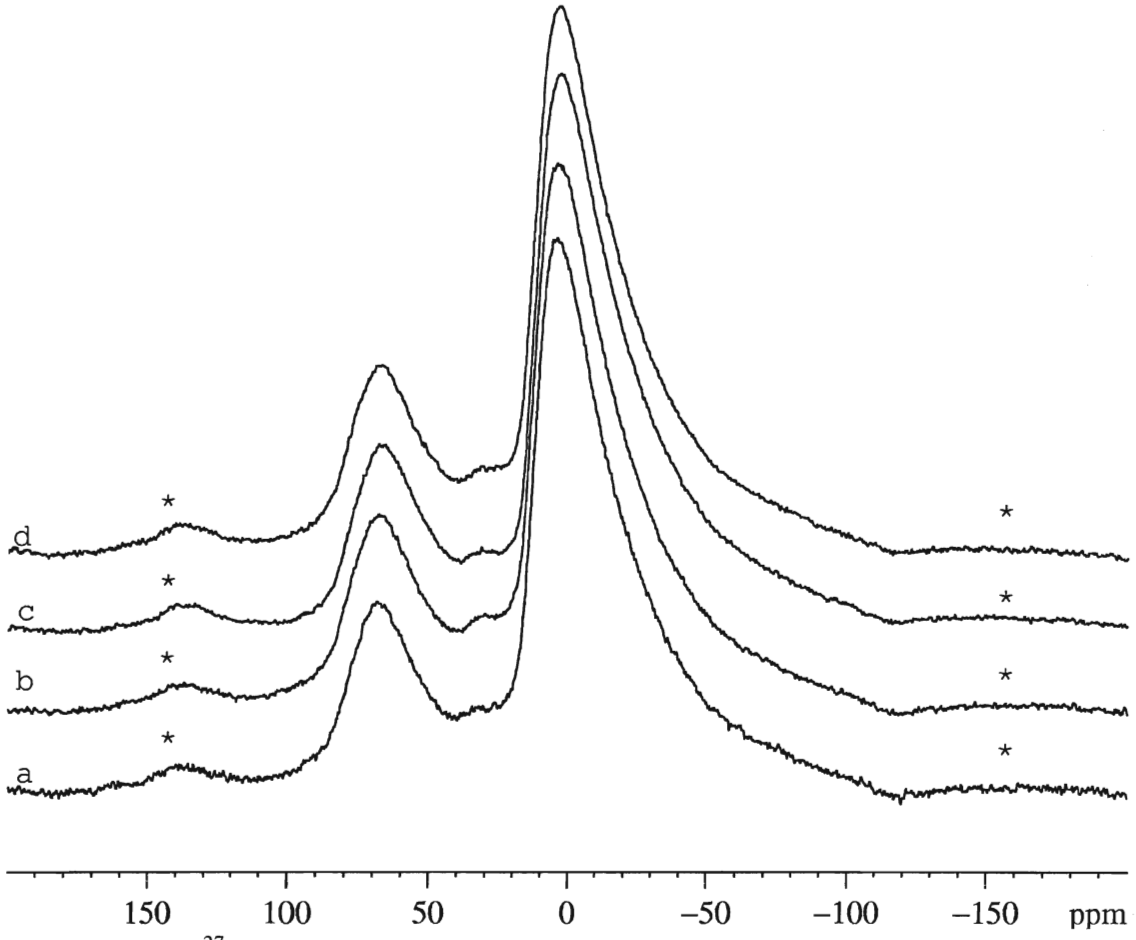

Figure 25:^{27}AL MAS-NMR spectra for supports made with acetophenone.
(2 ml water for gelation)

a: 2.1 mmol acetophenone, b: 4.2 mmol, c: 6.3 mmol, d: 8.4 mmol.

* Spinning Side Bands

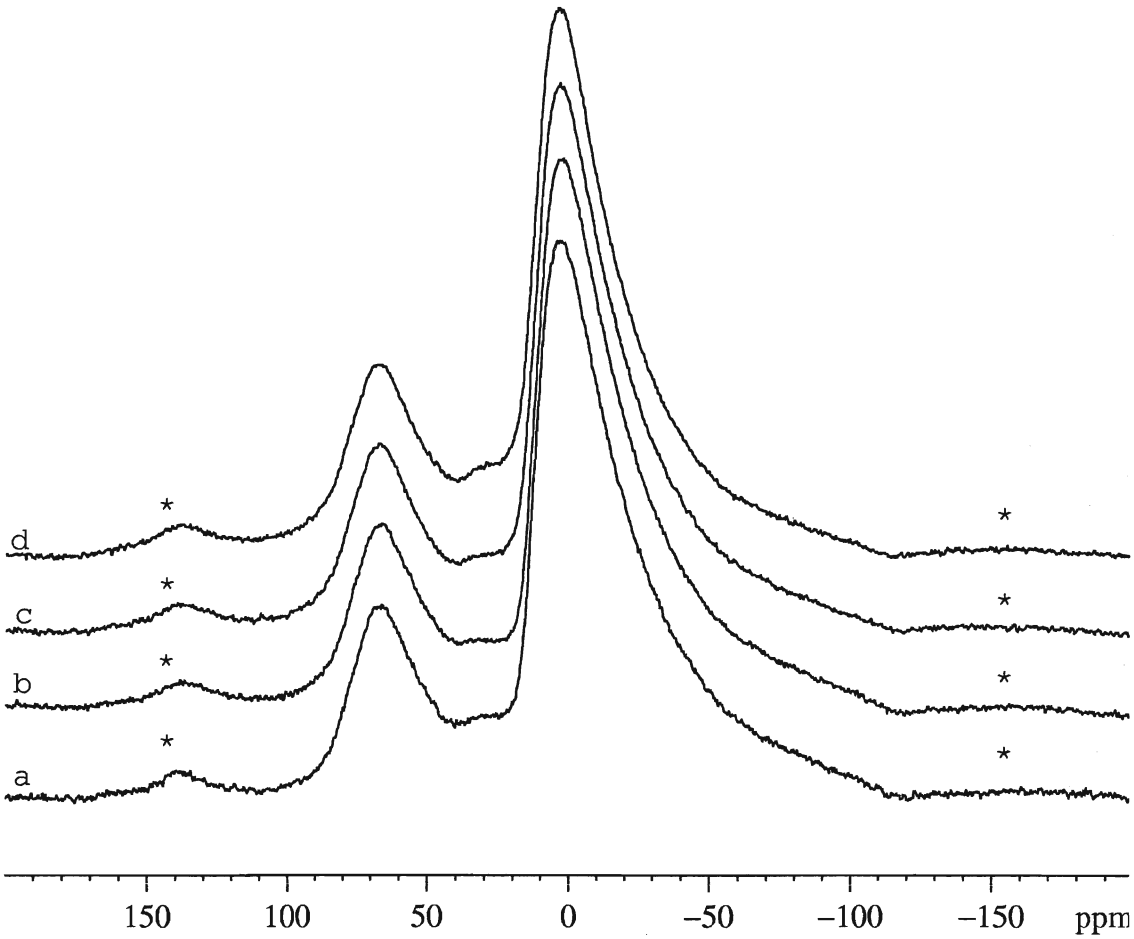

Figure 26:^{27}AL MAS-NMR spectra for supports made with acetophenone.
(4 ml water for gelation)

a: 2.1 mmol acetophenone, b: 4.2 mmol, c: 6.3 mmol, d: 8.4 mmol.

* Spinning Side Bands

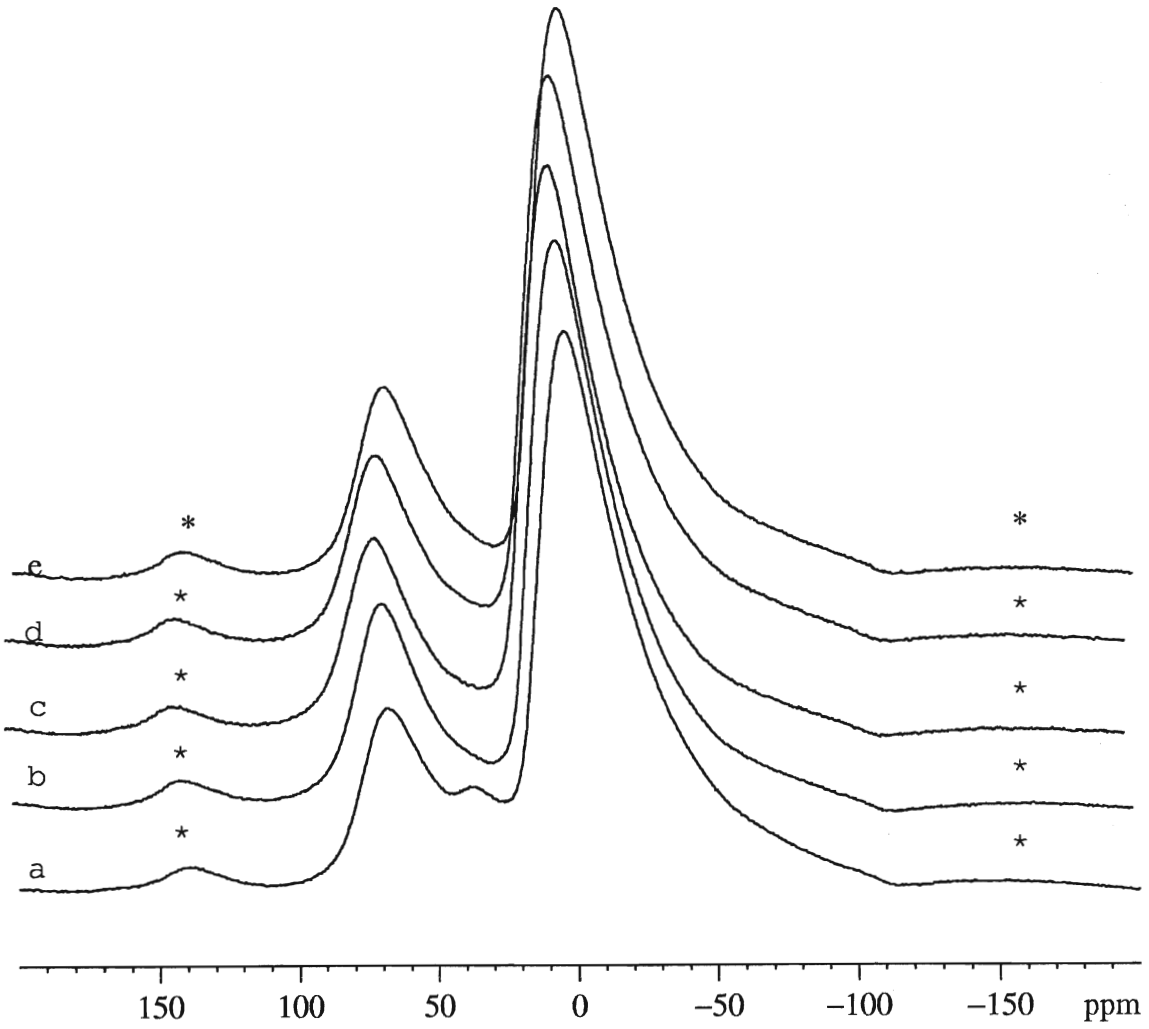

Figure 27: ^{27}Al MAS-NMR spectra for supports made with 1.1 mmol of dibenzoylmethane.
a: 2ml H2O, b: 4 ml H2O, c: 6 ml H2O, d: 8 ml H2O, e: 10ml H2O.
* Spinning Side Bands

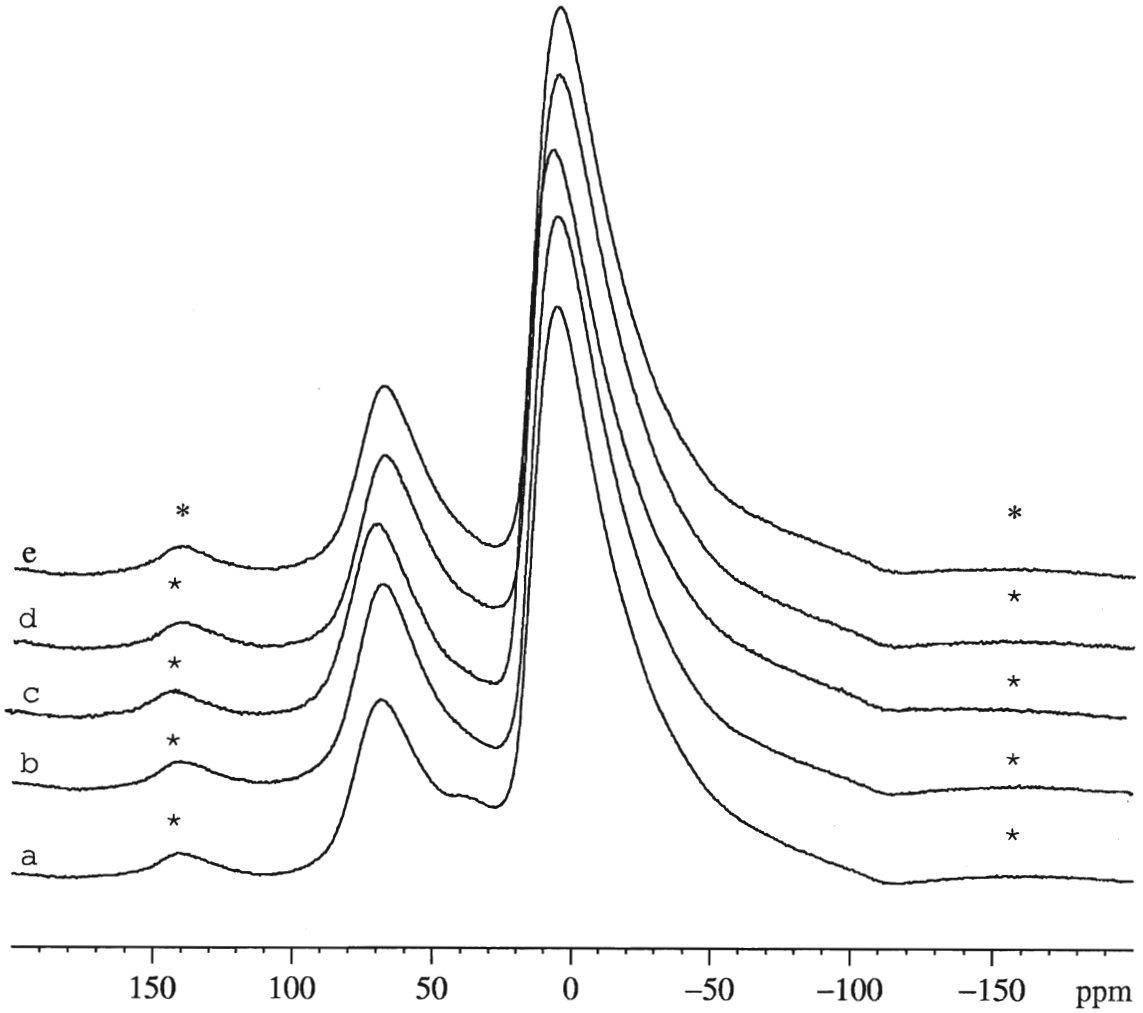

Figure 28:[27]Al MAS-NMR spectra for supports made with 2.2 mmol of dibenzoylmethane.
a: 2ml H2O, b: 4 ml H2O, c: 6 ml H2O, d: 8 ml H2O, e: 10ml H2O.
* Spinning Side Bands

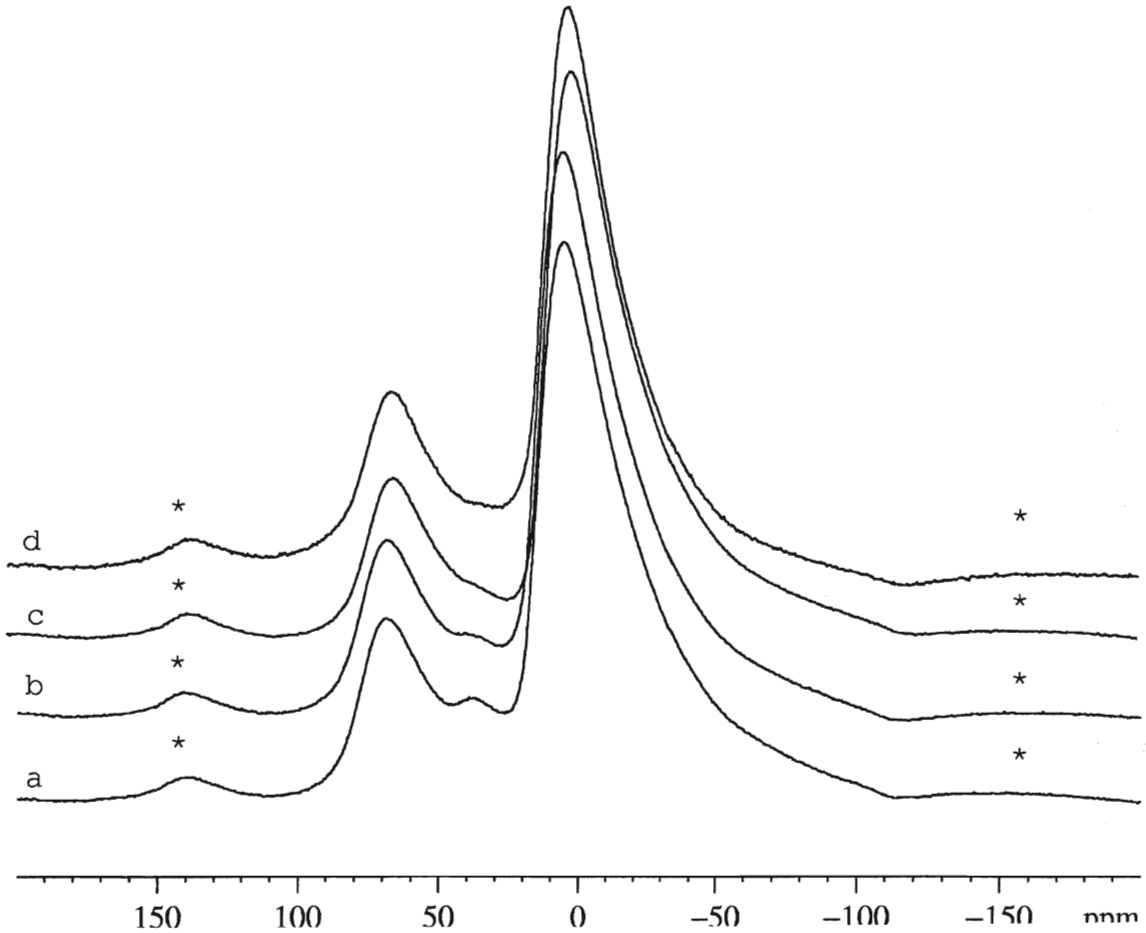

Figure 29:[27]AL MAS-NMR spectra for supports made with dibenzoylmethane.
(2 ml water for gelation)
a: 1.1 mmol dibenzoylmethane, b: 2.2 mmol, c: 3.3 mmol, d: 4.4 mmol.

* Spinning Side Bands

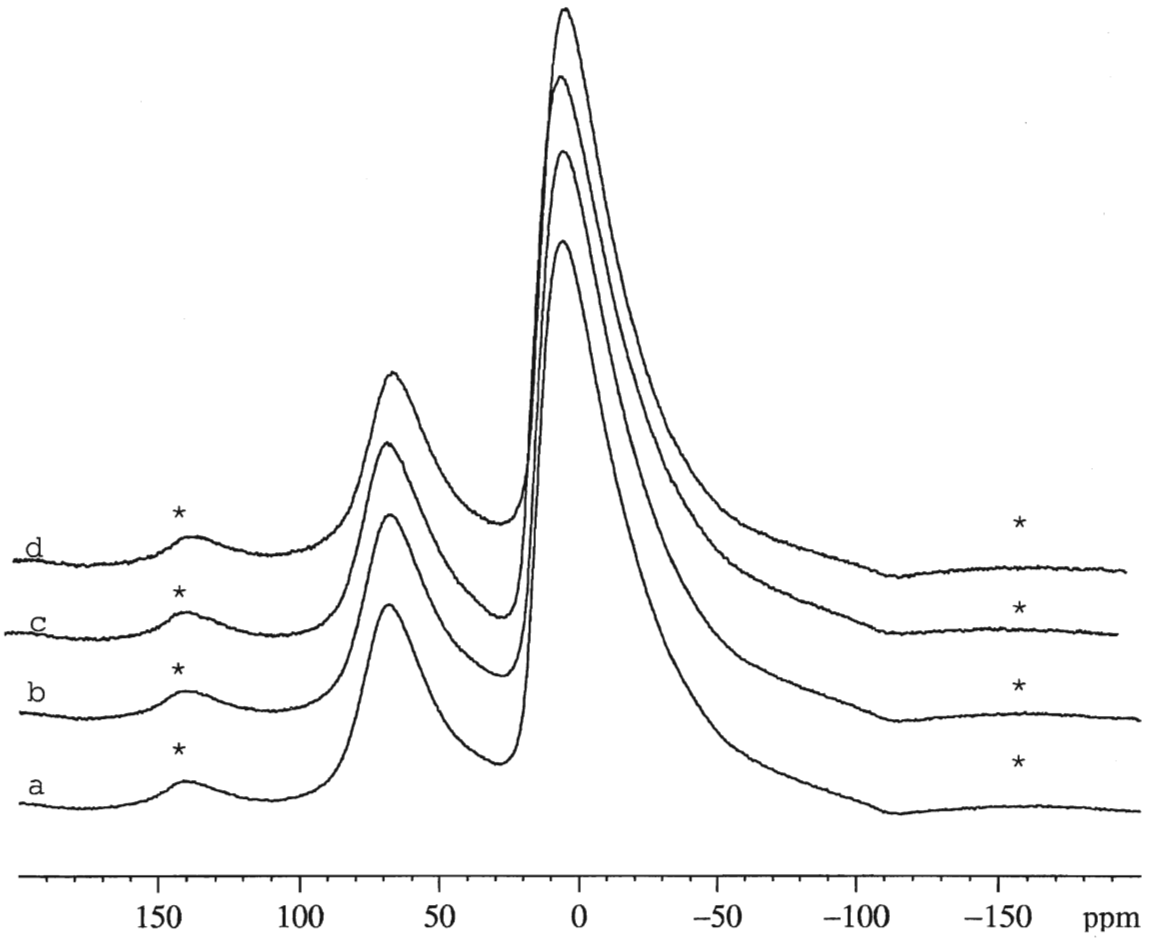

Figure 30:[27]AL MAS-NMR spectra for supports made with dibenzoylmethane.
(4 ml water for gelation)
a: 1.1 mmol dibenzoylmethane, b: 2.2 mmol, c: 3.3 mmol, d: 4.4 mmol.

* Spinning Side Bands

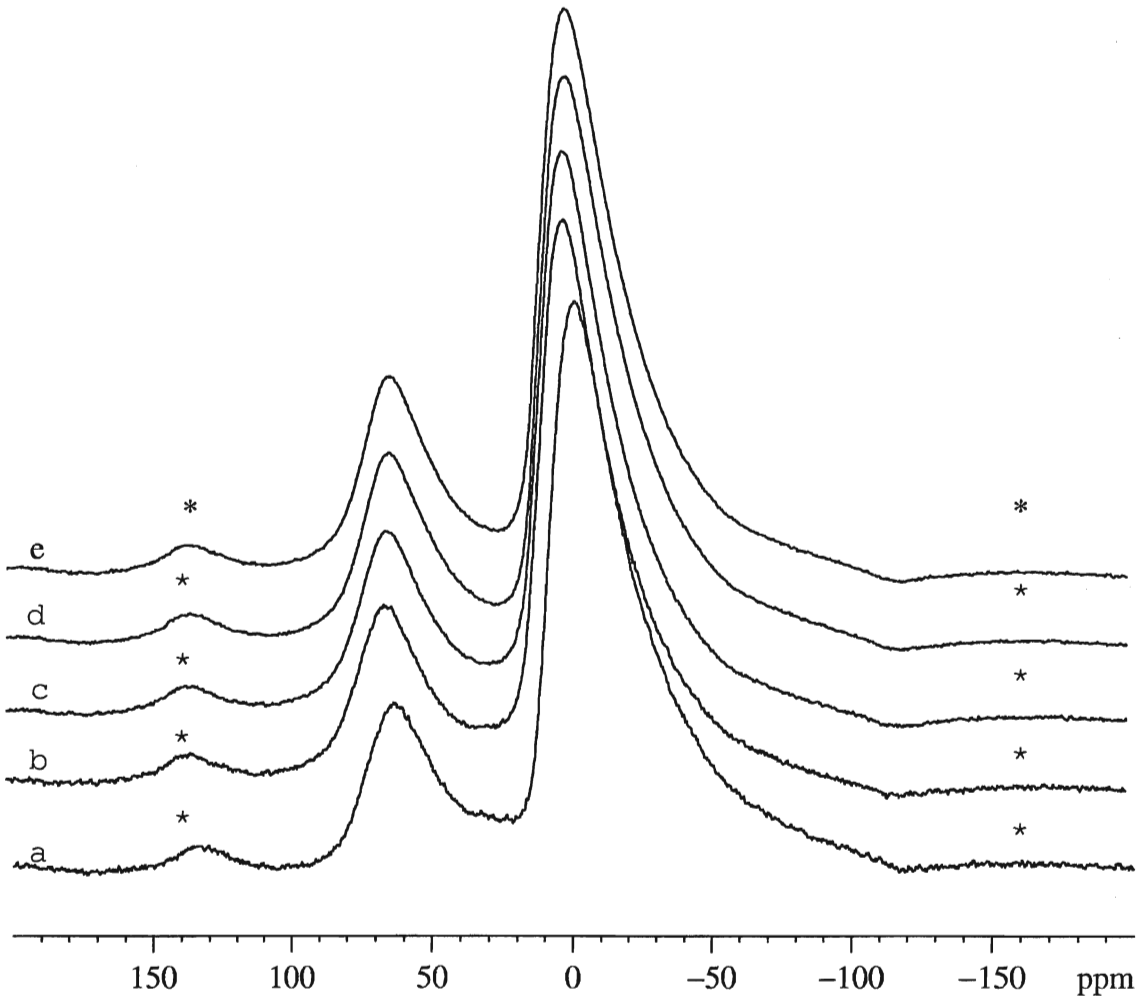

Figure 31:^{27}Al MAS-NMR spectra for supports made with 1.4 mmol of benzophenone. a: 2ml H2O, b: 4 ml H2O, c: 6 ml H2O, d: 8 ml H2O, e: 10ml H2O.

* Spinning Side Bands

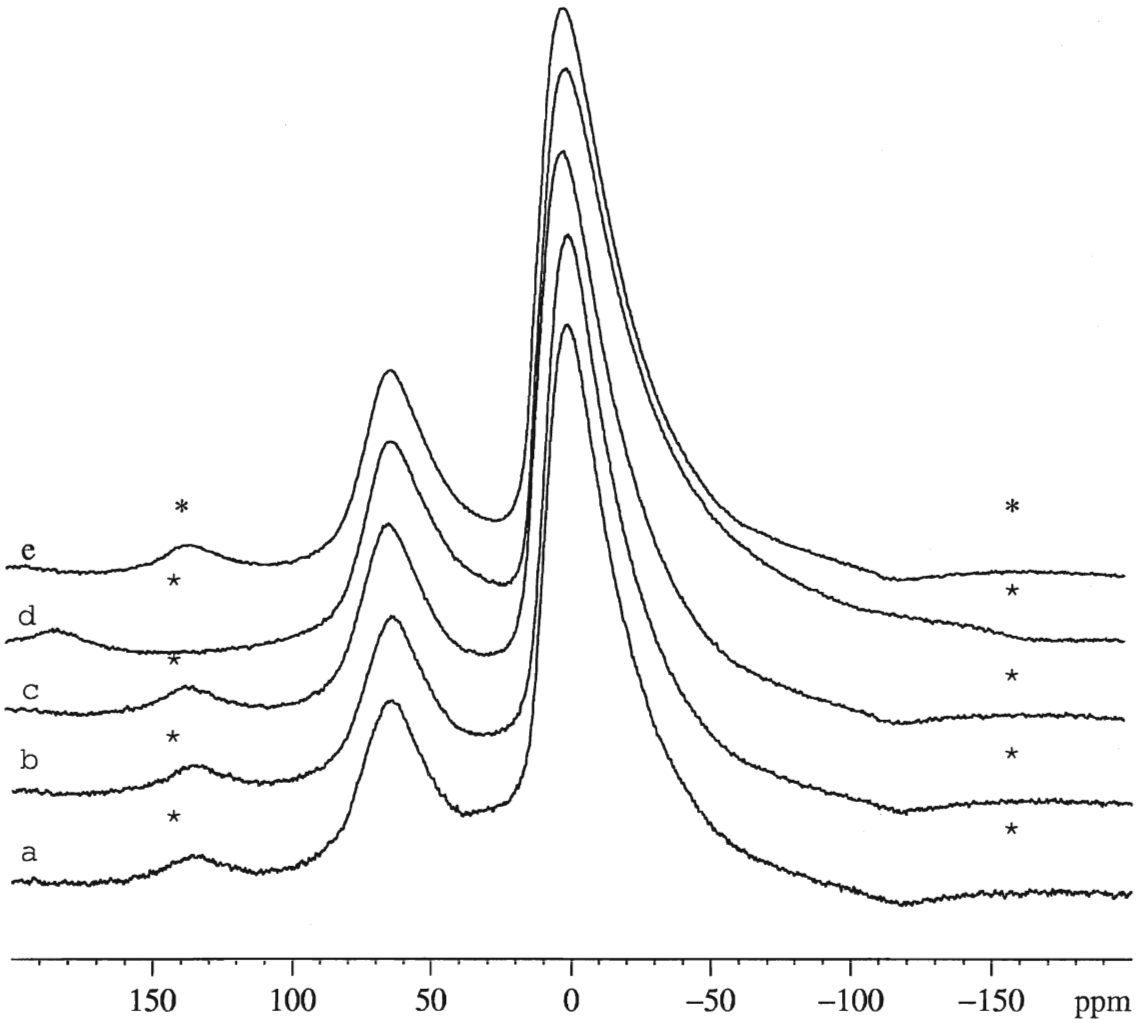

Figure 32:^{27}Al MAS-NMR spectra for supports made with 2.8 mmol of benzophenone. a: 2ml H2O, b: 4 ml H2O, c: 6 ml H2O, d: 8 ml H2O, e: 10ml H2O.

* Spinning Side Bands

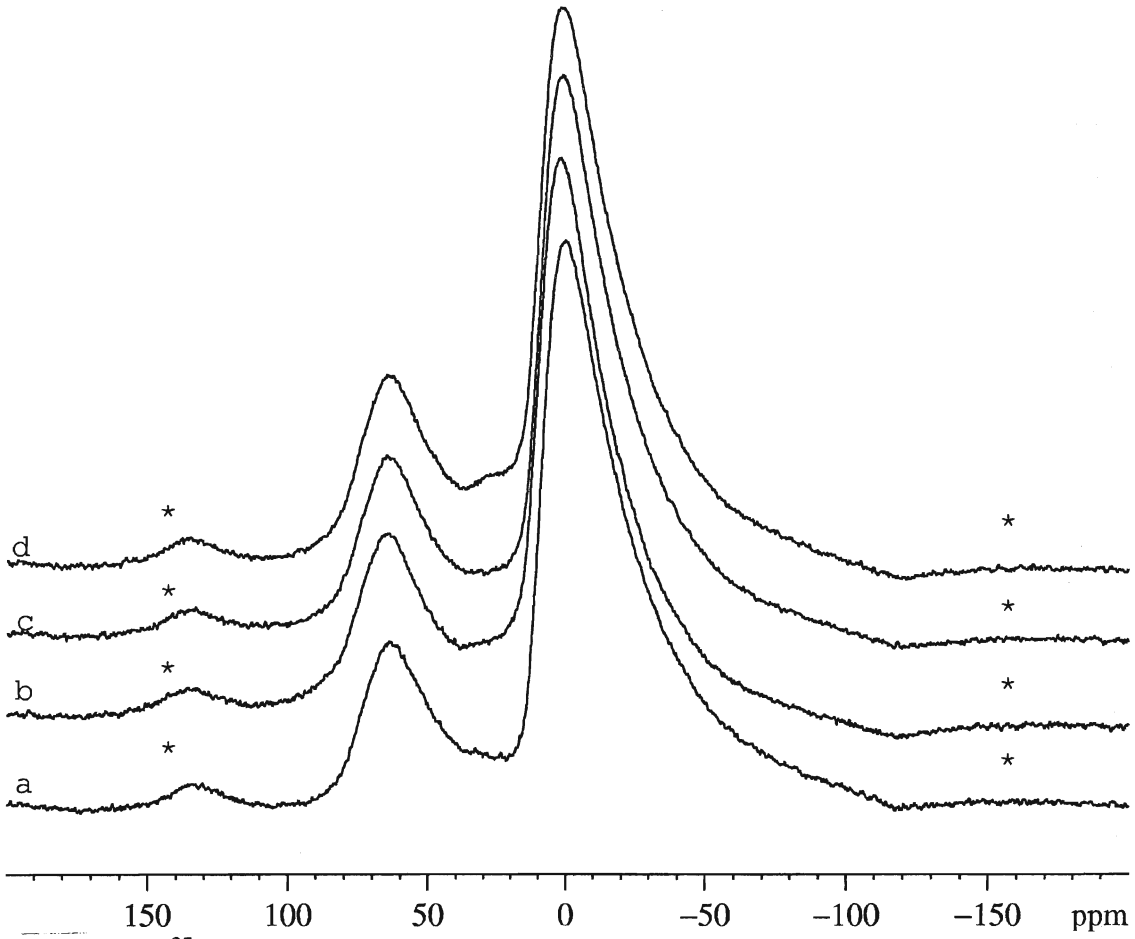

Figure 33:[27]AL MAS-NMR spectra for supports made with benzophenone.
(2 ml water for gelation)
a: 1.4 mmol benzophenone, b: 2.8 mmol, c: 4.2 mmol, d: 5.6 mmol.

* Spinning Side Bands

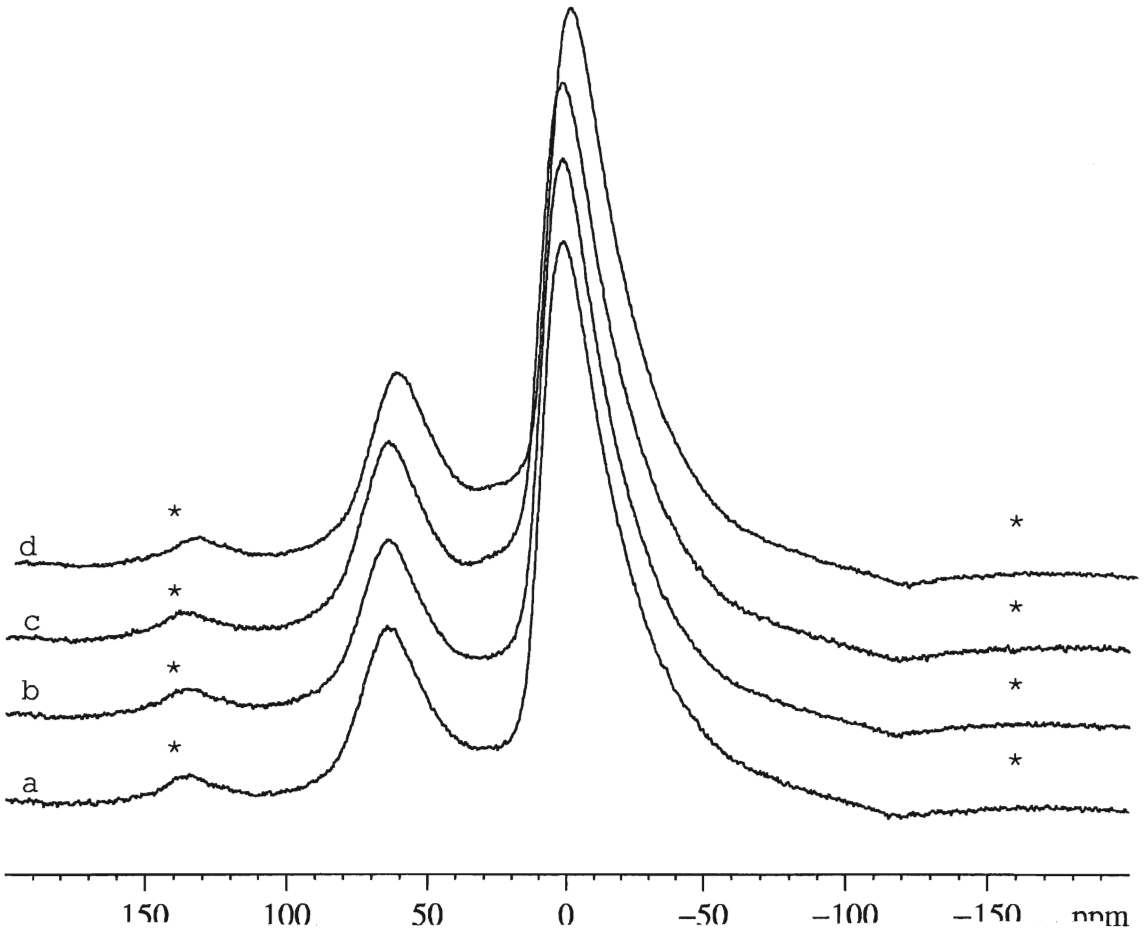

Figure 34: ^{27}AL MAS-NMR spectra for supports made with benzophenone.
(4 ml water for gelation)
a: 1.4 mmol benzophenone, b: 2.8 mmol, c: 4.2 mmol, d: 5.6 mmol.

* Spinning Side Bands

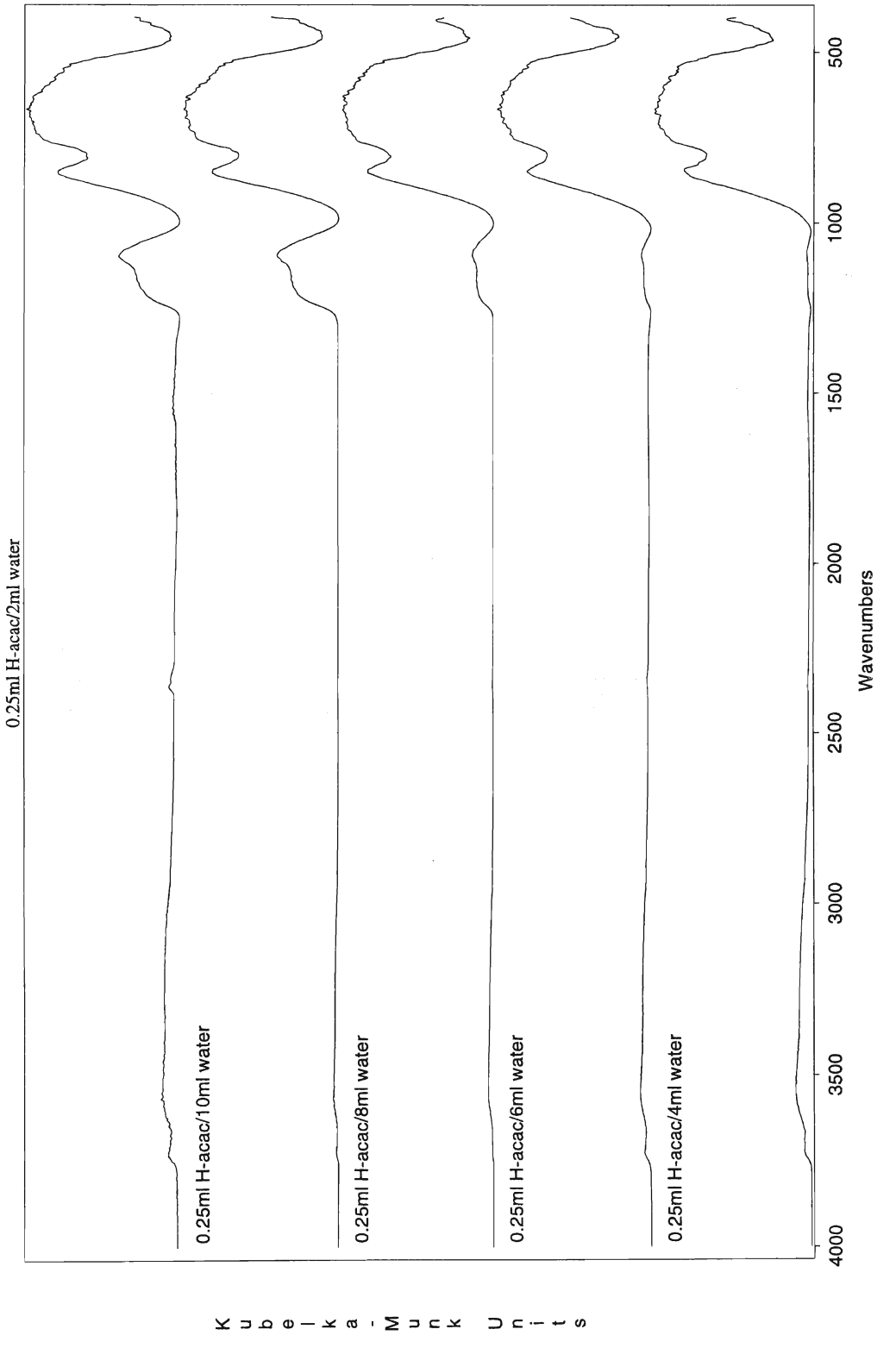

Figure 35: DRIFT spectra for alumina supports made with 2.4 mmol H-acac with various amounts of water used for gelation.

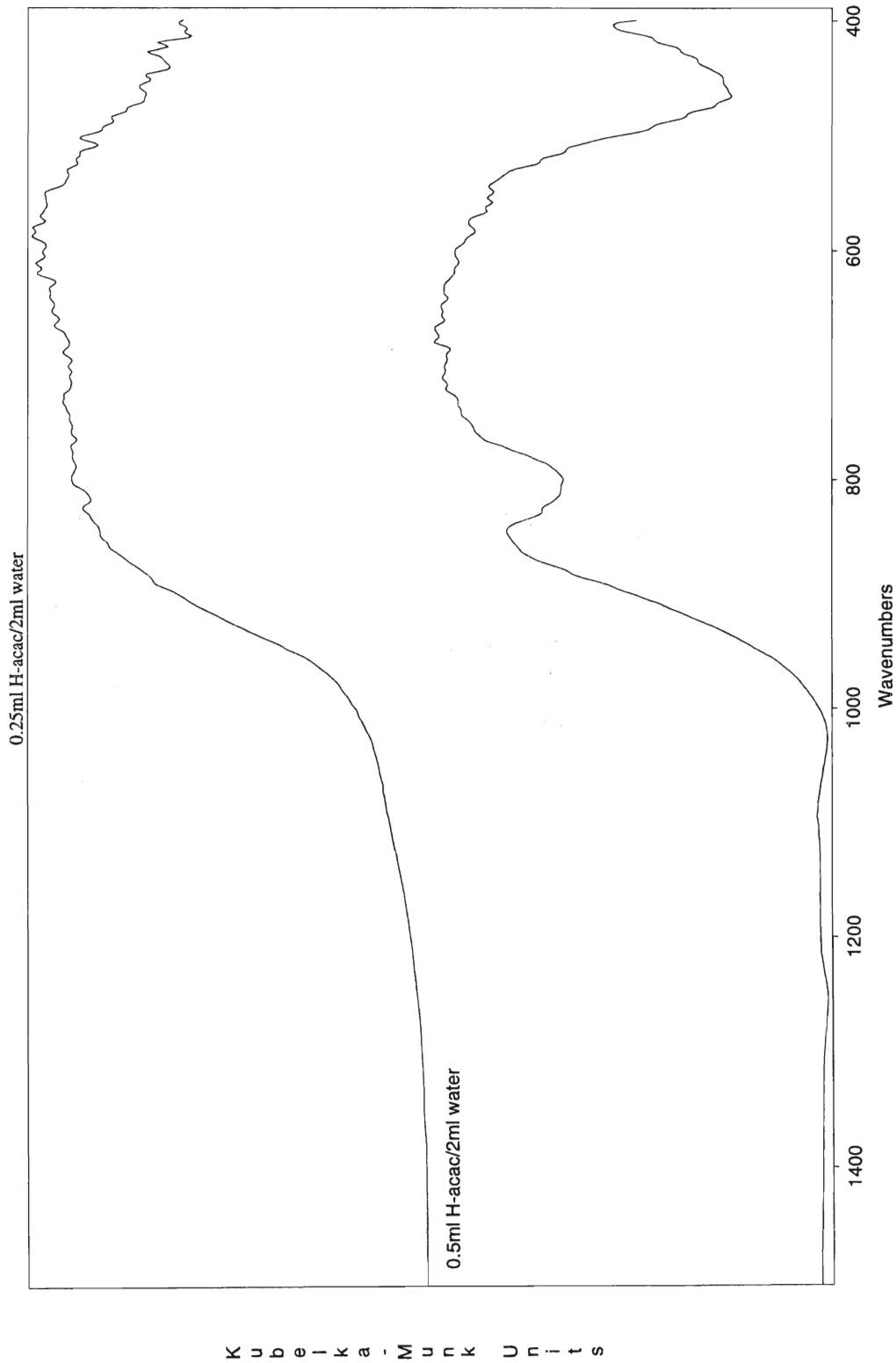

Figure 36: DRIFT spectra of alumina supports made with 2 ml water for gelation and various amounts of H-acac.

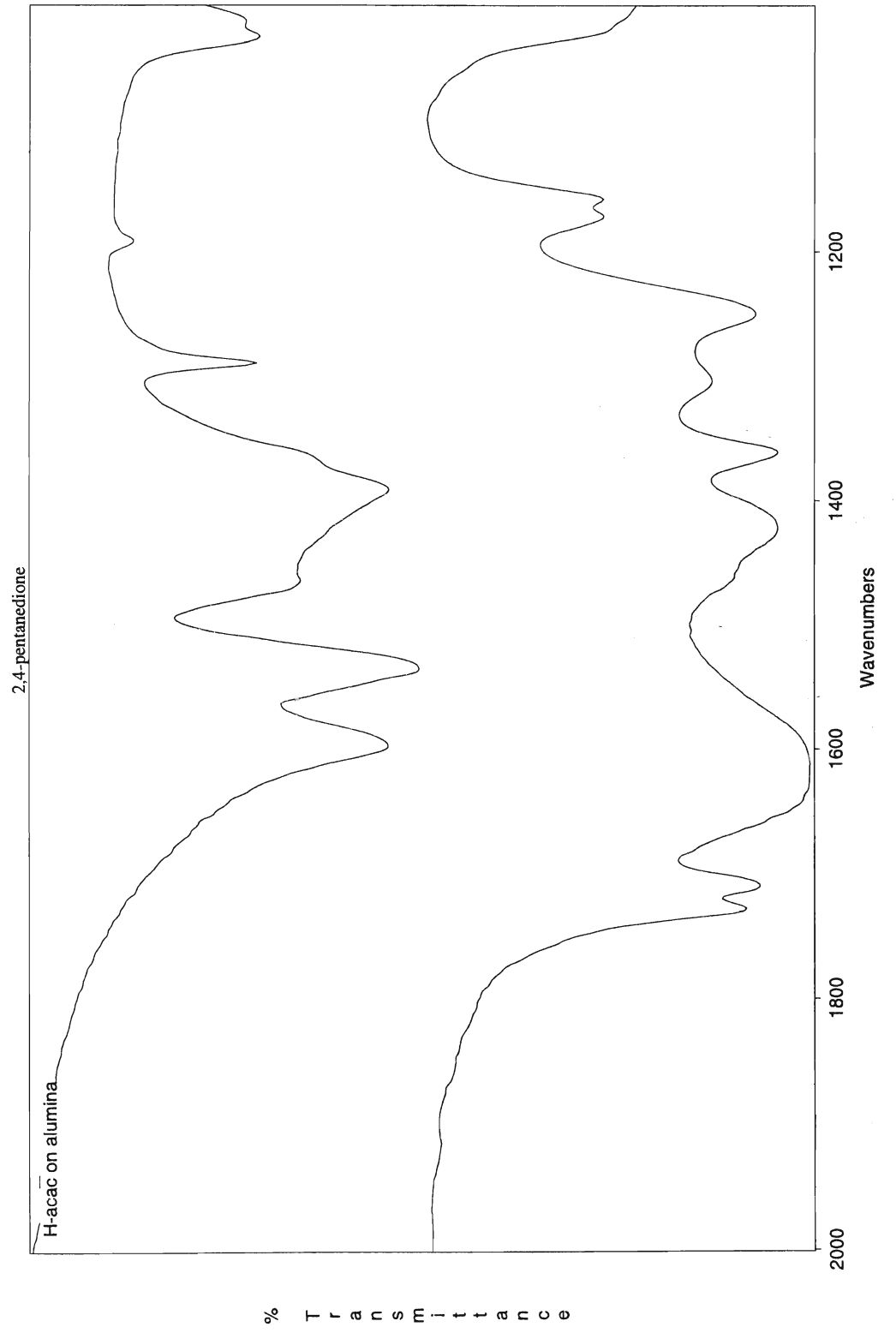

Figure 37: FTIR spectrum of alumina support made with H-acac (dried at room temperature) compared to FTIR spectrum of 2,4-pentanedione.

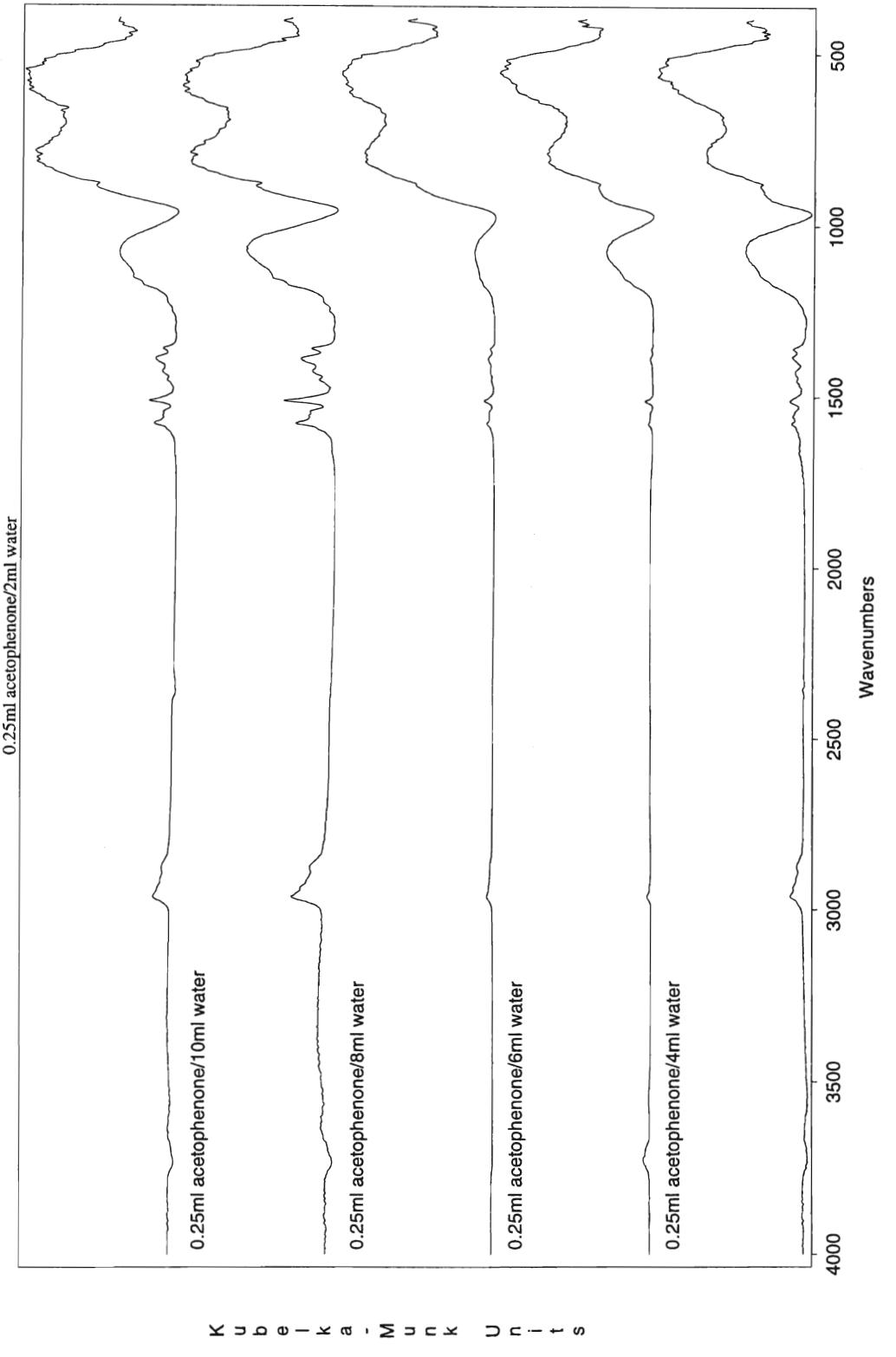

Figure 38: DRIFT spectra for alumina supports made with 2.1 mmol acetophenone with the amount of water for gelation varied.

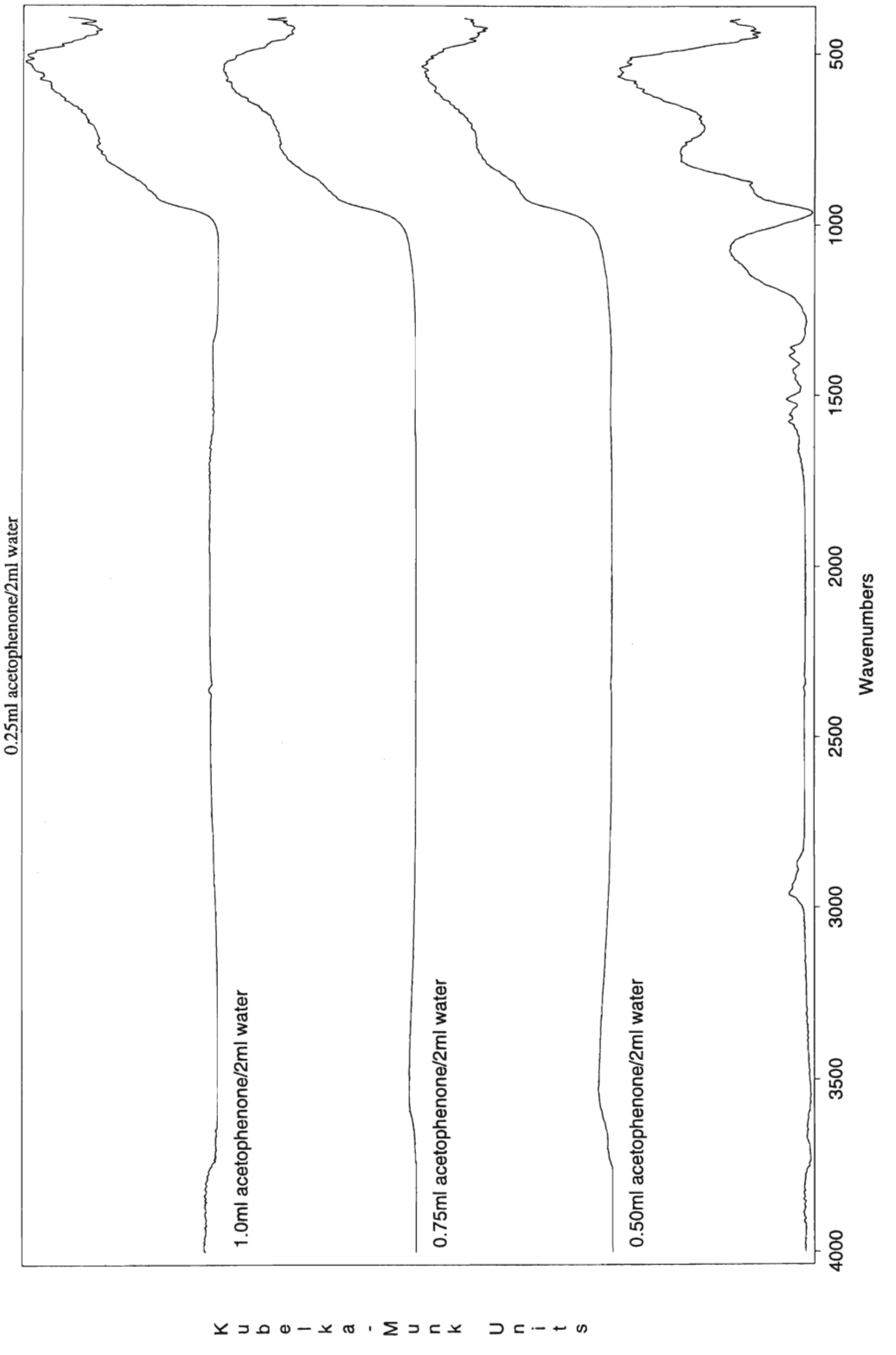

Figure 39: DRIFT spectra for alumina supports made with 2 ml of water for gelation with the amount of acetophenone varied.

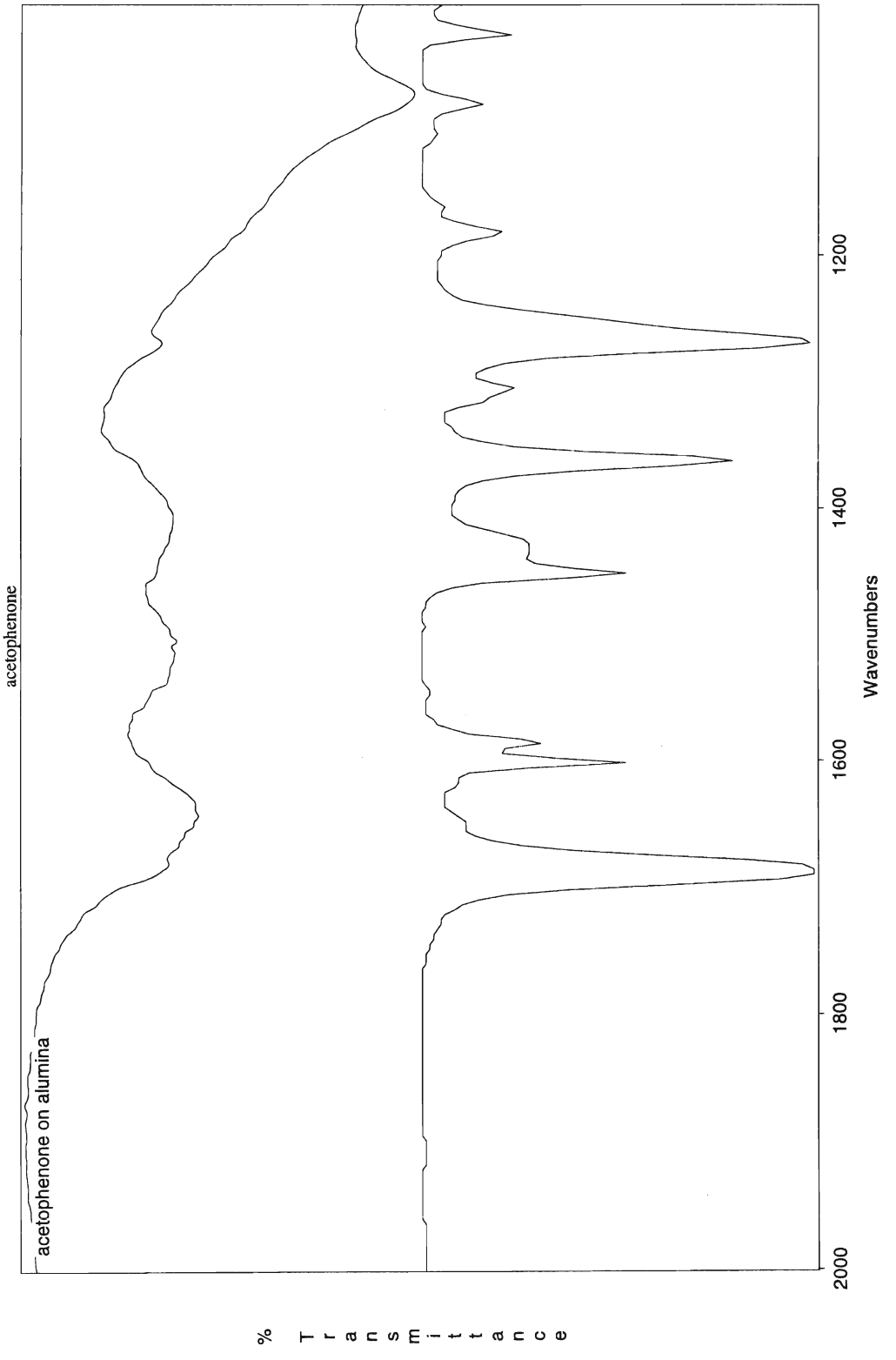

Figure 40: FTIR spectrum of alumina support made with acetophenone (dried at room temperature) compared to FTIR spectrum of acetophenone.

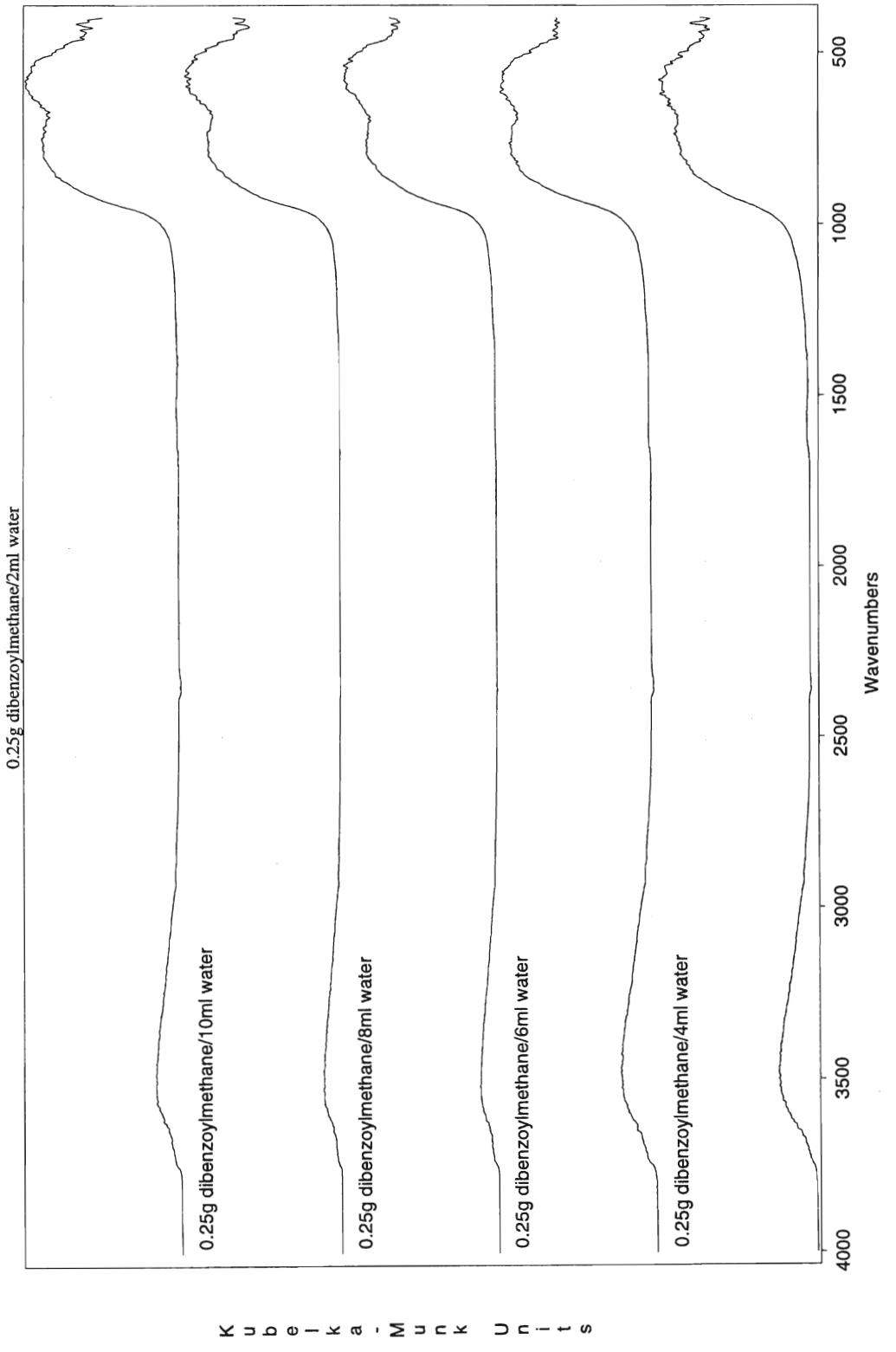

Figure 41: DRIFT spectra for alumina supports made with 1.1 mmol dibenzoylmethane with the amount of water for gelation varied.

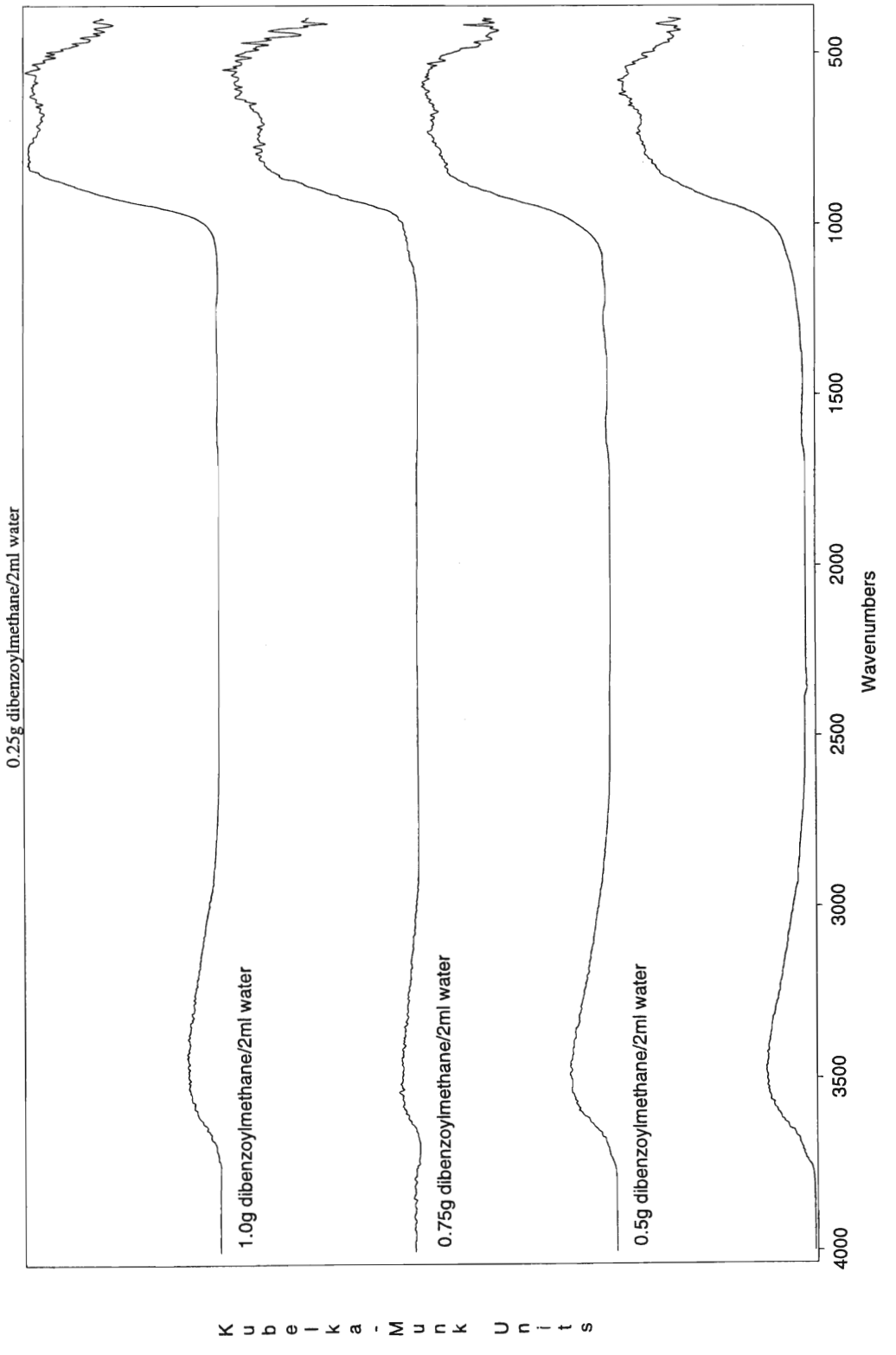

Figure 42: DRIFT spectra for alumina supports made with 2 ml of water for gelation with the amount of dibenzoylmethane varied.

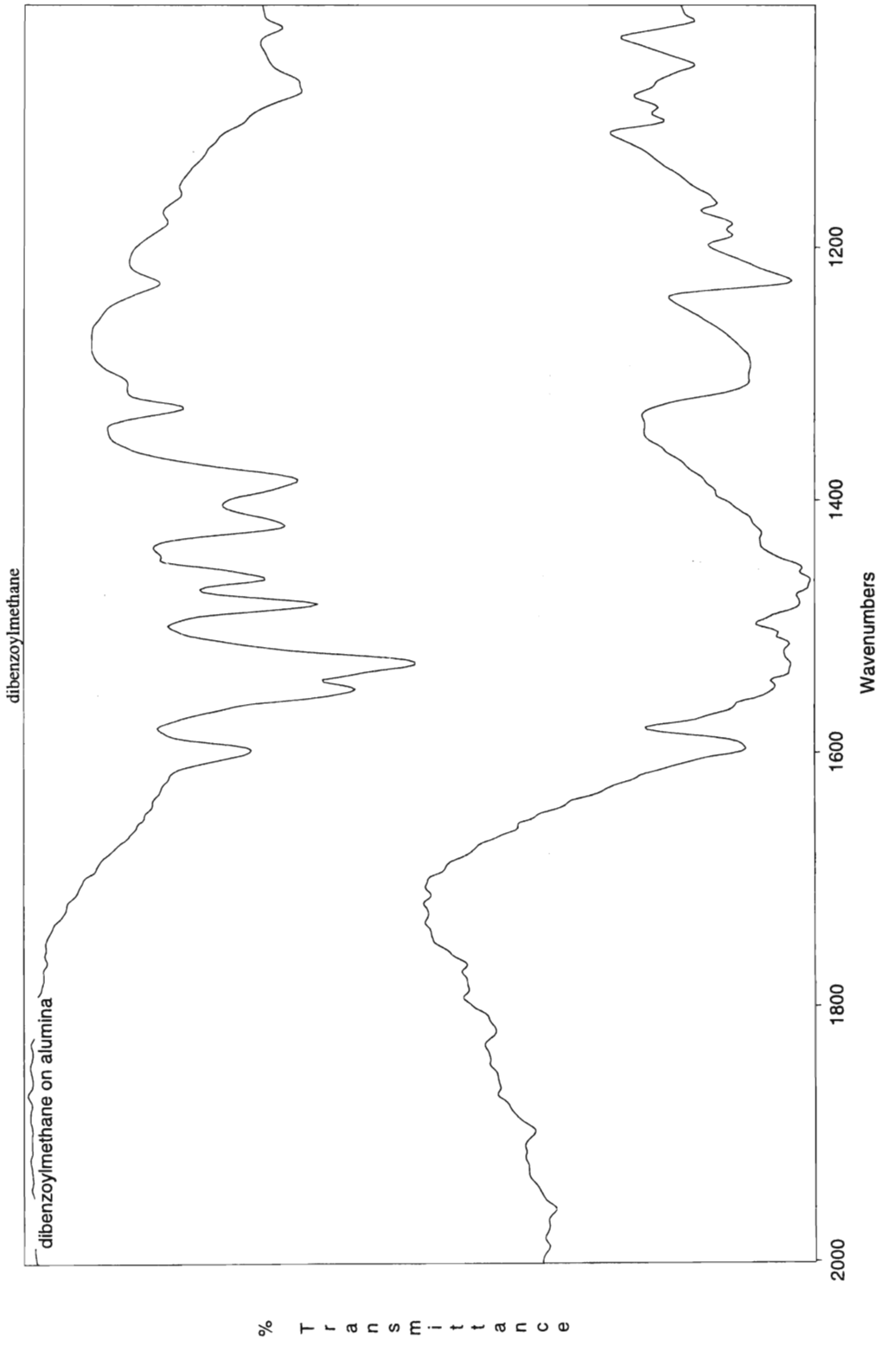

Figure 43: FTIR spectrum of alumina support made with dibenzoylmethane (dried at room temperature) compared to the FTIR spectrum of dibenzoylmethane.

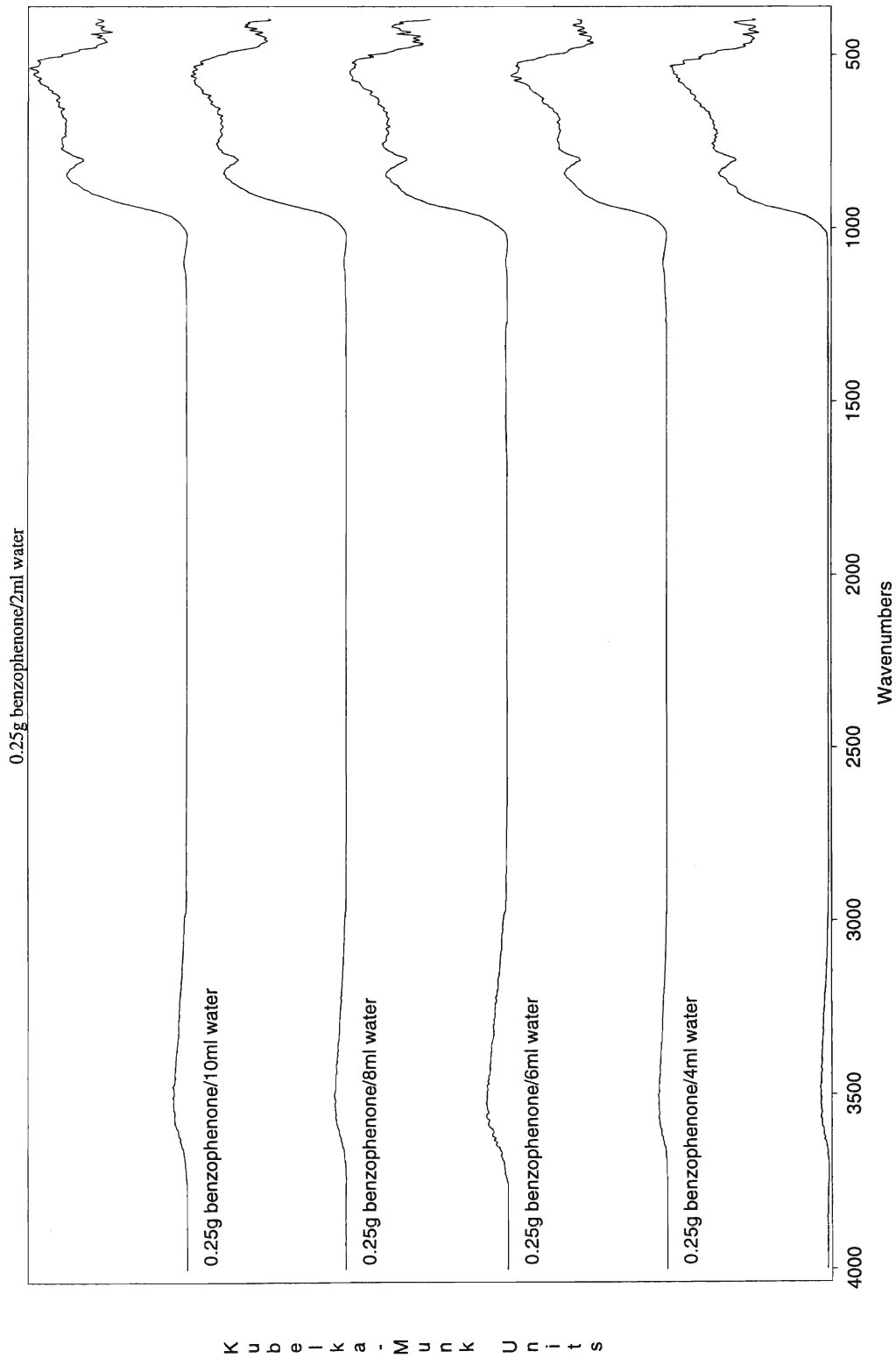

Figure 44: DRIFT spectra for alumina supports made with 1.4 mmol benzophenone with the amount of water for gelation varied.

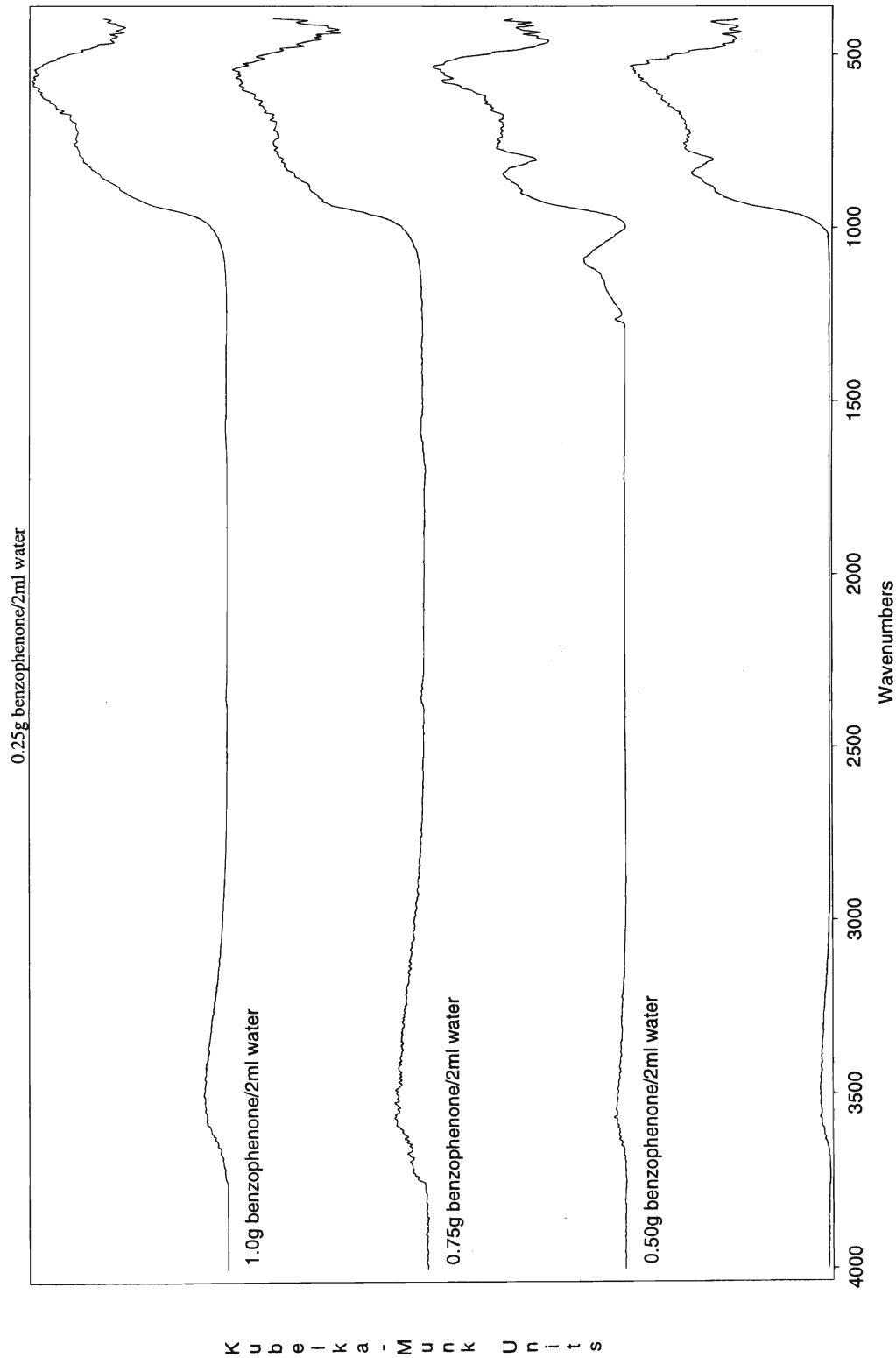

Figure 45: DRIFT spectra for alumina supports made with 2 ml of water for gelation and the amount benzophenone varied.

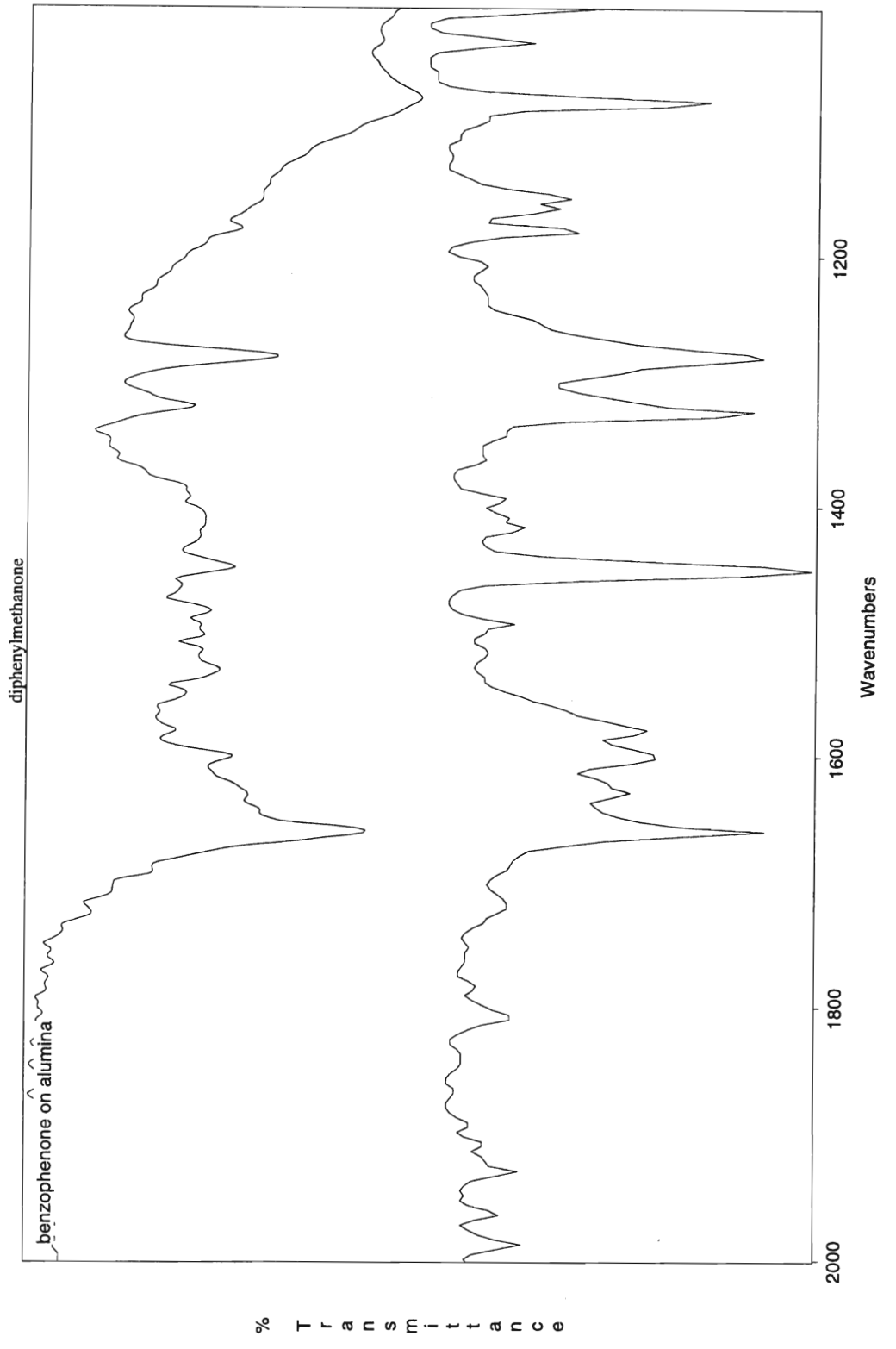

Figure 46: FTIR spectrum of alumina support made with benzophenone (dried at room temperature) compared to the FTIR spectrum of benzophenone.

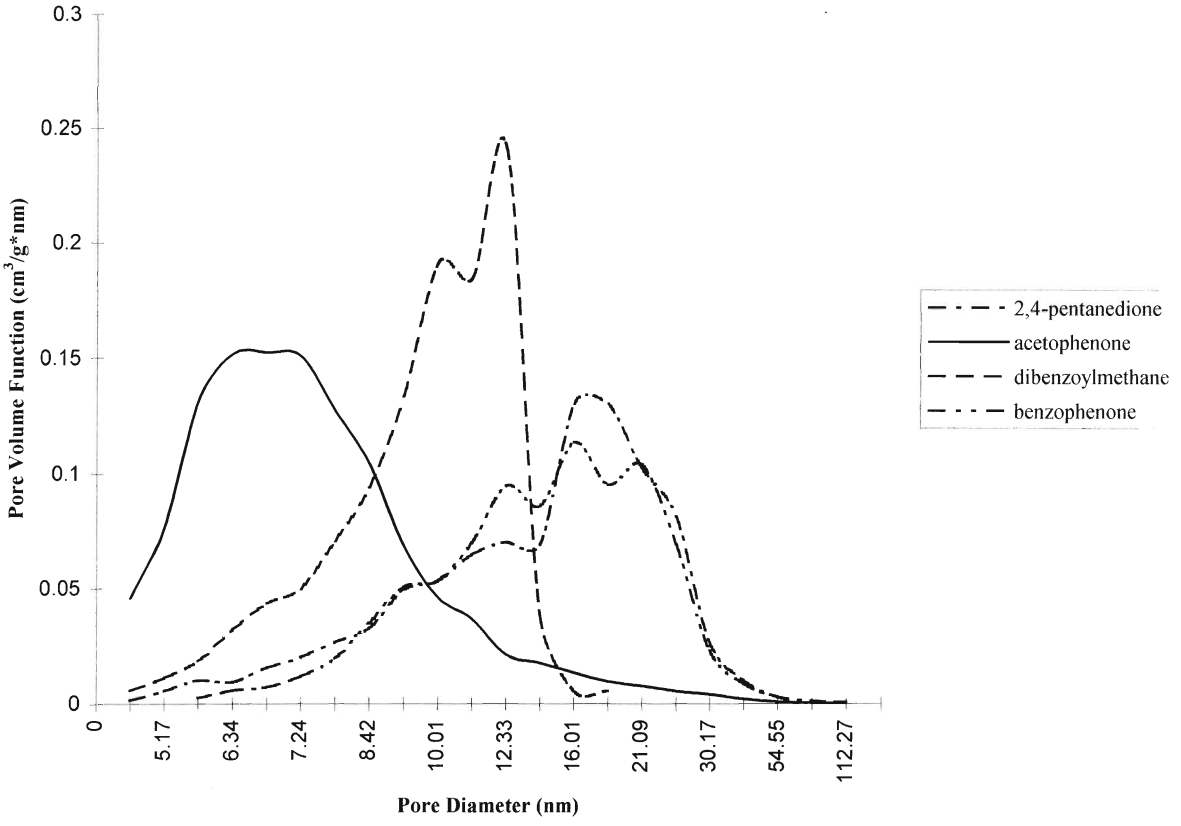

Figure 47: Optimum pore size distributions for alumina for alumina supports made with four different additives.

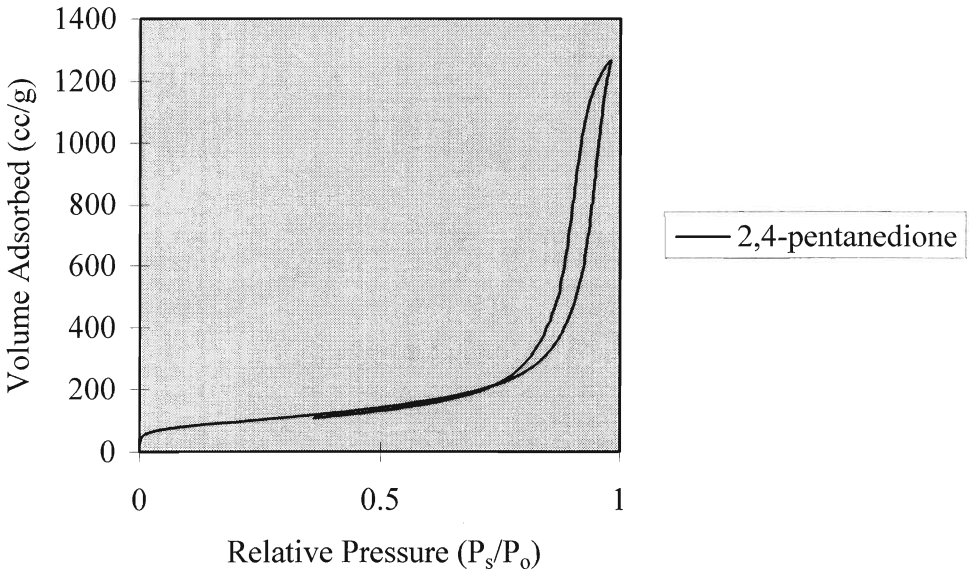

Figure 48: Isotherm for alumina support made with 2,4-pentanedione.

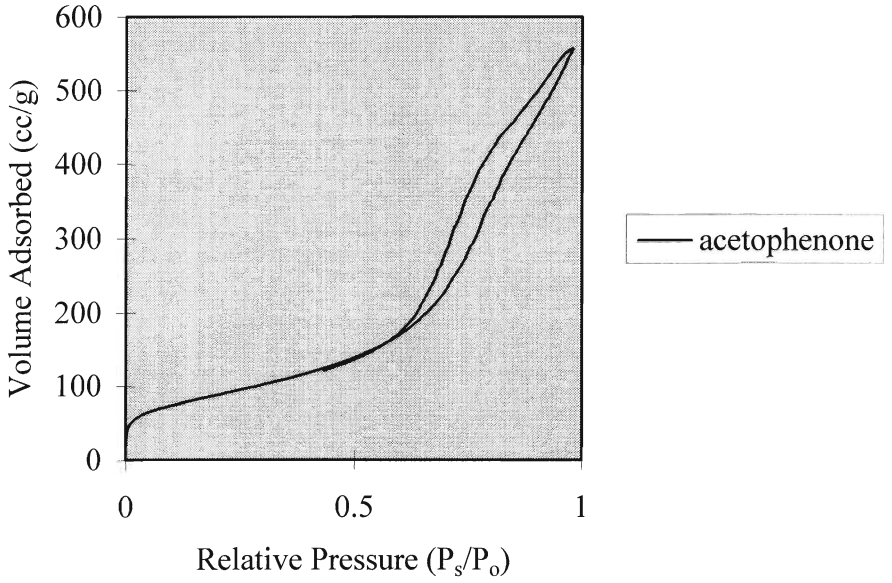

Figure 49: Isotherm for alumina support made with acetophenone.

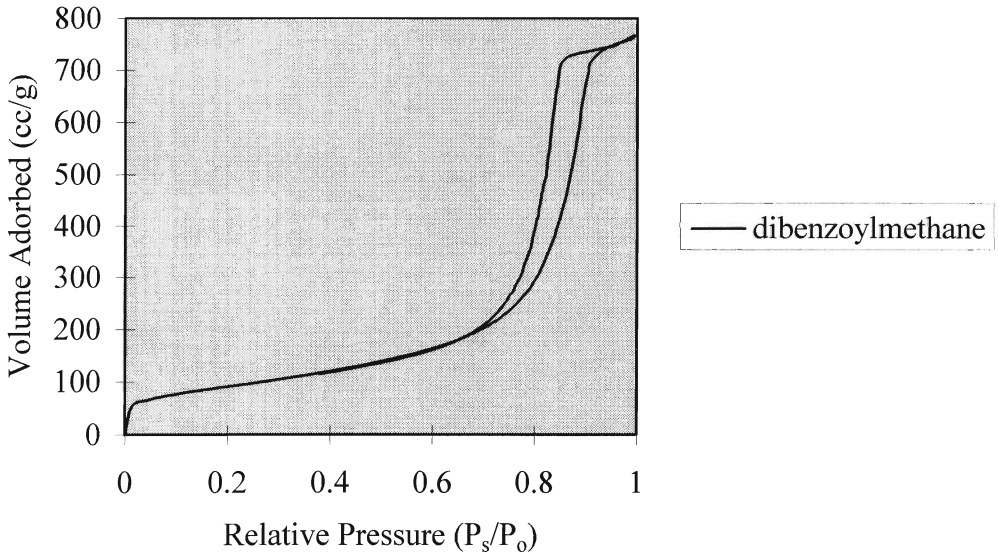

Figure 50: Isotherm for alumina support made with dibenzoylmethane.

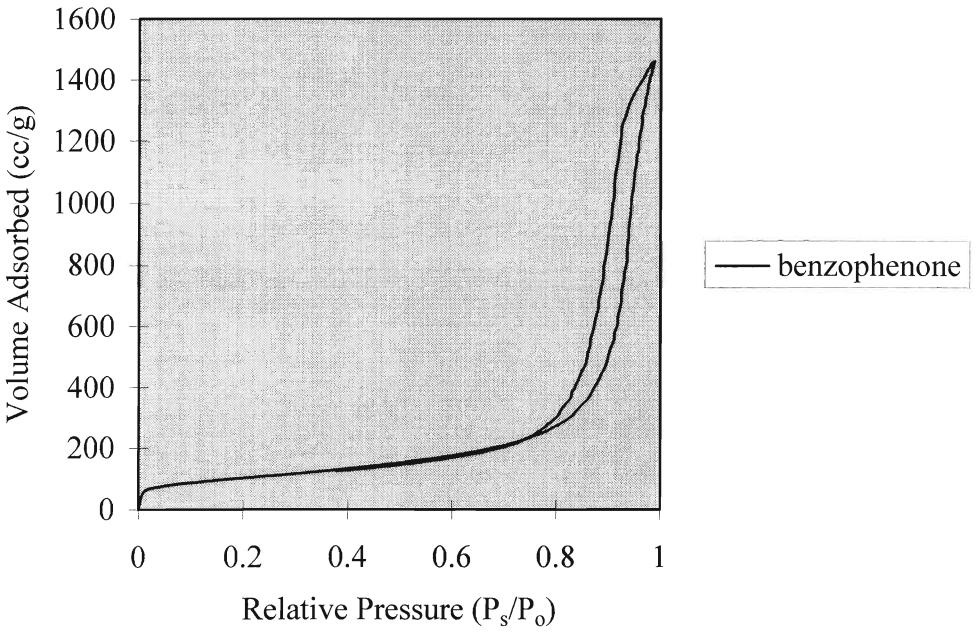

Figure 51: Isotherm for alumina support made with benzophenone.

3.3 $AlCl_3$ Work

Clark *et. al.*[48] have investigated the use of $AlCl_3$ on various supports as a Friedel-Crafts catalyst. The authors show that immobilizing the $AlCl_3$ on a support (silica, K10, alumina) gives activity on the order of $AlCl_3$ alone but with better selectivity toward the formation of monoalkylates with possibilities for separation and reuse of the catalyst. This work has attempted to extend that work to other types of supports with the aim of better selectivity and possibly application to various Friedel-Crafts alkylation reactions. With the work in our group on controlling the pore size distributions by the use of chemical additives for different supports, there are many supports to choose from.

This work used a synthetic aluminosilicate support (see Experimental) calcined at 500°C for the starting point of the study. Clark, *et. al.* provided a good starting point for the procedure chosen for the preparation and testing of the catalyst. The preparation and testing of the catalysts was done *in situ* and monitored by GC. Two major variables were taken into consideration. The first is the loading of the $AlCl_3$ on the support and the second is the ratio of benzene to 1-octene in the reaction.

Table 13 below gives a summary of the ratios of benzene:1-octene used in the reactions, the loading of $AlCl_3$, and the conversions. The figure given for % conversion is based on total conversion of 1-octene to products. A discussion of the conversion to desired product is given later.

Table 13: Ratios, loadings, total conversion from 1-octene

MOLAR RATIO BENZENE:1-OCTENE	AMOUNT OF $AlCl_3$ (mmol)	AMOUNT OF SUPPORT (g)	%CONVERSION
2:1	0.1	1	44
2:1	0.2	1	73
2:1	0.3	1	100
2:1	0.4	1	100
2:1	0.5	1	100
2:1	0.75	1	100
2:1	1.0	1	100
2:1	1.25	1	100
2:1	1.5	1	100
10:1	0.4	1	53
10:1	0.5	1	100
15:1	0.4	1	90
15:1	0.5	1	100
15:1	0.6	1	100
20:1	0.1	1	5
20:1	0.2	1	13
20:1	0.3	1	10
20:1	0.4	1	35
20:1	0.5	1	81
20:1	0.6	1	100

The 2:1 ratio was investigated first. This pinpointed the approximate loadings for the other ratios examined which is the reason there are not as many entries for the other ratios. As the ratio was increased, the loading of $AlCl_3$ required to give full conversion increased. Table 14 shows the percentages of the different products formed for each of the four ratios with the loading that gave just below 100% conversion and for the minimum loading which gave 100% conversion. It was apparent that products were formed when the reaction mixture turned yellow-brown and heat was evolved. After this was determined the flask was placed into a cold bath to control the temperature of the

reaction as the evolution of heat may have promoted further alkylations. The results given above reflect this.

Table 14: Activity of different ratios as GC %.

RATIO BENZENE:1-OCTENE	LOADING (mmol/g)	Methylheptyl benzene	Ethylhexyl benzene	OTHER PRODUCTS
2:1	0.2	52.3	31.4	16.3
2:1	0.3	37.0	35.5	27.5
10:1	0.4	54.5	45.5	none
10:1	0.5	69.9	30.1	none
15:1	0.4	56.3	43.7	none
15:1	0.5	50.8	42.0	7.2
20:1	0.5	49.5	29.7	20.8
20:1	0.6	52.9	47.1	none

The column designated as other products is in reference to several isomers of a disubstituted benzene system. From the table it is evident that there is an optimum ratio of benzene:1-octene which is 10:1. This ratio gives only monoalkylated products although there is still rearrangement. In this reaction, the benzene acts as both solvent and reagent. With an overloaded amount of $AlCl_3$ there is the possibility that free $AlCl_3$ is present in solution which may account for the increased amount of disubstitutions. The surface active site for the adsorbed $AlCl_3$ is thought to be -O-$AlCl_2$. When the ratio is increased, the occurrence of disubstitutions is reduced with the optimum ratios of 10:1 and 15:1. Figure 52 is a reproduction of the typical GC trace obtained for the reaction.

The actual desired product is octylbenzene but the major products obtained are (1-methylheptyl)benzene and (1-ethylheptyl)benzene as determined by mass spectral analysis. The intensities of these products are given in the Experimental section. This is due to the rearrangement of the 1-octene before substitution onto the benzene ring. In Friedel-Crafts alkylations, the intermediate is a carbocation. The stability of the

carbocation is the driving force in the rearrangement of the 1-octene. That is, a secondary carbocation is more stable than a primary intermediate, which is why the rearrangement occurs. An attempt to improve selectivity further and generate octylbenzene was undertaken with the use of less reactive reagents. 1-Chlorooctane and 1-octanol where tried once. Both gave no conversion and 1-octanol was dismissed as a possibility when I realized that the by-product of this reaction was water, which would destroy the catalyst. The 1-chlorooctane still needs to be investigated.

It should be noted here that this work on $AlCl_3$ was by no means fully investigated and can only be considered a preliminary look into this aspect of supported reagents. It was not pursued further as I decided to try a more complete investigation of the other two parts of this thesis. Chapter 5 gives some suggestions for future work on supported $AlCl_3$.

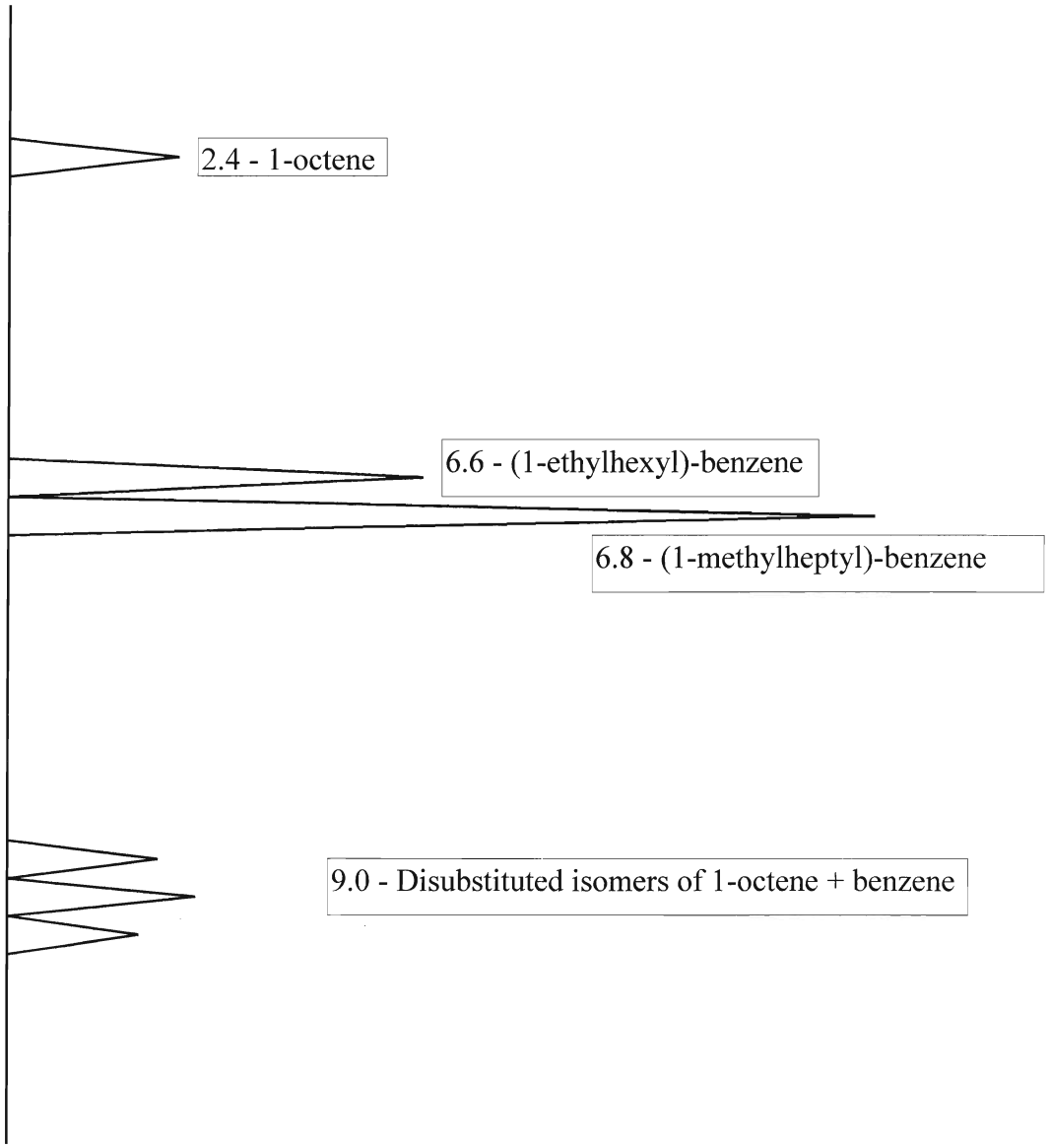

Figure 52: Reproduction of typical GC chromatogram for $AlCl_3$ test reaction. Shown with approximate retention times in minutes.

4. CONCLUSIONS

The aluminosilicate work was successful in the sense that a further probe into the structure of the catalyst was obtained. The ^{29}Si MAS-NMR spectra are broad and unresolved but as the fluoride concentration is increased the centre bands shifts to a higher field indicating that the structure of the aluminosilicate is different. The ^{27}Al MAS-NMR spectra show that upon increasing fluoride content the intensity of the $Al^{"V"}$ drops and the tetrahedral aluminum intensity increases indicating the formation of AlF_4^-, a tetrahedral species. It seems that the introduction of a fluoride inhibits the formation of the $Al^{"V"}$ which has been linked to enhanced activity. The reduction in activity observed here with increasing amounts of fluoride reinforce this.

The investigation into the alumina supports was a success. A method of making porous solids with a specific pore distribution and surface area has been devised. Chemical additives in the sol-gel synthesis is a powerful way of altering and "tailoring" desirable characteristics of a support This could be applied to other types of Friedel-Crafts reactions to optimize activity. There are several factors one may look for in determining a possible candidate for a good Friedel-Crafts catalyst. Nitrogen adsorption studies provide information on the shape and size of the pore. It was found that a high pore volume (≥2 cc/g), more than anything else indicated a support that when loaded with $ZnCl_2$ would exhibit high activity. Also, the type of hysteresis loop will indicate whether the pores are "ink bottle" shaped that may become clogged. In the case of dibenzoylmethane, the H2 hysteresis loop indicated "ink bottle" shaped pores and this support did not give a very active catalyst. The phenone additives used here gave an H4 type hysteresis loop with a high pore volume and the supports made very effective

Friedel-Crafts catalysts. Ketones with an aromatic ring beta to the carbonyl group are good additives to use in an alumina system to obtain a support with high surface area, pore volume and pore size distribution. The β-diketones do not provide supports with good properties for catalytic activity. The pores are formed by complexation of the aluminum with the organic additive. This can be confirmed by FTIR spectra which show a shift in either the carbonyl stretch or the aromatic skeletal region as compared to the spectrum of the additive. The H-acac, acetophenone and benzophenone show shifts in the carbonyl and/or aromatic stretches confirming the formation of a complex. The dibenzoylmethane did not and the alumina supports made with this additive made poor catalysts.

Aluminum chloride is still considered a powerful Friedel-Crafts catalyst. Using it in small amounts on a support would be useful. The preliminary work done here shows that there is potential for using $AlCl_3$ in a reaction with selectivity and safety.

5. FUTURE WORK

A study of more fluoride salts and more in depth ^{19}F MAS-NMR study could further the understanding of the effect of fluoride on the aluminosilicate support structure.

The alumina work still has much that could be done. There are several additives that could be used. The aromatic ketones proved to be good additives for this system, giving high pore volumes and large pore size distributions. It would be interesting to see if the straight chain ketones would produce the same types of results or if only the aromatic ketones are effective. Another area of investigation into this could involve solvent effects. In this study, no attempt was made to vary the amount or type of solvent used in the synthesis.

The support aluminum trichloride has much to be done as well. Using supports made with chemical additives and variation of the benzene:1-octene ratio with these supports could yield interesting results. NMR spectroscopy studies could also give insight into the reactive components of the catalyst. Substituted benzenes (like toluene) as the solvent and a reagent may reduce multiple alkylations of the aromatic ring so investigation into this could be done. Exploration of other alkylating agents such as chlorooctane could serve to improve the selectivity of this reaction.

REFERENCES

1. J.H. Clark, A.P Kybett & D.J Macquarrie, Supported Reagents-Preparation, Analysis and Applications, VCH Publishers Inc., New York, 1992.

2. A. Cornélis, P. Laszlo. Synthesis, 1985, 909.

3. A. Cornélis. In Preparative Chemistry Using Supported Reagents. P. Laszlo, editor. Academic Press Inc., Toronto. (1987).

4. W. Löwenstein. Am. Mineral., 1954, **39**, 92.

5. J.M. Miller, D. Wails, J.S. Hartman and J.L. Belelie, J. Chem. Soc., Faraday Trans., 1997, **93**(4), 2439.

6. W.D. Nesse, Introduction to Optical Mineralogy, 2nd. ed., Oxford University Press, New York, 1991.

7. C.Klein, C.S. Hurlbut Jr., Manual of Mineralogy, 21st. ed., John Wiley and Sons, Toronto, 1993.

8. R. Mokaya, W. Jones, J. Catal., 1995, **173**, 76.

9. J.H. Clark, A.P. Kybett, D.J. Macquarrie, S.J. Barlow and P. Landon, J. Chem. Soc., Chem. Comm., 1989, 1353.

10. Clayzic is a trademark of Contract Catalysts Ltd., Merseyside, U.K.

11. C.N. Rhodes, M. Franks, G.M.B. Parks and D.R. Brown, J. Chem. Soc., Chem. Comm., 1991, 804.

12. F. Asseid, FTIR and MAS-NMR Analysis fo Montmorillonite K10 Supported MF_2 Reagents and their Activity as Catalysts, Brock University, St. Catharines, 1992.

13. G.H. Posner, In Preparative Chemistry Using Supported Reagents, P. Laszlo, editor, Academic Press Inc., Toronto, 1987.

14. C.V.A. Duke, J.M. Miller, J.H. Clark and A.P. Kybett, Spectrochim. Acta., 1988, **44A**(11), 1207.

15. T. Ando, S.J. Brown, J.H. Clark, D.G. Cork, T. Hanafusa, J. Ichihara, J.M. Miller and M.S. Robertson, J.Chem Soc., Perkin Trans.II., 1986, 1133.

16. D. Villemin, J. Chem. Soc., Chem. Comm., 1983, 1092.

17. E. Santaniello, In Preparative Chemistry Using Supported Reagents, P. Laszlo, editor, Academic Press Inc., Toronto, 1987.

18. J.M. Miller, D. Wails, J.S. Hartman, K. Schebesh and J.L. Belelie, Can. J. Chem., 1998 (in press).

19. A.M. Buckley and M. Greenblatt, J. Chem. Ed., 1994, **71**(7), 599.

20. I.C. Tilgner, P. Fischer, F.M. Bohnen, H. Rehage and W.F. Maier, Microporous Mat., 1995, **5**, 77.

21. S.H. Patinkin and B.S. Friedman, In Friedel-Crafts and Related Reactions, Vol. II, Part I, G.A. Olah, editor, John Wiley and Sons, New York, 1964.

22. S.H. Pine, Organic Chemistry, 5th, ed., McGraw-Hill Inc., Toronto, 1987.

23. F.A. Drahowzal, In Friedel-Crafts and Related Reactions, Vol. II, Part I, G.A. Olah, editor, John Wiley and Sons, New York, 1964.

24. C.J. Brinker and G.W. Scherer, Sol-Gel Science: The Physics and Chemistry of Sol-Gel Processing, Academic Press Inc., Toronto, 1990.

25. J. Livage, F. Babonneau, M. Chatry and L. Coury, Ceramics International, 1997, 13.

26. J.M. Miller, D. Wails, J.S. Hartman and J.L. Belelie, J. Chem. Soc., Faraday Trans., 1998, **94**, 789.

27. K. Maeda, F. Mizukami, M. Watanabe, N. Arai, S. Niwa and M. Toba, J. Mat. Sci. Lett., 1990, **9**, 522.

28. T. Adachi and S. Sakka, J. Non-cryst. Sol., 1988, **99**, 118.

29. J.B. Lambert, H.F. Shurvell, D.A. Lightner and R.G. Cooks, Introduction to Modern Spectroscopy, Macmillan Publishing Company, New York, 1987.

30. J.W. Akitt, NMR and Chemistry: An Introduction to Modern NMR Spectroscopy, Chapman and Hall, New York, 1992.

31. G. Engelhardt and D. Michel, High Resolution Solid-State NMR of Silicates and Zeolites, John Wiley and Sons, Toronto, 1987.

32. A.-R. Grimmer, and B. Blümich, In NMR Basic Principle and Prgress 30: Solid State NMR I: Methods, P. Diehl, E. Fluck, H. Günther, R. Kosfeld and J. Seelig, editors, Springer-Verlag, New York, 1994.

33. W. Kolodziejski and J. Klinowski, In NMR Techniques in Catalysis, A.T. Bell and A. Pines, editors, Marcel Dekker Inc., New York, 1994.

34. A.D. Irwin, J.S. Holmgren and J. Jonas, J. Mat. Sci., 1988, **23**, 2908.

35. B.M. Witte, P.J. Grobet and J.B. Utterhoeven, J. Phys. Chem., 1995, **99**, 6961.

36. K.J.D. MacKenzie, R.H. Meinhold, J.E. Patterson, H. Schneider, M. Schmücker and D. Voll, J. Eur. Ceram. Soc., 1996, **16**, 1299.

37. J.M. Miller, Prog. Nuc. Mag. Reson., 1996, **28**, 255.

38. K.S.W. Sing, D.H. Everett, R.A.W. Haul, L. Moscou, R.A.Pierotti, J. Rouquérol and T. Siemieniewska, Pure and Appl. Chem., 1985, **57**(4), 603.

39. S.J. Gregg and K.S.W. Sing, Adsorption, Surface Area and Porosity, 2nd. ed., Academic Press, Toronto, 1982.

40. S. Brunauer, P.H. Emmett and E. Teller, J. Amer. Chem. Soc., 1938, **60**, 309.

41. E.P. Barrett, L.G. Joyner and P.P. Halenda, J. Amer. Chem. Soc., 1951, **73**, 373.

42. N.K. Roberts, In Surface Analysis Methods in Materials Science, D.J. O'Connor, B.A. Sexton, R.St.C. Smart, Springer-Verlag, New York, 1991.

43. M.P. Fuller and R.P. Griffiths, Anal. Chem., 1978, **50**(13), 1906.

44. J.M. Chalmers and M.W. MacKenzie, In Advances in Applied Fourier Transform, Infrared Spectroscopy, John Wiley and Sons, Toronto, 1988.

45. D.Tilak.B. Tennakoon, J.M. Thomas, W. Jones, T.A. Carpenter and S. Ramdas, J. Chem. Soc., Faraday Trans. I, 1986, **82**, 545.

46. C. Morterra and G. Magnacca, Catalysis Today, 1996, **27**, 497.

47. D.H. Lee and R.A. Condrate Sr., Mater. Lett., 1995, **23**, 241.

48. J.H. Clark, K. Martin, A.J. Teasdale and S.J. Barlow, J. Chem. Soc., Chem. Comm., 1995, 2037.

49. C.N. Rhodes, D.R. Brown, J. Chem. Soc., Faraday Trans., 1992, **88**, 2269.

50. C.N. Rhodes, D.R. Brown, J. Chem. Soc., Faraday Trans., 1993, **89**, 1387.

51. Hore, P.J., Nuclear Magnetic Resonance, 2nd. ed., Oxford University Press, Toronto, 1995.